NEW AND FUNCTIONAL CYCLIC CARBONATES FOR POLYMER APPLICATIONS

Cristina Maquilón Albaladejo

UNIVERSITAT ROVIRA i VIRGILI

New and Functional Cyclic Carbonates for Polymer Applications

CRISTINA MAQUILÓN ALBALADEJO

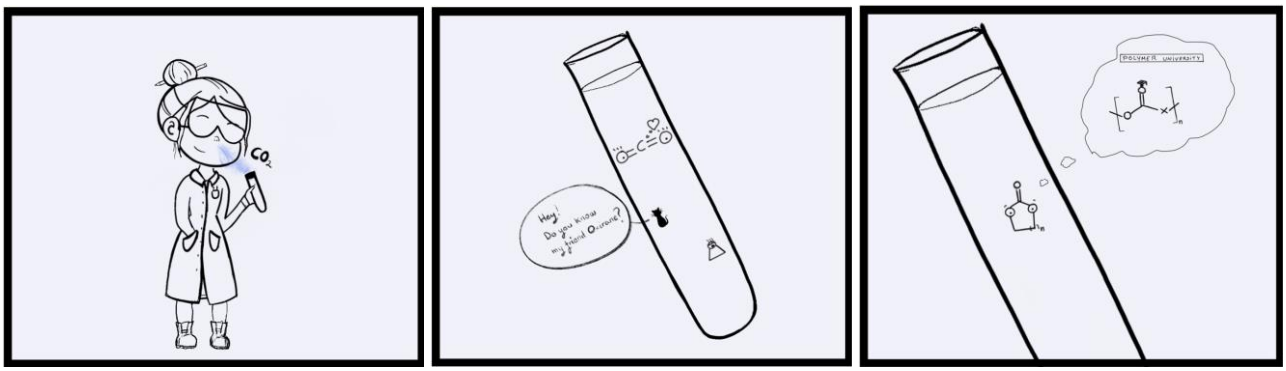

DOCTORAL THESIS
2021

UNIVERSITAT ROVIRA I VIRGILI
NEW AND FUNCTIONAL CYCLIC CARBONATES FOR POLYMER APPLICATIONS
Cristina Maquilón Albaladejo

UNIVERSITAT ROVIRA I VIRGILI
NEW AND FUNCTIONAL CYCLIC CARBONATES FOR POLYMER APPLICATIONS
Cristina Maquilón Albaladejo

PhD Thesis

"New and Functional Cyclic Carbonates for Polymer Applications"

Cristina Maquilón Albaladejo

Supervised by Prof. Dr. Arjan W. Kleij

Tarragona

October 2021

UNIVERSITAT ROVIRA i VIRGILI

ICIQ

UNIVERSITAT ROVIRA I VIRGILI
NEW AND FUNCTIONAL CYCLIC CARBONATES FOR POLYMER APPLICATIONS
Cristina Maquilón Albaladejo

Prof. Dr. Arjan W. Kleij, Group Leader at the Institute of Chemical Research of Catalonia (ICIQ) and Research Professor at the Catalan Institution for Research and Advanced Studies (ICREA),

I STATE that the present Doctoral Thesis, entitled "**New and Functional Cyclic Carbonates for Polymer Applications**" presented by Cristina Maquilón Albaladejo to receive the degree of Doctor, has been carried out under my supervision at the Institute of Chemical Research of Catalonia (ICIQ).

Tarragona, October 2021

Doctoral Thesis Supervisor
Prof. Dr. Arjan W. Kleij

UNIVERSITAT ROVIRA I VIRGILI
NEW AND FUNCTIONAL CYCLIC CARBONATES FOR POLYMER APPLICATIONS
Cristina Maquilón Albaladejo

A Margarita Pomares Sáez

UNIVERSITAT ROVIRA I VIRGILI
NEW AND FUNCTIONAL CYCLIC CARBONATES FOR POLYMER APPLICATIONS
Cristina Maquilón Albaladejo

"Learn more and more about less and less until you know everything about nothing!"

UNIVERSITAT ROVIRA I VIRGILI
NEW AND FUNCTIONAL CYCLIC CARBONATES FOR POLYMER APPLICATIONS
Cristina Maquilón Albaladejo

Acknowledgments

First, I would like to thank my supervisor Arjan Kleij for giving me the opportunity to carry out my doctoral thesis in his group. Likewise, thanks to all the former and present colleagues of the Kleij Group with whom I had the chance to spend all these years. También me gustaría agradecer a todas las unidades de soporte por hacer del ICIQ una familia y porque sin ellas esta tesis no habría sido posible.

I thank Dr. Claas Hövelmann and Dr. Christian Alter for accepting me during my short-stay and showing me the world of industry. Also, I would like to thank all their teammates for making me feel more than welcome from the very first day.

Finalment m'agradaria agraïr a tota la meva famila i amics pel suport incondicional que he rebut durant aquestos cuatre anys.

UNIVERSITAT ROVIRA I VIRGILI
NEW AND FUNCTIONAL CYCLIC CARBONATES FOR POLYMER APPLICATIONS
Cristina Maquilón Albaladejo

Financial Support

The present doctoral thesis has been made possible thanks to funding received from AEI/MINECO (FPI Severo Ochoa Fellowship, BES-2017-081151) and the Institute of Chemical Research of Catalonia (ICIQ) (CERCA Programme/Generalitat de Catalunya).

UNIVERSITAT ROVIRA I VIRGILI
NEW AND FUNCTIONAL CYCLIC CARBONATES FOR POLYMER APPLICATIONS
Cristina Maquilón Albaladejo

Curriculum Vitae

Cristina Maquilón Albaladejo was born on December 17, **1994** in Elche (Spain). She studied chemistry at the University of Alicante (UA) obtaining her BSc degree in June **2016**. Next, she moved to Madrid for her MSc studies in Organic Chemistry at the Autonomous University of Madrid (UAM). After obtaining her MSc in June **2017** she started her PhD studies in September under the supervision of Professor Arjan W. Kleij at the Institute of Chemical Research of Catalonia (ICIQ). The research studies performed during her PhD are described in this thesis. Her research was financially supported with an FPI Severo Ochoa Fellowship from the Spanish "Ministerio de Economía y Competitividad", MINECO. During her PhD she spent two months at BASF Coatings Gmbh (Münster, Germany) working on the synthesis of new biobased polyurethanes under the supervision of Dr. Claas Hövelmann and Dr. Christian Alter. The results described in this thesis have been communicated at different national and international conferences, such as the XXVII Reunión Bienal de Química Orgánica (RSEQO) in Santiago de Compostela (**2018**), ICIQ-INTECAT School in Montbrió (**2018**), the ICCDU XVII in Aachen (**2019**) and the EUGSC IV in Tarragona (**2019**).

UNIVERSITAT ROVIRA I VIRGILI
NEW AND FUNCTIONAL CYCLIC CARBONATES FOR POLYMER APPLICATIONS
Cristina Maquilón Albaladejo

List of Publications

The following publications are based on the work described in this thesis:

- "*Effect of an Al(III) Complex on the Regeo- and Stereoisomeric Formation of Bicyclic Organic Carbonates*" **Cristina Maquilón**, Bart Limburg, Victor Laserna, Diego Garay-Ruiz, Joan González-Fabra, Carles Bo, Marta Martínez Belmonte, Eduardo C. Escudero-Adán, and Arjan W. Kleij, *Organometallics* **2020**, *39*(9), 1642-1651.

- "*Phothochemical and Substrate-Driven CO_2 Conversion*" Bart Limburg, **Cristina Maquilón**, and Arjan W. Kleij, BOOK CHAPTER In: "Substrate-driven divergent CO_2 conversion" Ed. Shoubhik Das, Wiley-VCH, **2020**, *1* (ISBN: 978-3-527-34613-4).

- *"Photocatalytic Synthesis of Substituted Cyclic Carbonate Monomers for Ring-Opening Polymerization"* **Cristina Maquilón**, Francesco Della Monica, Bart Limburg, and Arjan W. Kleij, *Adv. Synth. Catal.* **2021**, *363* (16), 4033-4040.

The following publications relate to other activities during this thesis.

- "*Organocatalyzed Domino [3+2] Cycloaddition/Payne-Type Rearrangement using Carbon Dioxide and Epoxy Alcohols*". Sergio Sopeña, Mariachiara Cozzolino, **Cristina Maquilón**, Eduardo C. Escudero-Adán, Marta Martínez Belmonte and Arjan W. Kleij, *Angew. Chem. Int. Ed*. **2018**, *57*, 11203-11207.

UNIVERSITAT ROVIRA I VIRGILI
NEW AND FUNCTIONAL CYCLIC CARBONATES FOR POLYMER APPLICATIONS
Cristina Maquilón Albaladejo

Table of Contents

UNIVERSITAT ROVIRA I VIRGILI
NEW AND FUNCTIONAL CYCLIC CARBONATES FOR POLYMER APPLICATIONS
Cristina Maquilón Albaladejo

Preface

The work presented in this dissertation has been performed at the Institute of Chemical Research of Catalonia (ICIQ), during the period of October 2017 until September 2021 under the supervision of Professor Arjan W. Kleij. This thesis is divided into five sections: a general introduction containing the aims and outline of the thesis, three research chapters, and a chapter in which the overall conclusions of the work are presented. Each of the research chapters includes a brief introduction on the topic, followed by the collected results and their discussion, the main conclusions, and finally a detailed experimental section. References and their numbering are independently organized in each chapter.

UNIVERSITAT ROVIRA I VIRGILI
NEW AND FUNCTIONAL CYCLIC CARBONATES FOR POLYMER APPLICATIONS
Cristina Maquilón Albaladejo

List of abbreviations

In this doctoral thesis, the abbreviations and acronyms most commonly used in organic chemistry are based on the recommendations of the ACS "Guidelines for authors". Additional abbreviations are listed below:

APC	Aliphatic polycarbonate
BE	β-Elemene
BED	β-Elemene dioxide
BEDC	β-Elemene dicarbonate
BEDU	β-Elemene diurethane
BEMC	β-Elemene monocarbonate
CC	Cyclic carbonate
CCS	Carbon capture and storage
CCU	Carbon capture and utilization
CO_2	Carbon dioxide
DEE	Diethoxyethane
DFT	Density functional theory
DMAP	4-dimethylaminopyridine
DR	Double rub
DSC	Differential scanning calorimetry
GDMP	Ethylene glycol bis(3-mercaptopropionate)
MEK	Methyl ethyl ketone
MIBK	Methyl isobutyl ketone
NCO	Isocyanate
NIPU	Non-isocyanate polyurethane
PC	Polycarbonate
PEMTP	Pentaerythritol tetrakis(3-mercaptopropionate)
PHU	Polyhydroxyurethane
PU	Polyurethane
ROCOP	Ring-opening copolymerization
ROP	Ring-opening polymerization
TBAB	Tetrabutylammonium bromide
TGA	Thermogravimetric analyses

UNIVERSITAT ROVIRA I VIRGILI
NEW AND FUNCTIONAL CYCLIC CARBONATES FOR POLYMER APPLICATIONS
Cristina Maquilón Albaladejo

Chapter 1

General Introduction

Parts of this chapter were adapted from:

Limburg, B.; Maquilón, C.; Kleij, A. W. BOOK CHAPTER In: "*Substrate-driven divergent CO_2 conversion*" Ed. Shoubhik Das, Wiley-VCH, **2020**, *1* (ISBN: 978-3-527-34613-4).

UNIVERSITAT ROVIRA I VIRGILI
NEW AND FUNCTIONAL CYCLIC CARBONATES FOR POLYMER APPLICATIONS
Cristina Maquilón Albaladejo

1.1. Carbon dioxide

Carbon dioxide (CO_2) in its electronic ground state is a triatomic linear molecule. The central carbon, at its highest oxidation state (+4), is connected to the two oxygen atoms through two σ bonds and two π bonds which translates to a characteristic C=O bond length of 1.16 Å. The polarity of these bonds, as a result of the difference in electronegativity of the carbon and oxygen atoms, results in a partial positive charge at the carbon centre and partial negative charges located on the oxygen atoms. However, in this linear and centrosymmetric molecule, the dipole moments are directionally opposing leading to an overall non-polar molecule. The combination of the atomic orbitals in the valence shell produces 12 molecular orbitals. Thus, the molecular orbital diagram contains 4 bonding, 4 non-bonding and 4 antibonding orbitals that allocate the 16 valence electrons. These electrons are distributed in the bonding and non-bonding orbitals, leaving the antibonding orbitals empty (Figure 1.1).[1,2,3]

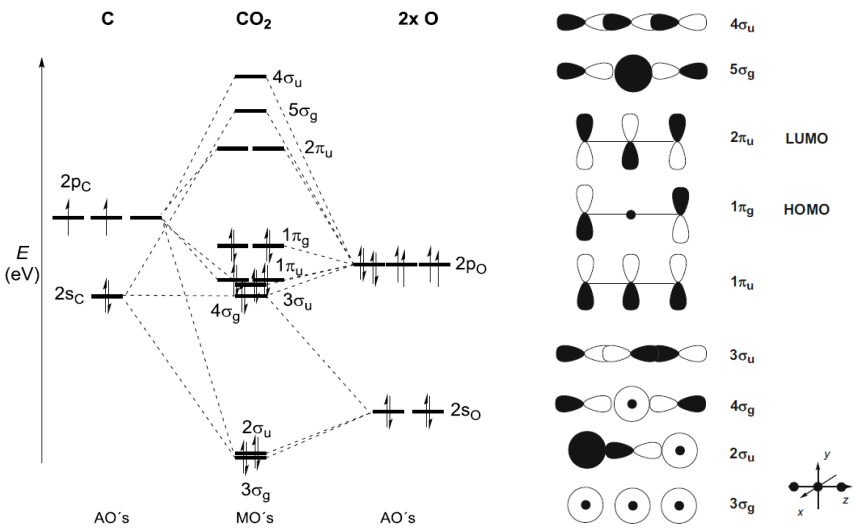

Figure 1.1. Molecular orbital diagram for CO_2.[4]

[1] Aresta, M.; Dibenedetto, A.; Quaranta, E. *Reaction Mechanisms in Carbon Dioxide Conversion*, Springer, Heidelberg, **2016**.
[2] Paparo, A.; Okuda, J. *Coord. Chem. Rev.* **2016**, *334*, 136-149.
[3] Alvarez, A.; Borges, M.; Corral-Perez, J. J.; Olcina, J. G.; Hu, L. J.; Cornu, D.; Huang, R.; Stoian, D.; Urakawa, A. *ChemPhysChem* **2017**, *18*, 3135-3141.
[4] The images have been extracted from references 1 and 2.

CO_2 has been present in the atmosphere since the early stages of our planet and represents one of the main components.[5,6] In fact, this greenhouse gas is considered essential for keeping habitable conditions on Earth due to its capability to absorb and emit infrared radiation. The contribution of CO_2 to the greenhouse effect is proportional to its concentration in the atmosphere.[7] This concentration is normally regulated by the long-term "carbon cycle", which is in turn influenced by the global temperature of the planet.[8,9]

Over the different glacial and interglacial Earth periods, the levels of CO_2 oscillated between values of 180-200 and 250-280 parts per million by volume (ppmv), respectively. Currently, Earth is going through an interglacial period where the concentration of CO_2 remained stable for more than 10,000 years with a value of 280 ppmv until the industrial revolution started around 1860.[10] The industrial revolution initiated a huge progress in technological innovation but also required a high energetic demand causing a steep increase in anthropogenic carbon emissions. Consequently, CO_2 levels in the atmosphere have been dramatically increasing up to 420 ppmv recorded on April 2021 (Figure 1.2).[11,12]

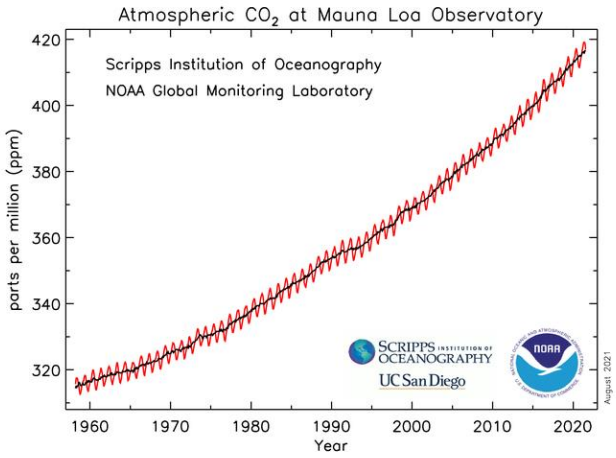

Figure 1.2. Recorded values of the CO_2 concentration in the atmosphere since 1958 at the National Oceanic Atmospheric Administration (NOAA).[10]

[5] Kasting, J. F.; Ackerman, T. P. *Science* **1986**, *234*, 1383-1385.
[6] Kasting, J. F.; Zahnle, K. J.; Walker, J. C. G. *Precambrian Res.* **1983**, *20*, 121-148.
[7] For details on the recently released IPCC report: https://www.ipcc.ch/report/ar6/wg1/.
[8] Mills, B. J. W.; Krause, A. J.; Scotese, C. R.; Hill, D. J.; Shields, G.A.; Lenton, T. M. *Gondwana Res.* **2019**, *67*, 172-186.
[9] Berner, R. A. *Nature* **2003**, *426*, 323-326.
[10] Lüthi, D.; Le Floch, M.; Bereiter, B.; Blunier, T.; Barnola, J.-M.; Siegenthaler, U. *Nature* **2008**, *453*, 379-382.
[11] Peter, S. C. *ACS Energy Lett*. **2018**, *3*, 1557-1561.
[12] Consult: https://gml.noaa.gov/ccgg/trends/mlo.html.

The accumulation of CO_2 in the atmosphere has had an impact on the carbon cycle, which is no longer able to be maintained as a controllable equilibrium through a balance of the different natural reservoirs or carbon sinks.[9] As a consequence, the greenhouse effect is reinforced and the radiative heating of the Earth's atmosphere increases, contributing to global warming and related negative effects.[13] The growing necessity of facing and mitigating this important issue has encouraged the scientific community to design and develop sustainable ways to reduce the atmospheric CO_2 concentration.

Among the most commonly used strategies, carbon capture & storage (CCS) and carbon capture & utilization (CCU) have arisen as potential solutions to store (CCS) and transform (CCU) this greenhouse gas. While CCS involves long-term CO_2 storage and does not provide any economic benefit, the aim of CCU is to convert CO_2 into value added products.[14] These chemical transformations can be classified depending on whether there is a formal carbon reduction occurring. When a reductive pathway takes place, CO_2 is transformed into other compounds that have the original carbon centre in a lower oxidation state such as in CO_2-derived fuels (CO, CH_4 and CH_3OH), carboxylic acids and formyl derivatives, among other products. Alternatively, in non-reductive methods, CO_2 is incorporated into organic structures while maintaining its original carbon (+4) oxidation state. This approach is often used for the preparation of carbonate and carbamate based compounds.[15,16,17] Within this area of research, our group has mainly focused on the use of CO_2 for the synthesis of cyclic carbonates[18,19,20] and polycarbonates.[21,22,23]

[13] Feldman, D.R.; Collins, W.D.; Gero, P.J.; Torn, M.S.; Mlawer, E.J.; Shippert, T.R. *Nature* **2015**, *519*, 339-343.
[14] Cuellar-Franca, R. M.; Azapagic, A. *J. CO_2 Util.* **2015**, *9*, 82–102.
[15] Fiorani, G.; Guo, W.; Kleij, A. W. *Green Chem.* **2015**, *17*, 1375–1389.
[16] Maeda, C.; Miyazaki, Y.; Ema, T. *Catal. Sci. Technol.* **2014**, *4*, 1482–1497.
[17] Song, Q.-W.; Zhou, Z.-H-; He, L.-H. *Green Chem.* **2017**, *19*, 3707–3728.
[18] Qiao, C.; Villar-Yanez, A.; Sprachmann, J.; Limburg, B.; Bo, C.; Kleij, A. W. *Angew. Chem. Int. Ed.* **2020**, *59* (42), 18446-18451.
[19] Laserna, V.; Martin, E.; Escudero-Adán, E.C.; Kleij, A.W. *ACS Catal.* **2017**, *7*, 5478-5482.
[20] Rintjema, J.; Guo, W.; Martin, E.; Escudero-Adán, E. C.: Kleij, A. W. *Chem. Eur. J.* **2015**, *21*, 10754-10762.
[21] Kindermann, N.; Cristòfol, À.; Kleij, A. W. *ACS Catal*. **2017**, *7*, 3860-3863.
[22] Martín, C.; Kleij, A. W. *Macromolecules* **2016**, *49*, 6285-6295.
[23] For recent reviews on CO_2-derived polymers/monomers see: (a) Grignard, B.; Gennen, S.; Jérôme, C.; Kleij, A. W.; Detrembleur, C. *Chem. Soc. Rev*. **2019**, *48*, 4466-4514. (b) Yadav, N.; Seidi, F.; Crespy, D.; D'Elia, V. *ChemSusChem* **2019**, *12*, 724−754.

1.2 Synthesis and application of cyclic carbonates

Conventionally, the formation of cyclic carbonates (CCs) is carried out using phosgene as a reagent but this has disadvantages associated with its high toxicity as well as being dangerous to handle. Consequently, finding more sustainable alternative routes to access CCs has been the subject of intense studies over the past 20 years.[24] As a result, the synthesis of cyclic carbonates is well-established providing easy access to more sophisticated scaffolds, which can eventually lead to increasingly complex products such as polymers. Greener transformations for the synthesis of CCs involve the use of CO_2 and diverse co-reagents including diols, halohydrins, (homo)allyl- and propargyl alcohols and cyclic ether such as epoxides and oxetanes (Figure 1.3).[25,26] In particular, the use of cyclic ethers has been become a highlypopular and versatile way of preparing CCs with different degrees of functionalization and substitution.[27]

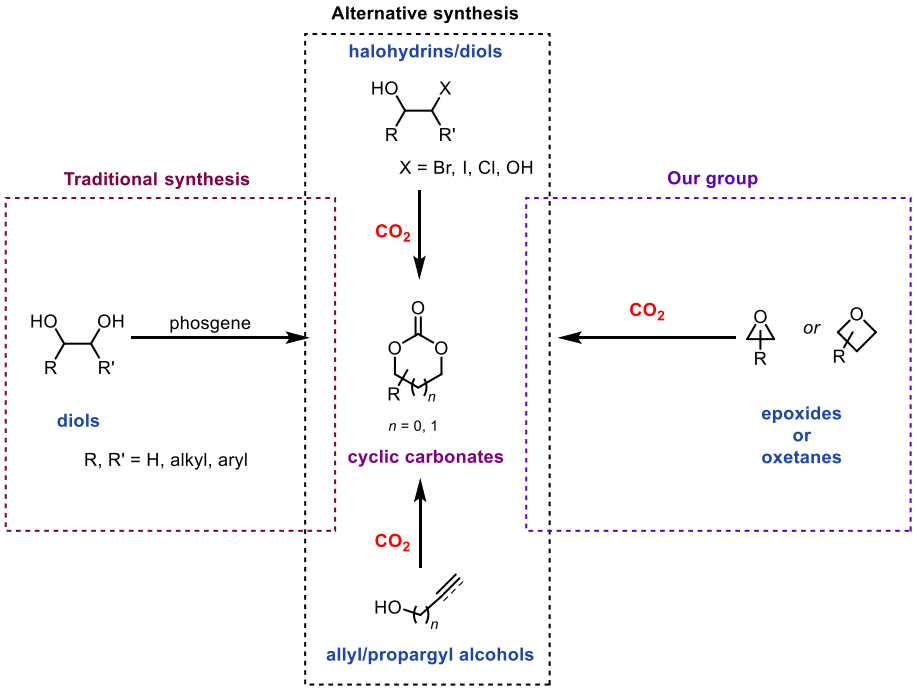

Figure 1.3. Most popular synthetic approaches for the synthesis of CCs.

[24] Burk, R. M.; Roof, M. B. *Tetrahedron Lett*. **1993**, *34*, 395-398.
[25] Reithofer, M. R.; Sum, Y. N.; Zhang, Y. *Green Chem*. **2013**, *15*, 2086-2090.
[26] Chen, K.; Shi, G.; Dao, R.; Mei, K.; Zhou, X.; Li, H.; Wang, C. *Chem. Commun*. **2016**, *52*, 7830-7833.
[27] Limburg, B.; Cristofol, A.; Della Monica, F.; Kleij, A. W. *ChemSusChem* **2020**, *13*, 6056-6065.

Our group has dedicated much effort towards developing new synthetic routes to CCs with cyclic ethers employed as privileged reagents.[15,18-20,27] For example, the cycloaddition of epoxides or oxetanes with CO_2 produces 5- (5MCCs) and 6-membered cyclic carbonates (6MCCs), respectively. Interestingly, in this field, we demonstrated recently that the use of epoxy alcohols provides new and unexpected reactivity.[27] Specifically, the alcohol group of these substrates is actively involved in the CO_2 incorporation process, thus allowing a different manifold to be operated. When the alcohol is positioned alpha to the epoxide, a *trans*-configured 5MCC is obtained (Figure 1.4a).[19] Alternatively, with the hydroxyl group positioned beta to the epoxy alcohol, typically challenging to access 6MCCs are produced through a two-step process that involves the unusual rearrangement of a 5- into a 6-membered carbonate and *O*-protection (Figure 1.4b).[18] The synthesis of both *trans*-5MCCs and 6MCCs represents a challenge within the field of carbonate chemistry (see also Chapter 2 of this thesis). However, due to their enhanced reactivity towards ring-opening[28] compared to thermodynamically stable *cis*-configured 5MCCs, they possess high potential as monomers for creating new polymer formulations.[23]

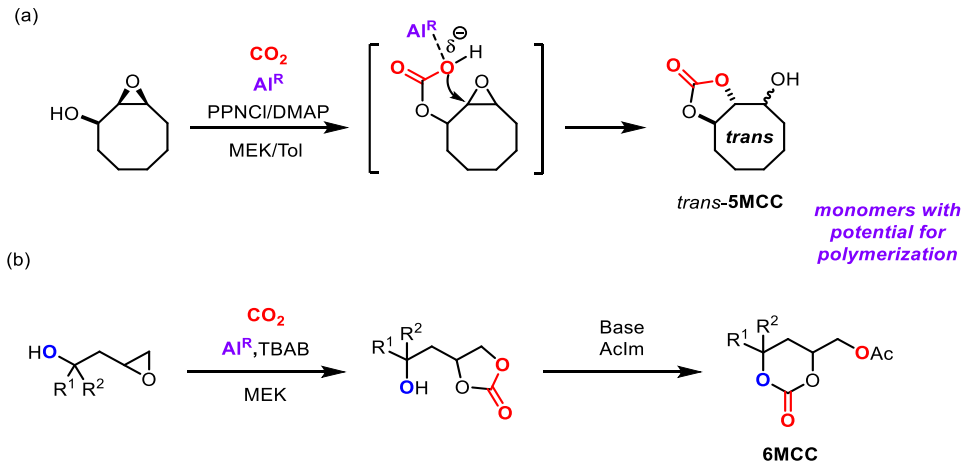

Figure 1.4. (a) Synthesis of a rare *trans*-configured cyclic carbonate from an epoxy alcohol and CO_2. (b) 6MCC formation via a step-wise process using β-epoxy alcohols. AcIM = acetyl imidazole.

[28] (a) McGuire, T. M.; López-Vidal, E. M.; Gregory, G. L.; Buchard, A. *J. CO_2 Util.* **2018**, *27*, 283−288. (b) Gregory, G. L.; Jenisch, L. M.; Charles, B.; Kociok-Köhn, G.; Buchard, A. *Macromolecules* **2016**, *49*, 7165−7169.

Cyclic carbonates are currently used in a wide range of applications, including their use as polar aprotic solvents, possible electrolytes for lithium ion batteries, organic synthetic intermediates,[29] fuel additives and precursors for polymeric materials.[16,23] While the latter application can be regarded as a sub-domain of CO_2 chemistry still being in relative infancy, interesting progress has been noted over the last few years. Moreover, with a growing need to improve the sustainability of plastics in the mid and long term, it represents a timely field of investigation.

1.3. Cyclic carbonate-based polymer chemistry

Polymers are versatile materials and are essential for modern life owing to an extremely broad window of material properties and hence (consumer) applications. Unfortunately, to date, the most commonly used polymers are produced from fossil sources such as crude oil and are not (bio)degradable or recyclable. As a result, they tend to accumulate in our environment and present a threat to our eco-systems and health.[30] A possible solution to this problem would be the development of polymers form bio-based monomers and, even more ideally, from bio-monomers that afford polymers with biodegradation and repurposing potential. In this regard, CCs are promising monomer candidates that have already shown useful reactivity towards the formation of polycarbonates (PCs)[31] and non-isocyanate polyurethane (NIPUs).[32]

CCs can be converted into PCs via a ring-opening polymerization process (ROP) which represents a chain-growth polymerization (Figure 1.5a) and this reactivity is mostly associated with the use of 6MCCs. The ROP process starts off with the attack of a suitable initiator (**In**) on a CC monomer, generating a reactive alkoxide that can attack a subsequent monomer producing, after n-1 repetitive steps, a polymer chain. Depending on the nature of the initiator and resultant reactive centre, anionic, cationic or radical ROP can take place.[33] CCs can also participate in polyaddition reactions that involve di/poly-carbonate monomers and diamines

[29] Guo, W.; Gómez, J. E.; Cristòfol, À.; Xie, J.; Kleij, A. W. *Angew. Chem. Int. Ed*. **2018**, *57*, 13735-13747.
[30] (a) Geyer, R.; Jambeck, J. R.; Law, K. L. *Sci. Adv.* **2017**, *3*, e1700782. For information on the "plastic soup" please refer to: https://www.plasticsoupfoundation.org/en/.
[31] (a) Liu, S.; Wang, X. *Curr. Opin. Green Sust. Chem.* **2017**, *3*, 61-66. (b) Arai, R.; Seto, K.; Bell, A.; Sugimoto, H. *Polym. J.* **2018**, *50*, 301–307.
[32] Ghasemlou, M.; Daver, F.; Ivanova, E.; Adhikari, B. *Eur. Polym. J.* **2019**, *118*, 668-684. (b) Chen, Z.; Hadjichristidis, N.; Feng, X.; Gnanou, Y. *Macromolecules* **2017**, *50*, 2320–2328. (c) Fleischer, M.; Blattmann, H.; Mülhaupt, R. *Green Chem*. **2013**, *15*, 934–942.
[33] Nuyken, O.; Pask, S. D. *Polymers*. **2013**, *5*, 361–403.

giving rise to the formation of NIPUs (Figure 1.5b).[23] In particular, the reactivity of 5MCCs towards ring-opening by suitable (poly)amines is well-documented.[34]

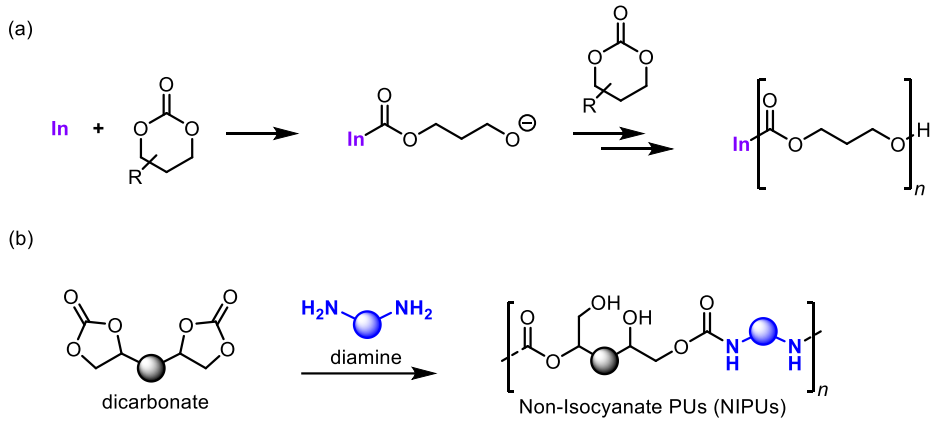

Figure 1.5. (a) PC synthesis from CCs via ROP. (b) NIPU production from the polyaddition between dicarbonates and diamines.

1.4. Thesis outline and objectives

Taking into account our group expertise surrounding the non-reductive and catalytic transformation of CO_2 and the absolute need to develop more sustainable ways to access polymers, this thesis has as the main focus ***the development of new CO_2-based transformations that provide access to structurally versatile cyclic carbonates for potential use in polymer science***. Connected to this main objective, this thesis will devote particular attention to: (**1**) the synthesis of new functional and structurally modular CC monomers, (**2**) investigation of novel larger-ring cyclic carbonates and their potential as monomers in ROP processes and (**3**) the study of the relationship between the nature and substitution pattern of these monomers on their "polymerizability" and the influence on the resultant polymer properties.

In **Chapter 2**, a bicyclic epoxy alcohol substrate is presented that allows the preparation of different stereo- and regio-isomeric bicyclic carbonates. Empirical data is presented showing that the nature of the catalyst has a crucial role in controlling the chemo-selectivity and a

[34] (a) Guo, W.; González-Fabra, J.; Bandeira, N. A. G.; Bo, C.; Kleij, A. W. *Angew. Chem. Int. Ed*. **2015**, *54*, 11686-11690. (b) Blain, M.; Jean-Gérard, L.; Auvergne, R.; Benazet, D.; Caillol, S.; Andrioletti, B. *Green Chem*. **2014**, *16*, 4286–4291.

combination of spectroscopic and structural analyses revealed the formation and identification of two unusual *trans*-configured bicyclic carbonates. The formation of some of these carbonate products is rationalized on the basis of computational data and control experiments.

Chapter 3 discloses a novel route towards 6MCCs using a photocatalytic approach that permits access a range of novel larger-ring carbonates from γ-mono and γ-disubstituted *O*-protected allylic alcohols in moderate to appreciable yields. ROP studies performed with a selection of these 6MCCs demonstrates that the substitution pattern and stereoelectronic nature of the substituents strongly influences the potential of these carbonates to serve as ROP monomers. A small collection of poly(carbonates) were prepared and a clear dependence between the thermal properties and the monomer substitution was noted.

In the final part of this thesis, **Chapter 4**, a new terpene based dicarbonate is presented that can be produced from the natural compound β-elemene. The synthesis of this β-elemene dicarbonate can be easily scaled up to multi-gram quantities which permitted its use as a ditopic monomer upon combination with commercially relevant diamines to give access to novel NIPU structures. The thermal and physical properties of these (oligomeric) NIPUs were investigated (in collaboration with BASF Coatings GmbH) to assess the suitability of β-elemene dicarbonate and related derivatives to serve as bio-monomers in future coating applications.

Chapter 2

Stereodivergent Synthesis of Bicyclic Hydroxycarbonates

The results described in this chapter have been published in:

Maquilón, C.; Limburg, B.; Laserna, V.; Gray-Ruiz, D.; González-Fabra, J.; Bo, C.; Martínez Belmonte, M.; Escudero-Adán, E. C.; Kleij, A. W. *Organometallics* **2020**, *39*, 1642–1651

UNIVERSITAT ROVIRA I VIRGILI
NEW AND FUNCTIONAL CYCLIC CARBONATES FOR POLYMER APPLICATIONS
Cristina Maquilón Albaladejo

2.1. Introduction

Carbon dioxide is a readily available carbon feedstock with potential to become an alternative for some fossil fuel based chemistry.[1,2,3] The use of carbon dioxide in organic synthesis has had a major impact on the discovery of new transformations.[4,5,6] Moreover, catalytic conversion of this C_1 building block has shown an upsurge of more challenging enantioselective and stereodivergent transformations.[7,8,9,10] Within the area of nonreductive CO_2 transformations, the field of cyclic carbonate synthesis has witnessed a spectacular growth over the past decade.[11] Yet, the diastereoselective formation of cyclic organic carbonates remains underdeveloped.[12]

One of the most popular approaches towards the formation of cyclic carbonates is the [3+2] cycloaddition reaction of CO_2 with epoxides.,[13] which typically involves a double S_N2 pathway and implies retention of the configuration of the starting material.[14] The reaction starts with epoxide ring opening induced by the catalyst (typically including a co-catalytic nucleophile such as a halide), followed by CO_2 activation by a metal-alkoxide intermediate and finally a cyclization step in which the cyclic carbonate product is released (Figure 2.1a) while regenerating the catalyst for subsequent turnover. Being among the most effective catalytic systems for this type of cycloaddition reaction, our group has focused on [3+2] cycloaddition reaction using aluminum triphenolate complexes combined with a nucleophilic cocatalyst, the latter usually being an ammonium halide salt (Figure 2.1b). These Al(III) complexes have found

[1] Liu, Q.; Wu, L.; Jackstell, R.; Beller, M. *Nat. Commun*. **2015**, *6*, 5933.
[2] Rajjak Shaikh, R.; Pornpraprom, S.; D'Elia, V. *ACS Catal*. **2018**, *8*, 419-450.
[3] Wei, J.; Ge, Q.; Yao, R.; Wen, Z.; Fang, C.; Guo, L.; Xu, H.; Sun, J. *Nat. Commun*. **2017**, *8*, 15174.
[4] Song, Q.-W.; Zhou, Z.-H.; He, L.-N. *Green Chem*. **2017**, *19*, 3707-3728.
[5] Gui, Y.-Y.; Zhou, W.-J.; Ye, J.-H.; Yu, D.-G. *ChemSusChem* **2017**, *10*, 1337-1340.
[6] Maeda, C.; Miyazaki, Y.; Ema, T. *Catal. Sci. Technol*. **2014**, *4*, 1482-1497.
[7] Sopeña, S.; Cozzolino, M.; Maquilón, C.; Martínez Belmonte, M.; Escudero-Adán, E. C.; Kleij, A. W. *Angew. Chem. Int. Ed*. **2018**, *57*, 11203-11207.
[8] Guo, W.; González-Fabra, J.; Bandeira, N. A. G.; Bo, C.; Kleij, A. W. *Angew. Chem. Int. Ed*. **2015**, *54*, 11686-11690.
[9] Ren, X.; Zheng, Z.; Zhang, L.; Wang, Z.; Xia, C.; Ding, K. *Angew. Chem., Int. Ed*. **2017**, *56*, 310-313.
[10] Ran, C.; Chen, X.; Gui, Y.; Liu, J.; Song, L.; Ren, K.; Yu, D. *Sci. China Chem.* **2020**, *63*, 1446-1351.
[11] Maeda, C.; Taniguchi, T.; Ogawa, K.; Ema, T. *Angew. Chem. Int. Ed.* **2015**, *54*, 134-138.
[12] Laserna, V.; Martin, E.; Escudero-Adán, E. C.; Kleij, A. W. *ACS Catal.* **2017**, *7*, 5478-5482.
[13] Guo, L.; Lamb, K. J.; North, M. *Green Chem.* **2021**, *23*, 77–118.
[14] Della Monica, F.; Kleij, A. W. *Catal. Sci. Technol.* **2020**, *10*, 3483–3501.

broad application in CO_2 valorization reactions[15,16] as well as in epoxide cycloaddition reactions.[17]

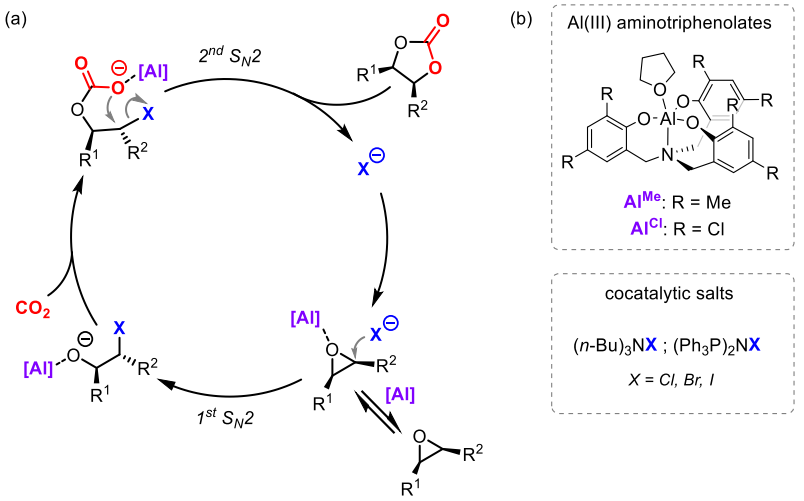

Figure 2.1. (a) Catalytic [3 + 2] cycloaddition mechanism via a double inversion pathway in the presence of a binary catalyst. (b) Binary catalytic systems based on Al(III) aminotriphenolate complexes [Al] and halide sources.

Recent work illustrated that specific (bifunctional) catalysts may affect the reaction pathway involving epoxy alcohols and CO_2 thereby leading to regio- and stereo-isomeric cyclic carbonate products.[18,19] In this regard, our group reported that when epoxy alcohols are used as substrates, alternative manifolds to the typical [3+2] cycloadditions operate. In this alternate scenario, the hydroxyl moiety is actively involved into the activation of CO_2 and affects the selectivity towards the formation of different cyclic carbonate isomeric products. This alternative pathway has been denoted as "substrate-controlled".[12,20]

[15] Laserna, V.; Fiorani, G.; Whiteoak, C. J.; Martin, E.; Escudero-Adán, E.; Kleij, A. W. *Angew. Chem. Int. Ed.* **2014**, *53*, 10416-10419.
[16] Carmen Martín, Arjan W. Kleij *Macromolecules* **2016**, *49*, 6285-6295.
[17] Rintjema, J.; Kleij, A. W. *ChemSusChem* **2017**, *10*, 1274-1282.
[18] Castro-Osma, J. A.; North, M.; Offermans, W. K.; Leitner, W.; Müller, T. E. *ChemSusChem* **2016**, *9*, 791-794.
[19] Huang, R.; Rintjema, J.; González-Fabra, J.; Martín, E.; Escudero-Adán, E. C.; Bo, C.; Urakawa, A.; Kleij, A. W. *Nat. Catal*. **2019**, *2*, 62-70.
[12] Laserna, V.; Martin, E.; Escudero-Adán, E. C.; Kleij, A. W. *ACS Catal.* **2017**, *7*, 5478-5482.
[20] Rintjema, J.; Epping, R.; Fiorani, G.; Martín, E.; Escudero-Adán, E. C.; Kleij, A. W. *Angew. Chem. Int. Ed*. **2016**, *55*, 3972-3976.

The reaction between *cyclic* epoxy alcohols and CO_2 leads to the formation of bicyclic hydroxycarbonates with different stereoconfigurations. The relative configuration of the hydroxyl group and the cyclic carbonate is either *syn* or *anti*, whereas the stereochemistry of the carbonate ring itself is either *cis* or *trans* (Figure 2.2.). During a previous study we observed the formation of rare (*syn/anti*) *trans*-configured bicyclic carbonates. *Trans*-carbonates are potentially useful precursors for the synthesis of polycarbonates, this due to their lower thermodynamic stability in comparison to their corresponding *cis*-configured analogues. These bicyclic hydroxycarbonates may also be used as synthons for stereodefined 1,2,3-triols and act as synthetic precursors for more complex organic molecules.[12]

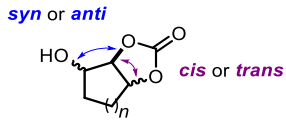

Figure 2.2. *Syn*/*anti* and *cis*/*trans* designations in bicyclic hydroxycarbonates.

The structure of these carbocycles (such as illustrates in Figure 2.2) fortunately does not give rise to any regioisomers as no symmetry-breaking element is present. Instead, we envisioned that the introduction of a double bond in the backbone of the epoxy alcohol substrate would create an opportunity to study the potential formation and identification of such regioisomers. Following the conventional [3 + 2] cycloaddition path (see Figure 2.4), a type A regioisomer would be produced. This isomer contains the carbonate ring attached to the same ring carbons as the original epoxide. Alternatively, when the alcohol group is involved in the carbonate formation, the generation of a type B regioisomer via a substrate-controlled process would be favored, incorporating in this case the initial hydroxyl group in the cyclic carbonate moiety (Figure 2.4).

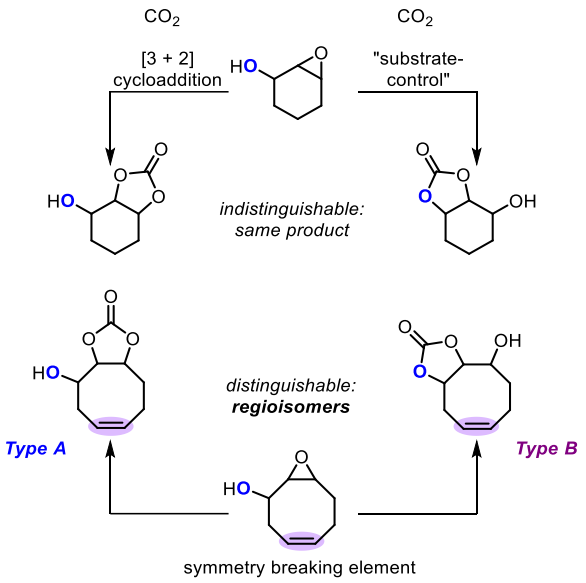

Figure 2.3. Possible formation of regioisomeric bicyclic carbonates through [3+2] cycloaddition or a substrate-controlled pathway.

The formation of cyclic organic carbonates under high stereo- and regiocontrol remains highly attractive for new synthetic applications. We observed within the development of the project described in this chapter that different combination of catalysts and reaction conditions led selectively to different isomeric bicyclic carbonate products. Interestingly, we were able to access two unexpected carbonate products different from those produced using standard binary catalysis.

In order to set up our studies, we selected an eight membered bicyclic epoxy alcohol substrate because of the commercially availability and accessibility of its precursors. Furthermore, the flexibility of an eight-membered ring should facilitate the formation of typically more strained and challenging to synthesize *trans*-configured carbonates. Theoretically, up to eight possible isomeric products can be formed from a single starting material as shown in Figure 2.5. Three out of these eight isomers have been prepared selectively, and additionally two other minor isomers have also been identified.

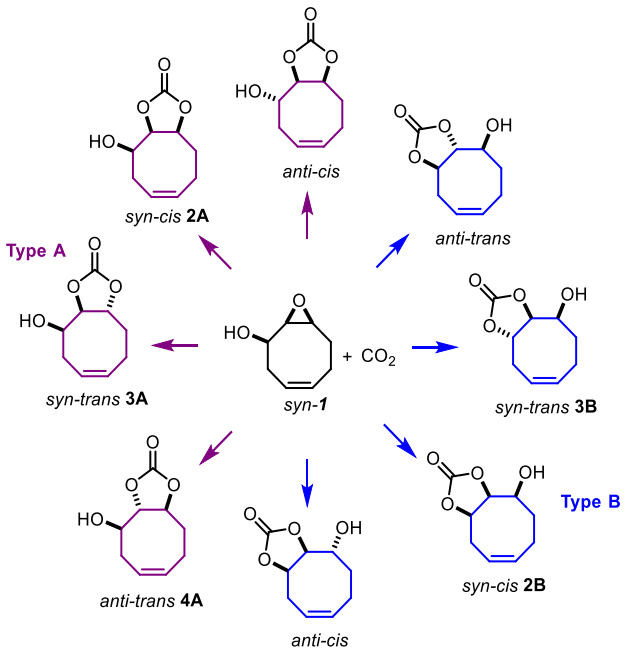

Figure 2. 4. Possible stereo- and regio-isomers obtained from a single cyclooctene epoxyalcohol through either traditional [3+2] cycloaddition or a substrate-controlled catalysis.

The results described in this chapter provide a stepping stone towards the design of stereocontrolled manifolds in which the use of carbon dioxide and more complex cyclic carbonate can be merged productively.

2.2 Results and Discussion

Three different types of high pressure systems were used (Figure 2.6) to carry out the experiments reported in this chapter. First, a HEL multireactor system allowed us to perform several tests under similar pressure and temperature conditions in small scale, whereas an AMTEC multireactor provided further control over individual reactor temperatures and pressures while using larger scale preparations. Thirdly, standard stainless steel autoclave reactors allowed us to monitor the temperature and pressure of the reaction, and also to scale up pre-optimized protocols.

Figure 2.5. High pressure reactor systems used to achieve the results of this chapter: a HEL (left), AMTEC (middle), and standard autoclave high pressure reactor system (right).

Tetrabutylammonium bromide-catalyzed synthesis of hydroxycarbonate 2B

It is well known that (ammonium) halides can catalyze the [3+2] cycloaddition of epoxides with CO_2. Typically, a double S_N2 pathway (see Figure 2.1a) would produce cyclic carbonates while retaining the original stereoconfiguration of the starting materials. The simplicity of this catalytic system prompted us to first investigate the conversion of epoxy alcohol *syn*-**1** into the corresponding bicyclic carbonates using various halide sources (Table 2.1, next page). Based on previous work carried out in our group, the initial reaction conditions were set up at 80 ºC, 40 bar of CO_2 pressure and using methyl ethyl ketone (MEK, butanone) as solvent. The first screening experiments were performed in a HEL pressure multireactor with tetrabutylammonium bromide (TBAB) as the halide source and first scrutinizing the catalyst loading (Table 2.1). The reaction promoted by TBAB at a 1 mol% loading gave only a 20% of *syn*-**1** conversion leading to a mixture of two carbonates in a 4:1 ratio (Entry 1). A gradual increase of the TBAB loading revealed eventually that full conversion was achieved using 25 mol%, improving concomitantly the selectivity towards the major product (Entries 2-5). Under these conditions, we were able to unambiguously identify both isomers. *Syn-cis* **2B** isomer was the major product formed in 92%

selectivity with 8% of the minor carbonate formed being *syn-cis* **2A**. Both identifications were supported by various 1D/2D NMR techniques, and crystallographic measurements (*vide infra*).

Table 2.1. Screening of the TBAB loading for the coupling of epoxy alcohol *syn*-**1** and CO_2.[a]

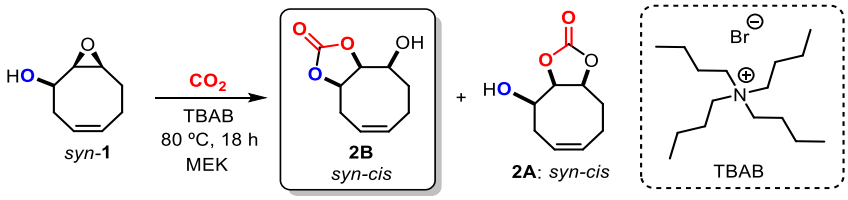

Entry	TBAB (mol%)	Conversion *syn*-**1** (%)[b]	Selectivity **2B**:**2A** (%)[b]
1	1	20	80:20
2	10	85	88:12
3	15	85	89:11
4	20	90	87:13
5	25	>99	92:8

[a]Reaction conditions: 80 ºC, 40 bar CO_2, 18 h, substrate *syn*-**1** (0.50 mmol, 70 mg, 2.5 M), MEK = methyl ethyl ketone. [b]Based on ^{1}H NMR integration of the crude product taking only the starting material and carbonate products into account.

Further screening showed that the nature of the counterion did not result in a significant improvement of the selectivity for the synthesis of **2B** (Table 2.2, Entries 2-4). Also, other halide sources were tested showing similar outcome, suggesting that the chemo-selectivity does not depend on the type of nucleophilic catalyst (Entries 5-9). As expected, low conversions were observed when catalysts with poor solubility in the reaction mixture were used (Entries 4, 8-9).

Table 2.2. Screening of halide sources in the synthesis of carbonate **2B**.[a]

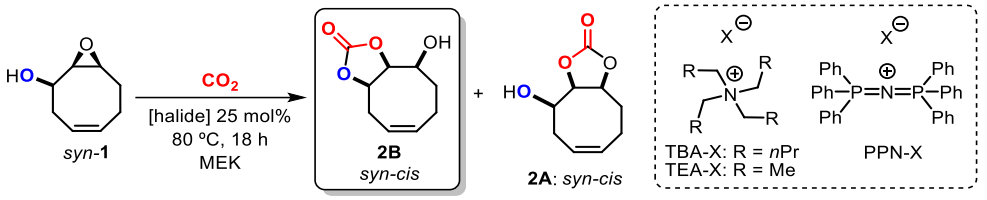

Entry	Catalyst (mol%)	Conversion *syn*-**1** (%)[b]	Selectivity **2B**:**2A** (%)[b]
1	TBAB	>99	92:8
2	PPNBr	>99	88:12
3	TEAB	>99	91:9
4	NaBr[c]	40	87:13
5	TEAI	>99	88:12
6	PPNI	>99	89:11
7	TBAI	>99	88:12
8	PPNCl[c]	79	93:7
9	TBACl[c]	56	93:7

[a]Reaction conditions: 80 ºC, 40 bar CO_2, 18 h, substrate *syn*-**1** (0.50 mmol, 70 mg, 2.5 M), catalyst 25 mol%, MEK = methyl ethyl ketone. [b]Based on ^{1}H NMR integration of the crude product taking only the starting material and carbonate products into account. [c]The reaction mixture was heterogeneous.

Next, we moved towards the screening of various solvents for this transformation (Table 2.3, next page). Among the solvents screened, the use of dimethyl sulfoxide (DMSO) and dimethylformamide (DMF) gave lower conversion of the *syn*-**1** epoxide accompanied by a lower selectivity towards **2B** (Entries 2-3). The utilization of diethoxyethane (DEE) showed a slightly lower substrate conversion but provided good product selectivity (entry 4). Finally, by using acetonitrile (ACN) and toluene (TOL) (Entries 5-6), full conversion of *syn*-**1** was accomplished but with rather similar results to the ones obtained with MEK. Thus, MEK was finally selected as the solvent for further studies.

Table 2.3. Solvent optimization for the synthesis of carbonates **2B** and **2A**.[a]

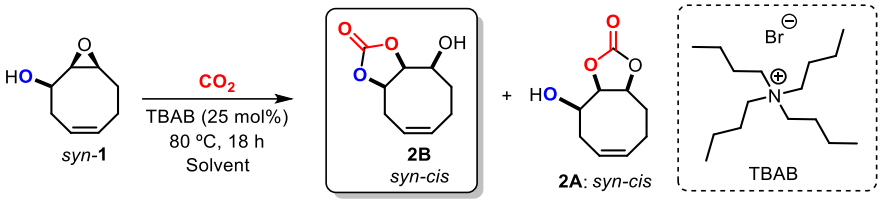

Entry	Solvent	Conversion *syn*-**1** (%)[b]	Selectivity **2B**:**2A** (%)[b]
1	MEK	>99	92:2
2	DMSO	68	66:34
3	DMF	87	78:22
4	DEE	97	91:9
5	ACN	>99	88:12
6	TOL	>99	93:7

[a]Reaction conditions: 80 ºC, 40 bar CO_2, 18 h, substrate *syn*-**1** (0.50 mmol, 70 mg, 2.5 M), MEK = methyl ethyl ketone. DEE stands for diethoxyethane. [b]Based on ^{1}H NMR integration of the crude product taking only the starting material and carbonate products into account.

Then, in an AMTEC multireactor, the influence of the CO_2 pressure was evaluated. During this part of the study, lower conversions of *syn*-**1** were detected probably due to the different type of reactor (cf., CO_2 solubilization, different volume-to-area ratio) used, but we could observe that the pressure did not have a significant impact on the selectivity of the reaction, with a selectivity of 88% to 92% towards **2B** using a 10 bar up to 40 bar CO_2 pressure, respectively (Table 2.4, next page).

Table 2.4. Screening of the CO_2 pressure in an AMTEC multireactor system.[a]

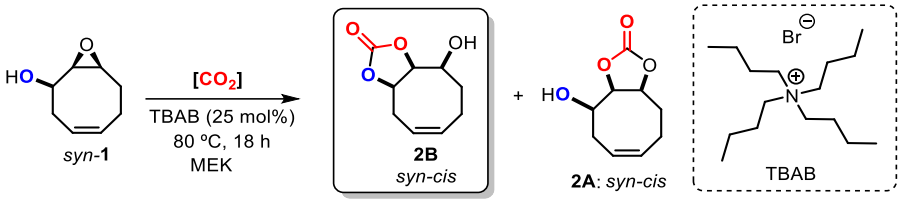

Entry	$[CO_2]^0$ (bar)	Conversion *syn*-**1** (%)[b]	Selectivity **2B**:**2A** (%)[b]
1	40	48	92:8
2	30	52	90:10
3	20	54	87:13
4	10	56	88:12

[a]Reaction conditions: 80 ºC, 18 h, substrate *syn*-**1** (0.50 mmol, 70 mg, 2.5 M), MEK = methyl ethyl ketone. [b]Based on ^{1}H NMR integration of the crude product taking only the starting material and carbonate products into account.

Finally, to further optimize the yield of **2B**, a screening of reaction temperatures between 60 ºC and 80 ºC was carried out at 1 mmol scale in an autoclave system (Table 2.5). The results revealed that the preparation of **2B** is best performed at 80 ºC reaching full conversion of *syn*-**1** and with a 65% isolated yield of the product.

Table 2.5. Optimization of the isolated yield of *syn-cis* cyclic carbonate **2B**.[a]

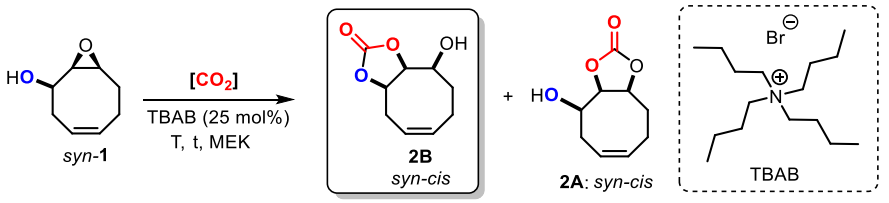

Entry	T (ºC)	t (h)	Conversion *syn*-**1** (%)[b]	Selectivity **2B**:**2A** (%)[b]	Yield **2B** (%)[b]
1	60	84	78	90:10	53
2	70	48	80	90:10	65
3	80	48	99	90:10	76 (65)[c]

[a]Reaction conditions: temperature indicated, 40 bar CO_2, *syn*-**1** (1.0 mmol, 140 mg, 1.0 M), TBAB (82 mg), MEK. [b]Based on ^{1}H NMR integration of the crude product using 1,3,5-trimethoxy-benzene as internal standard. [c]Isolated yield in brackets.

The pure isolated isomers **2B** and **2A** could be crystallized and analyzed by X-ray crystallography. The X-ray diffraction studies revealed that two regioisomeric cyclic carbonates (Figure 2.6) had been formed under the optimized conditions. Both carbonates clearly show a

syn-cis stereoconfiguration. The minor carbonate product **2A** corresponds to a type A isomer, where the carbonate ring is attached to the same carbon centers as the initial epoxide. This is the expected product for a typical double S_N2 pathway in a formal [3 + 2] cycloaddition of epoxides with CO_2. The major, unexpected isomer **2B** has the initial hydroxyl group incorporated in the carbonate ring of the bicyclic structure.

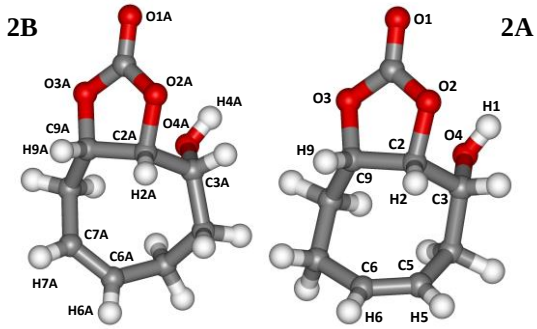

Figure 2.6. LEFT: X-ray molecular structure determined for *syn-cis* **2B** (major isomer). Some selected pertinent bond lengths (Å) and dihedral angles (º) with esd´s in parentheses: C(6A)-C(7A) = 1.3323(8); O(2A)-C(2A)-C(9A)-O(3A) = 27.20(5), O(2A)-C(2A)-C(3A)-O(4A) = -70.22(5). RIGHT: X-ray molecular structure determined for *syn-cis* **2A** (minor isomer). Some selected pertinent bond lengths (Å) and dihedral angles (º) with esd´s in parentheses: C(5)-C(6) = 1.3324(17), O(2)-C(2)-C(9)-O(3) = 22.49(9), O(2)-C(2)-C(3)-O(4) = -54.62(11).

Contrary to what would be anticipated from a standard double inversion pathway, the major isomer turned out to be *syn-cis* **2B**. This observation prompted us to consider the involvement of a free alcohol group directing the outcome of the reaction, and the formation of **2B** might thus be the result of an unknown manifold. Based on the retention of the initial stereoconfiguration, with all the ring substituents residing at the same face of the molecule, an overall double inversion process should be an integral part of this new manifold. In order to shed light on the formation of the major regioisomer **2B**, density functional theory (DFT) based calculations were performed. Both the α and the β attack of the bromide onto the epoxy alcohol were considered. Likewise, the concerted processes combining the epoxide ring opening and subsequent linear carbonate formation were also computed (Figure 2.8).

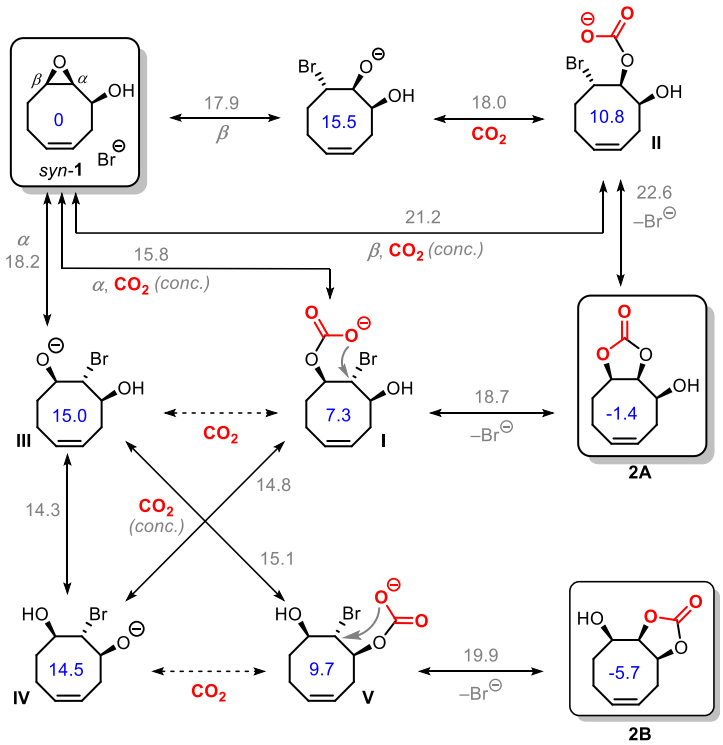

Figure 2.7. DFT computed pathways for the formation of **2A** and **2B.** All energies are relative to the energy of *syn*-**1** and in kcal/mol. Note that the value in ***blue*** refer to the free energies of the respective intermediates, whereas the ***grey*** numbers refer to the energies of the respective transition states.

The DFT studies revealed that the stepwise formation of *syn-cis* **2A** via an *α* attack showed a significant lower energetic span (ΔG relative to *syn*-**1**) if compared with the ring opening through the *β* position, 18.7 kcal/mol versus 22.6 kcal/mol respectively. When the concerted pathways to the linear carbonate intermediates **I** and **II** were studied, we found that, comparing with the stepwise manifold, the *β* attack entailed a higher ΔG value, while the pathway from an *α* attack is even more favored. Therefore, the formation of isomer **2A** is suggested to happen through initial *α* attack. The calculated energies indicated that all reaction steps should be reversible under the experimental conditions of 80 ºC and 40 bar CO_2 pressure. Since the synthesis of carbonate **2B** is not possible through a mechanism involving *β* attack, other possible pathways from the *α* epoxide ring opening were explored. Alkoxide **III** can isomerize through an intramolecular proton transfer from the alcohol unit to intermediate **IV**. This new alkoxide can produce via CO_2 activation a linear carbonate **V** that upon cyclization would lead to isomer **2B**. The manifold via *α* attack accounts for the formation of both carbonate isomers **2A** and **2B**.

Noteworthy, the substantial difference in the free energy of both products, -1.4 kcal/mol and -5.7 kcal/mol for **2A** and **2B** respectively, indicates that the expected thermodynamic product would be carbonate **2B**. Thus, these DFT results align well with the experimental major formation of **2B** isomer since thermodynamics are controlling the final product ratio. To complete this study, kinetic modeling was performed simulating experimental reaction conditions. The results fitted well with the experimental observation, predicting a 95% selectivity for **2B** compared with a 92% selectivity observed at 25 mol% TBAB (for further information see the Experimental Section, Figure 2.27)

Al^{Cl} catalyzed formation of *syn-trans* hydroxycarbonate 3B

The use of halide-based catalysts has shown an unexpected reactivity between epoxy alcohol *syn*-**1** and CO_2. This result prompted us to consider other potential catalytic systems that could affect the outcome of this coupling reaction. The use of Aluminum aminotriphenolate complexes have been vastly explored in our group, and they have been frequently used in various CO_2 valorization reactions. These Al(III) complexes have proven to be powerful Lewis acids promoting different transformations involving epoxides/oxetanes (ring opening polymerization and cyclic carbonate/carbamate synthesis, among other transformations). One advantage of these complexes is the possibility of fine-tuning the Lewis acidity and steric/electronic features by changing the substituents on the aromatic ring of the aminotriphenolate ligand. Thus, in addition to the results discussed so far, we decided to examine the effect of the additional use of these Aluminum complexes on the transformation of *syn*-**1** in presence of CO_2.

The Al^{Me} and Al^{Cl} complexes were employed in combination with TBAB (Table 2.6, next page) as binary catalysts. Initially, using a [Al] loading of 1 mol% and a 1:1 ratio of Al^{Me}:TBAB, full conversion of the substrate *syn*-**1** was observed producing a mixture of cyclic carbonate products (Entry 1). Out of the mixture, four major isomers were identified as *syn-cis* **2B**, *syn-trans* **3A**, *syn-trans* **3B** and *anti-trans* **4A**. Whereas **2B** had already been fully characterized, the crystallization of two other products, **3B** and **4A**, allowed us to assign the molecular connectivities and the stereoconfiguration by X-ray diffraction (Figure 2.9). Both carbonate structures show a *trans* configured cyclic carbonate. While **3B** has the hydroxyl group in a *syn* position with respect to the carbonate ring, **4A** has an *anti* configuration between the same fragments. The fourth product, produced in minor amounts, was assigned by 1D/2D NMR as the last remaining possible *syn* isomer **3A** (see Experimental Section 2.4). In the presence of an aluminum catalyst, the pathway previously described using exclusively TBAB for the formation

of minor isomer **2A** by formal [3 + 2] cycloaddition, was under these experimental conditions slow enough to be neglected.

Table 2.6. Conversion of *syn*-**1** in the presence of Al(III) complex Al^{Me} or Al^{Cl} combined with TBAB.[a]

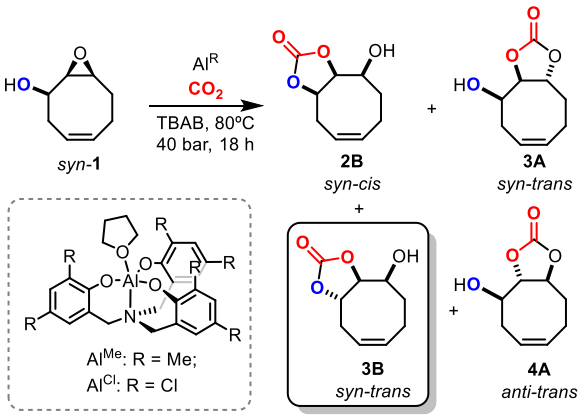

Entry	[Al] (mol%)	TBAB (mol%)	Selectivity **2B**:**3A**:**3B**:**4A** (%)[b]	Yield **3B** (%)[b]
1	Al^{Me} (1.0)	1.0	16:22:34:28	n.d.
2	Al^{Me} (1.0)	10	27:17:38:18	n.d.
3	Al^{Cl} (1.0)	2.5	0:15:74:11	n.d.
4	Al^{Cl} (1.0)	1.0	0:6:81:16	n.d.
5	Al^{Cl} (5.0)	5.0	4:6:90:0	n.d.
6	Al^{Cl} (7.5)	7.5	2:9:89:0	n.d.
7	Al^{Cl} (10)	10	3:6:91:0	n.d.
8[c]	Al^{Cl} (5.0)	5.0	7:13:80:0	42 (29)[d]
9[c,e]	Al^{Cl} (5.0)	5.0	2:6:92:0	33[g]
10[c,f]	Al^{Cl} (5.0)	5.0	0:7:93:0	16[g]

[a]Reaction conditions: 18 h, 80 ºC, 40 bar CO_2, *syn*-**1** (0.5 mmol, 70 mg, 2.5 M), TBAB (16 mg, 5.0 mol%), MEK. Substrate conversion was >99% in all cases. [b]Based on ^{1}H NMR integration of the crude product; numbers refer to conversion into carbonates. [c]Reactions were carried out in an autoclave equipped with a 20 mL Teflon insert, using *syn*-**1** (1.0 mmol, 140 mg, 1.0 M) and Al^{Cl}/TBAB (5.0 mol% each), 80 ºC, 40 bar, 24 h. [d]In brackets, the isolated yield of *syn-trans* **3B** after column purification. [e]Temperature: 70 ºC. [f]Pressure: 10 bar CO_2. [g]A different unidentified product is produced in large amounts. n.d. = not determined.

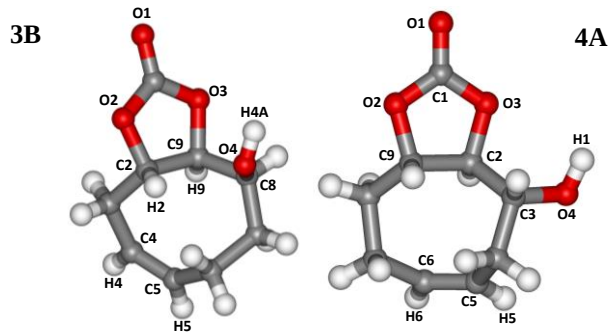

Figure 2.8. LEFT: X-ray molecular structure determined for *syn-trans* **3B**. Some selected pertinent bond lengths (Å) and dihedral angles (º) with esd´s in parentheses: C(4)-C(5) = 1.3384(15); O(2)-C(9)-C(2)-O(3) = 4.07(9), O(3)-C(9)-C(8)-O(4) = 71.02(9). RIGHT: X-ray molecular structure determined for *anti-trans* **4A**. Some selected pertinent bond lengths (Å) and dihedral angles (º) with esd´s in parentheses: C(5)-C(6) = 1.329(2), O(2)-C(9)-C(2)-O(3) = 15.56(12), O(3)-C(2)-C(3)-O(4) = -66.30(14).

Once the carbonate products **3B** and **4A** had been identified, a further screening of the reaction parameters was performed with the aim to find conditions to prepare either of these carbonate products with improved selectivity. We observed that by increasing the Al^{Me}:TBAB ratio from 1:1 to 1:10 and using a 10 mol% loading of TBAB, a slightly higher selectivity towards **2B** was observed (Entry 2). Based on previous results using TBAB, we expected that the employment of a higher TBAB:Al^{R} ratio would favor the formation of **2B** isomer. Interestingly, the higher Lewis acidity of Al^{Cl} compared to Al^{Me} showed a positive effect in the selectivity of the reaction. Next, a 1:1 Al^{Cl}:TBAB ratio was scrutinized at loadings of each component ranging from 1mol% to 10 mol% (Entries 4-7). At a loading of 1 mol%, an 81% carbonate selectivity was found towards *syn-trans* **3B** over the other carbonate isomers, this value being much higher than the 34% obtained when using Al^{Me} (Entry 4 vs 1). The higher Lewis acidity of catalyst Al^{Cl} is likely responsible for the suppression of the formation of **2B**. To our delight, **3B** was provided in a 90% selectivity at 5 mol% catalyst loading (Al^{Cl}:TBAB = 1:1, Entry 5). A further increase in the amount of catalyst loading did not result in selectivity improvement (Entries 6-7), while the inhibition of the formation of **4A** was in generally noted. In line with previous results, increasing the ratio of TBAB:Al^{Cl} to 2.5:1 slightly lowered the selectivity for **3B** compared to a ratio of 1:1 at 1 mol% loading of both components (Entry 3 vs 4).

With the best catalytic system for selective formation of **3B** in hand (Entry 5), we then further optimized the yield in an autoclave reactor at larger scale (Entries 8-10). Using the optimized conditions, the product was obtained with a slightly lower selectivity (80%) and a

42% NMR yield (with an overall 55% carbonate yield, Entry 8). Lowering the temperature and pressure of the reaction led to lower yields of **3B** (Entries 9-10). Finally, isomer **3B** was isolated in 29% yield after column chromatography. Due to the similar R_f values of the various carbonate products, further improvement of the isolated yield was not feasible. Note that significant amounts of unidentified products were produced.

In order to explain the modest yields obtained for **3B** compared with previous isomer *syn-cis* **2B**, control experiments were performed. First, to check the stability of substrate *syn*-**1**, a solution thereof in MEK was heated up at 80 ºC in the presence of internal standard 1,3,5-trimethoxybenzene. ^{1}H NMR showed no degradation of the substrate after 18 h pointing at a high stability of the starting material at elevated temperature. In contrast, when the same experiment was repeated adding 5 mol% of Al^{Cl}, a gradual decrease in the concentration of the substrate with time was noted. The progress of the experiment followed by ^{1}H NMR showed that only 33% of the substrate was remaining after 18 h and only traces could be detected after 3 days. Since other decomposition products were not observed, the latter experiment was carried out in d_8-toluene as solvent. The same decomposition trend was observed for *syn*-**1** (though slower) with 60% of the substrate left after 18 h. A significant amount of material precipitated out from the solution. Both the solution and the precipitated solid were measured by ^{1}H NMR and IR showing virtually identical results. Whereas the NMR spectra displayed broadened signals, the IR spectrum pointed at the formation of an oligo-/polyether compound. It appears that at elevated temperature, strong Lewis acids are able to induce ring opening of the epoxide.

Recently, we described that similar Al(III) aminotriphenolate complexes can activate epoxy alcohols following proton transfer to one of the phenolate donor atoms of the complex providing an Al-alkoxide species. In absence of any reagent, this nucleophilic alkoxide should be able to promote the ring opening of second epoxy alcohol molecule, leading eventually to the formation of an oligoether. This side-reactivity was recently reported by Fiorani *et al.* in the synthesis of terpene-based cyclic carbonates under fairly similar reaction conditions (85 ºC, 10-40 bar; using 1 mol% of Al^{Cl}).[21] These data suggest that the instability of the staring material in the reaction condition and the generally long reaction time can contribute to the modest yields for this reaction.

[21] Fiorani, G.; Stuck, M.; Martín, C.; Martínez-Belmonte, M.; Martin, E.; Escudero-Adán, E. C.; Kleij, A. W. *ChemSusChem* **2016**, *9*, 1304-1311.

Al^{Me} catalyzed synthesis of hydroxycarbonate *anti-trans* 4A

As previously discussed, an increase of the TBAB concentration led to the suppression of isomer *anti-trans* **4A** (Table 2.6). Thus, we reasoned that omission of the halide additive would favor the formation of this *trans* configured cyclic carbonate.

However, it seems that the presence of a cocatalyst is required for the desired reaction to proceed, since only decomposition of starting material *syn*-**1** (polyether formation) was observed. Consequently, we decided to evaluate the nature of the cocatalyst replacing the halide sources for *N*-heterocyclic bases. Table 2.7 (see next page) gathers the results obtained during the test of several *N*-heterocyclic bases. Initially, the presence of 4-dimethylaminopyridine (DMAP) resulted into an 82% selectivity towards the desired carbonate isomer **4A** (Entries 1-2). Further variation of the catalytic system (i.e., changing the type of base and its relative amount, Entries 3-12) led eventually to full substrate conversion and 86% selectivity for **4A** (Entry 7). Interestingly, the use of DIPEA in the presence or absence of the Al(III) complex suppresses the formation of any carbonate product, indicating that relatively nucleophilic bases are required for the reaction to occur. Instead, rather low conversion of *syn*-**1** was observed, and unidentified byproducts were produced (Entries 10-11). In contrast, using DBU in the *absence* of Al complex led to a lower selectivity for **4A** and lower substrate conversion (Entry 12).

Table 2.7. Optimization of the reaction conditions leading to *anti-trans* carbonate **4A**.[a]

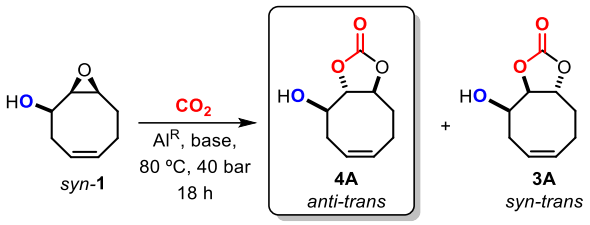

Entry	[Al] (mol%)	Base (mol%)	Selectivity **4A**:**3A** (%)[b]
1	Al^{Me}, 1.0	DMAP, 10	79:21
2	Al^{Me}, 5.0	DMAP, 20	82:18
3	Al^{Me}, 1.0	DBU, 10	79:21
4	Al^{Me}, 5.0	DBU, 5.0	76:24
5	Al^{Me}, 5.0	DBU, 15	82:18
6	Al^{Me}, 5.0	DBU, 20	85:15
7	Al^{Me}, 5.0	DBU, 25	86:14
8	Al^{Cl}, 5.0	DMAP, 5.0	84:16
9	Al^{Cl}, 5.0	DBU, 5.0	81:19
10	Al^{Cl}, 5.0	DIPEA, 5.0	0:0
11	-	DIPEA, 10	0:0
12	-	DBU, 10	61:39[c]

[a]Reaction conditions: 80 ºC, 40 bar CO_2, *syn*-**1** (0.5 mmol, 70 mg, 2.5 M), base (type and amount indicated), MEK. [b]Based on ^{1}H NMR integration of the crude product. Carbonates **2A**, **2B** and **3B** could not be detected. With the exception of entries 10, 11 and 12, the conversion was quantitative. [c]The conversion in this reaction was 52%. Abbreviations: DMAP = 4-dimethylaminopyridine, DBU = 1,8-diazabicyclo(5.4.0)undec-7-ene, DIPEA = diisopropylethylamine.

With the best conditions in hand, the yield for *anti-trans* **4A** was further maximized performing larger scale experiments in an autoclave reactor (Table 2.8). The observation of substantial amounts of oligoether byproducts prompted us to initially use lower reaction temperatures. However, the NMR yield of *anti-trans* **4A** was not positively affected and changing the pressure or the reaction time resulted in lower conversions of the substrate *syn*-**1** (Entries 1-3). Raising the reaction temperature to 80 ºC produced **4A** in 59% NMR yield (Entry 4). Further variations were probed, including lowering the loading of the catalytic system (Entries 3 and 6), eliminating the pre-purging step of the reactor prior to pressurizing at 40 bar with the aim to reduce possible loss of the volatile *syn*-**1** (Entry 7), and changing the solvent (Entry 8). Increasing the reaction time to 48 h using the conditions of Entry 4 led to similar results, evidencing the stable character of the carbonate products under experimental conditions.

From the crude product the desired *anti-trans* **4A** was isolated in 25% yield with a 57% NMR yield (Entry 9). It is noteworthy to highlight that the isolation and characterization of *trans*-fused cyclic carbonates is difficult and rare, and only few examples have been reported in literature.[12,22,23]

Table 2. 8. Optimization of the yield of *anti-trans* carbonate **4A** obtained from *syn*-**1**.[a]

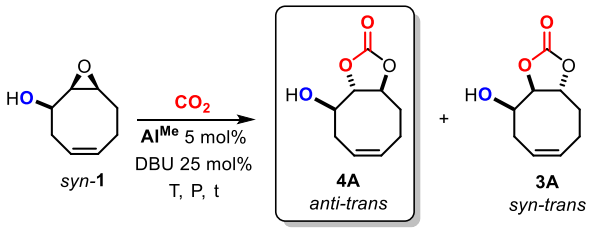

Entry	T/P (ºC/bar)	t (h)	Conversion *syn*-**1**(%)[b]	4A (%)[b]	3A (%)[b]	Rest (%)[c]
1	70/40	24	>99	49	17	34
2	70/10	24	79	47	19	13
3[e]	70/40	18	89	45	22	22
4	80/40	24	>99	59	14	27
5	80/10	24	94	47	14	33
6[e]	80/40	24	>99	44	14	42
7[f]	80/40	24	>99	54	14	32
8[g]	80/40	24	>99	40	13	47
9	80/40	48	>99	57 (25)[d]	18	25

[a]Reaction conditions: autoclave reactors were used equipped with a 20 mL Teflon insert; temperature/pressure indicated, *syn*-**1** (1.0 mmol, 140 mg, 2.5 M), Al^{Me} (22 mg, 5 mol%), DBU (37 µL, 25 mol%), TMB (189.2 mg, 1 equiv), MEK. [b]Determined by ^{1}H NMR ($CDCl_3$) using TMB as internal standard. [c]Remaining mass balance of all unidentified products based on ^{1}H NMR ($CDCl_3$) analysis. [d]In brackets, the isolated yield for **4A** is reported. [e]Using 5.0 mol% DBU and 1.0 mol% Al^{Me}. [f]The reactor was not purged with CO_2 prior to the experiment. [g]Using toluene as solvent.

[22] McGuire, T. M.; López-Vidal, E. M.; Gregory, G. L.; Buchard, A. *J. CO₂ Util.* **2018**, *27*, 283-288.
[23] Gregory, G. L.; Jenisch, L. M.; Charles, B., Kociok-Köhn, G.; Buchard, A. *Macromolecules* **2016**, *49*, 7165-7169.

2.3. Conclusions

The results in this chapter clearly demonstrate that bicyclic epoxy alcohols open up new possibilities for the synthesis of carbonates with unusual stereo-configurations. However, the evaluation of bicyclic substrates with a symmetrical backbone do not allow to identify possible regio-isomerism. Therefore, in this work a detailed study towards the reactivity of a bicylic epoxy alcohol with a symmetry-breaking element (a double bond) was conducted, and its coupling with CO_2 examined. The latter feature greatly facilitates the analysis of the conversion of epoxy alcohol *syn*-**1** into various regio- and diastereoisomeric products through different manifolds. The use of bicyclic epoxy alcohol *syn*-**1** in this respect provides unexpected reactivity in several cases different from classical [3+2] cycloaddition chemistry. The new modus operandi permitted the formation of two rare *trans* configured carbonates and a *cis* configured one as major products, as well as, two other identified minor carbonates representing five out of a maximum of eight possible isomers that can be generated from a single epoxy alcohol substrate by modulating the reaction conditions and the nature of the (binary) catalyst. However, further exploration of these manifolds and a better mechanistic understanding are crucial factors to advance the selective synthesis of more complex carbonate structures under high stereo- and regiocontrol.

2.4. Experimental Section

General considerations

The Al complexes[24] Al^{Me} and Al^{Cl} and epoxy alcohol *syn*-**1**[25] were prepared according to previously reported procedures. Carbon dioxide was purchased from PRAXAIR and used without further purification. Solvents used in the synthesis of the complexes were dried using an Innovative Technology PURE SOLV solvent purification system. Solvents used in the catalytic screening were used as received. ^{1}H and ^{13}C and 2D NMR spectra were recorded on a Bruker AV-300, AV-400 or AV-500 spectrometer, and signals are referenced to the residual solvent peak. FT-IR measurements were carried out using a Bruker Optics FTIR Alpha spectrometer. Mass spectrometric analyses and X-ray diffraction analysis were performed by the Research Support Area (RSA) at ICIQ.

[24] Whiteoak, C. J.; Kielland, N.; Laserna, V.; Castro-Gómez, F.; Martin, E.; Escudero-Adán, E. C.; Bo, C.; Kleij, A. W. *Chem. - Eur. J.* **2014**, *20*, 2264−2275.
[25] Itoh, T.; Jitsukawa, K.; Kaneda, K.; Teranishi, S. *J. Am. Chem. Soc.* **1979,** *101*, 159−169.

General catalytic procedure using autoclave reactors

Typical conditions are as follows: epoxy alcohol *syn*-**1** (1.0 mmol, 140 mg, 1.0 M), TBAB (16-82 mg, 5-25 mol%) and Al complex Al^{Cl} (28 mg, 5.0 mol%), MEK (200 µL) and internal standard TMB (189.2 mg, 1 equiv) were charged into a stainless steel autoclave equipped with a 20 mL Teflon insert. After the autoclave was sealed three cycles of pressurization/depressurization were carried out. After reaching the selected reaction temperature (typically 80 ºC), the autoclave was pressurized with CO_2 to the desired pressure (typically 40 bar) and left stirring. At the end of the chosen time interval, the autoclave was cooled to rt and then carefully depressurized. An aliquot of the reaction mixture was taken for analysis and the conversion, selectivity and yield were determined by ^{1}H NMR spectroscopy in $CDCl_3$. The desired products were then obtained by chromatographic purification as indicated below.

General catalytic procedure using an autoclave-based HEL multi-reactor

A typical procedure is as follows: epoxy alcohol *syn*-**1** (70 mg, 0.50 mmol, 2.5 M), Al-complex Al^{Cl} (5.0 mol%), TBAB (5.0-25 mol%) and MEK (200 µL) were added into a glass insert. The HEL system was closed and after three pressurization/depressurization cycles using 10 bar of CO_2 the reactor was charged with 40 bar CO_2 pressure. Then the reactor was heated to the desired temperature and the mixtures were stirred for 18 h. Finally, the HEL reactor was cooled down to rt, carefully depressurized and opened. For each of the reaction mixtures an aliquot was taken and analyzed by ^{1}H NMR ($CDCl_3$) to determine conversions and selectivity.

General catalytic procedure using autoclave AMTEC multi-reactor

Typical set up is as follows: the TBAB (25 mol%) was weighed into a steel vessel, after which an overnight leak test was carried out at 30 bar. Then, epoxy alcohol *syn*-**1** (140 mg, 1 mmol) was dissolved in MEK (500 µL) and carefully added. The reactors were warmed up to 80 ºC and finally pressurized with CO_2 (10, 20, 30 and 40 bar). After the set reaction time the multi-reactor was cooled down and depressurized and an aliquot was taken and analyzed by ^{1}H NMR ($CDCl_3$) to determine the conversion and selectivity.

Synthesis of *syn-cis* cyclic carbonate 2B

A mixture of *syn*-epoxy alcohol *syn*-**1** (140 mg, 1.0 mmol) and TBAB (82 mg, 25 mol%) dissolved in 1.0 mL of MEK was introduced into a 30 mL stainless steel reactor. After three cycles of pressurization and depressurization, the reactor was charged with 40 bar of CO_2. Then

the reaction mixture was heated to 80 ºC and magnetically stirred for 24 h. Finally, the reactor was cooled down to rt and carefully depressurized. The crude product was purified by flash chromatography on silica gel (hexane:ethyl acetate, 2:1 v/v) affording the title compound (120 mg, 65% yield) as a white solid. Single crystals were obtained by recrystallization from CH_2Cl_2/hexane at room temperature. **^{1}H NMR** (400 MHz, CDCl3): δ = 5.94 (dtd, J = 10.3, 8.0, 1.0 Hz, 1H), 5.66 – 5.48 (m, 1H), 4.73 (ddd, J = 12.6, 7.3, 4.2 Hz, 1H), 4.52 (dd, J = 7.4, 1.2 Hz, 1H), 4.36 – 4.30 (m, 1H), 3.41 – 3.29 (m, 1H), 2.99 – 2.84 (m, 1H), 2.80 – 2.68 (m, 1H), 2.43 (ddd, J = 11.6, 6.6, 4.2 Hz, 1H), 2.16 – 2.05 (m, 1H), 1.96 – 1.86 (m, 1H), 1.59 – 1.46 (m, 1H) ppm. **^{13}C NMR** (126 MHz, CDCl3): δ = 155.8, 135.8, 123.8, 84.1, 80.0, 72.9, 33.8, 26.5, 19.7 ppm. **IR** (neat): ν = 3456 (OH), 1758 (C=O) cm^{-1}. **HRMS** (ESI+, MeOH): m/z calcd. for $[C_9H_{12}NaO_4]^+$, 207.0633; found, 207.0637.

Synthesis of *syn-trans* cyclic carbonate 3B

A mixture of *syn*-epoxy alcohol *syn*-**1** (140 mg, 1.0 mmol), Al catalyst Al^{Cl} (16 mg, 5.0 mol%) and TBAB (28 mg, 5.0 mol%) dissolved in MEK (1.0 mL) was introduced into a 30 mL stainless steel reactor. After three cycles of pressurization and depressurization, the reactor was charged with 40 bar of CO_2. Then the reaction mixture was heated to 80 ºC and magnetically stirred for 24 h. Finally, the reactor was cooled down to rt and carefully depressurized. Flash chromatography on silica gel (hexane:ethyl acetate, 2:1 v/v) afforded the title compound as a 91:9 mixture of *syn-trans* **3B** and a minor isomer (78 mg, 42% yield) as a white solid. Note that more extensive column purification was possible, but due to similar R_f values for the carbonate products only 29% of pure *syn-trans* **3B** was obtained. Recrystallization from CH_2Cl_2/hexane at room temperature afford single crystals. **^{1}H NMR** (400 MHz, CDCl3): δ = 5.75-5.64 (m, 1H), 5.54 (ddd, J = 11.8, 7.9, 5.7 Hz, 1H), 5.48-5.38 (m, 1H), 4.55 (dd, J = 7.9, 1.3 Hz, 1H), 4.30-4.21 (m, 1H), 3.06-2.85 (m, 1H), 2.50-2.31 (m, 1H), 2.23-2.12 (m, 1H), 2.10-1.93 (m, 2H), 1.65-1.51 (m, 1H) ppm. **^{13}C NMR** (126 MHz, CDCl3): δ = 154.6, 131.1, 123.6, 84.9, 74.1, 66.4, 34.1, 32.2, 20.3 ppm. **IR** (neat) ν = 3427 (OH), 1793 (C=O) cm^{-1}. **HRMS** (ESI+, MeOH): m/z calcd. for $[C_9H_{12}NaO_4]^+$, 207.0633; found, 207.0630.

Synthesis of *anti-trans* cyclic carbonate 4A

A mixture of *syn*-epoxy alcohol *syn*-**1** (140 mg, 1 mmol), Al complex Al^{Me} (22 mg, 5.0 mol%) and DBU (8.0 mg, 5.0 mol%) dissolved in 1.0 mL of MEK was introduced into a 30 mL stainless steel reactor. After three cycles of pressurization and depressurization, the reactor was charged with 40 bar of CO_2. Then the reaction mixture was heated to 80 ºC and magnetically

stirred for 24 h. Finally, the reactor was cooled down to rt and carefully depressurized. Flash chromatography on silica gel (hexane:ethyl acetate, gradient from 2:1 to 1:1 v/v) afforded the title compound as a colorless oil (46 mg, 25% yield). Crystals of **4A** were obtained from a saturated solution in $CDCl_3$/Hexane at –20 ºC. **^{1}H NMR** (500 MHz, CDCl3): δ = 5.82-5.68 (m, 2H), 4.50-4.38 (m, 2H), 3.91-3.78 (m, 1H), 2.51-2.37 (m, 2H), 2.37-2.28 (m, 1H), 2.27-2.15 (m, 2H), 1.82-1.62 (m, 1H) ppm. **^{13}C NMR** (126 MHz, CDCl3): δ = 154.1, 130.8, 126.1, 86.8, 79.2, 70.9, 29.8, 29.4, 21.0 ppm. **IR** (neat): ν = 3473 (OH), 1787 (C=O) cm^{-1}. **HRMS** (ESI+, MeOH): m/z calcd. for $[C_9H_{12}NaO_4]^+$, 207.0633; found, 207.0631.

Assigned NMR spectra

Product **2A** was isolated as a mixture of **2A**:**2B** (91:9). X-ray crystallography proved the identity of **2A** as explained in the main text. Below only the resonances belonging to **2A** are assigned.

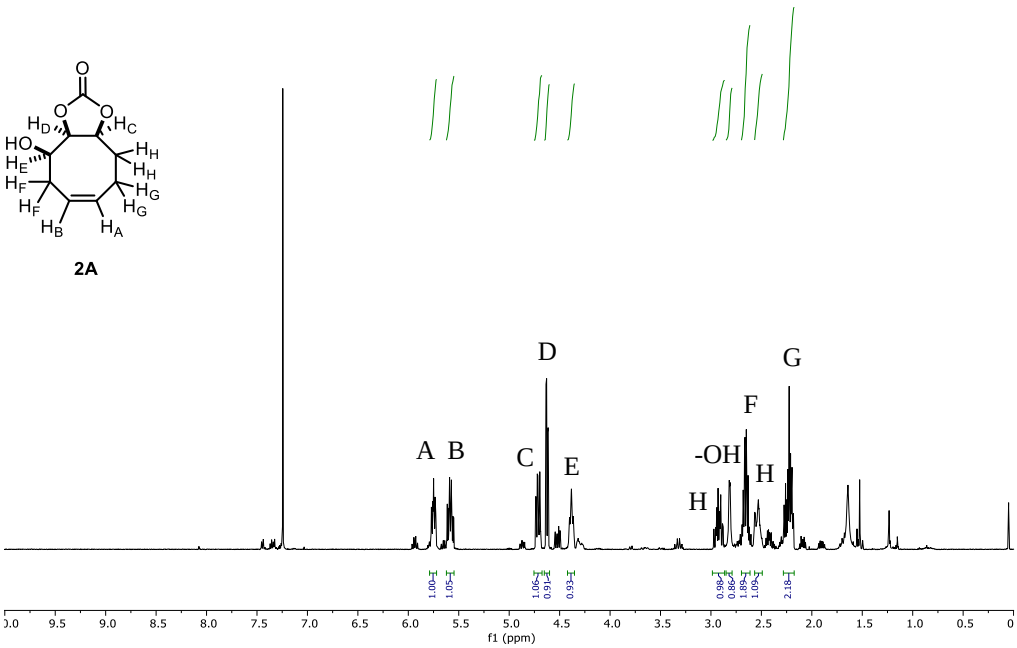

Figure 2.9. ^{1}H NMR analysis (500 MHz, Chloroform-*d*) for a 91:9 mixture of **2A**:**2B**.

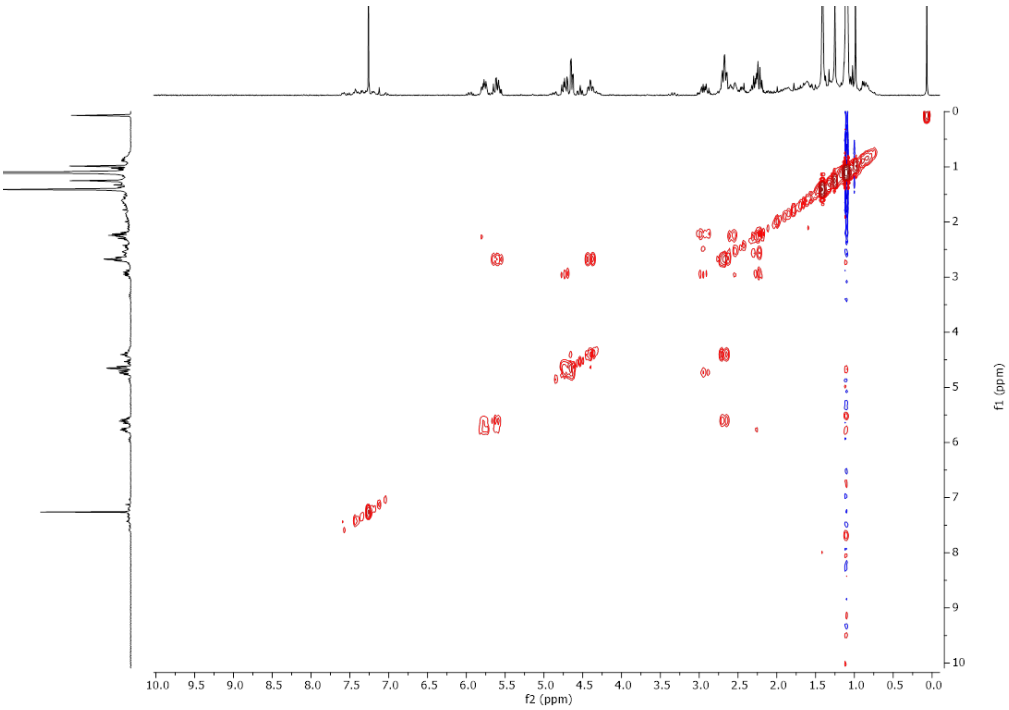

Figure 2.10. 2D ^{1}H-^{1}H COSY-NMR (500 MHz, Chloroform-*d*) for a 91:9 mixture of **2A**:**2B**.

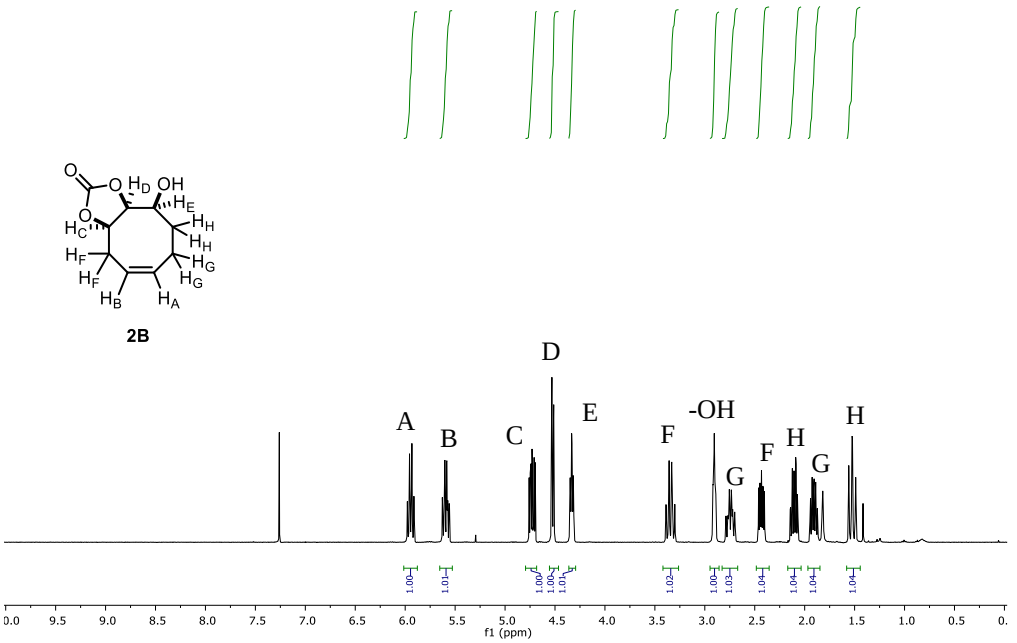

Figure 2.11. ^{1}H NMR (500 MHz, Chloroform-*d*) for pure **2B**.

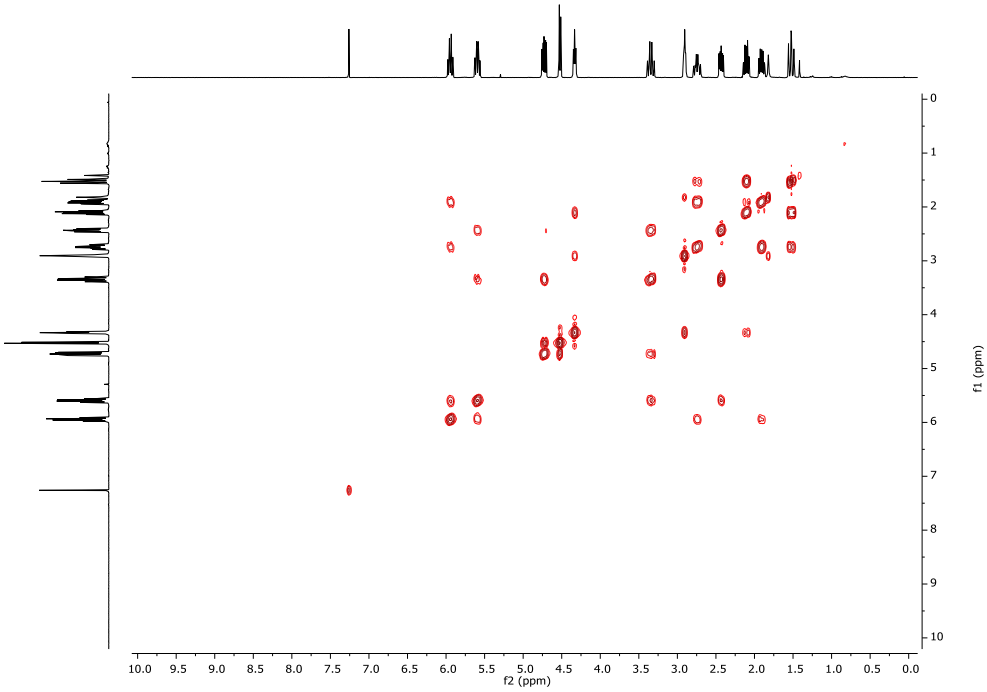

Figure 2.12. 2D ^{1}H-^{1}H COSY-NMR (500 MHz, Chloroform-*d*) for pure **2B.**

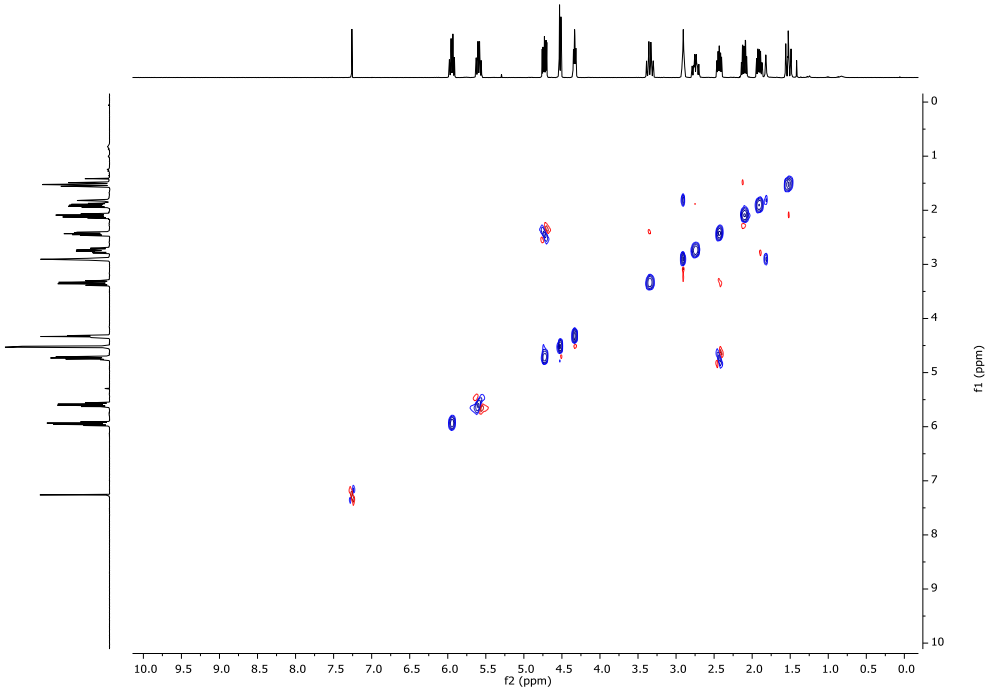

Figure 2.13. 2D 1H-1H NOESY-NMR (500 MHz, Chloroform-d) for pure **2B**.

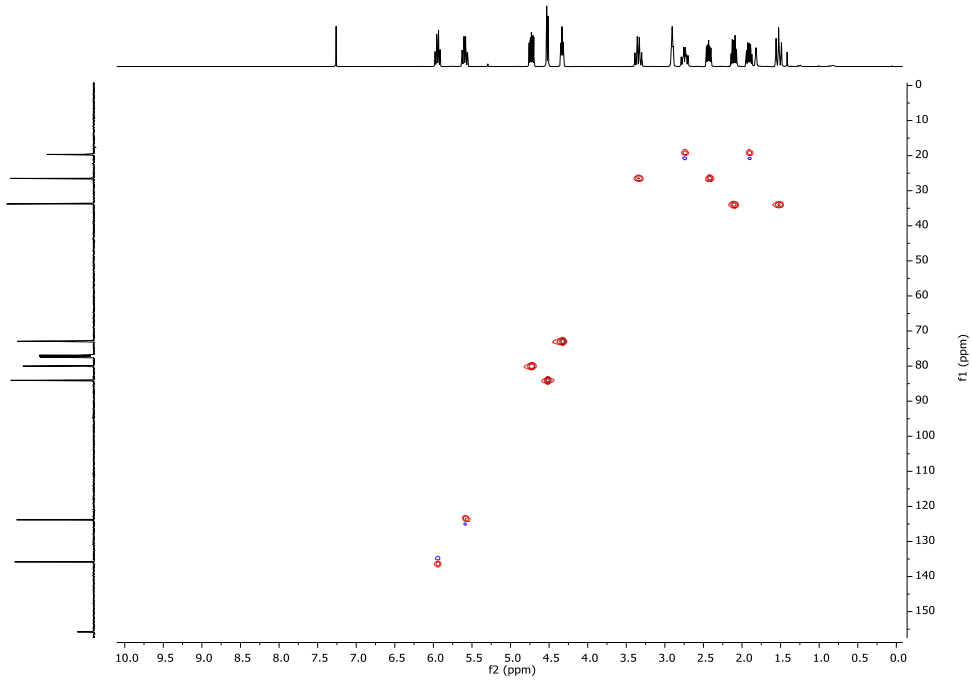

Figure 2.14. 2D ^{1}H-^{13}C HSQC-NMR (500 MHz, Chloroform-*d*) for pure **2B**.

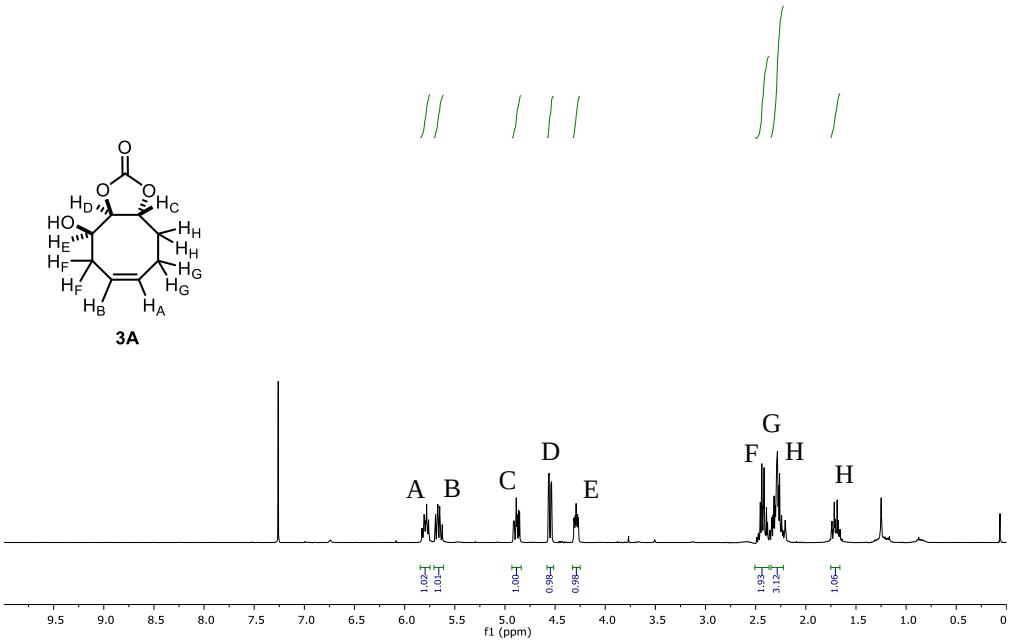

Figure 2.15. ^{1}H NMR analysis (Chloroform-d) for pure **3A**.

Product **3A** was assigned based on characteristic cross-peaks in the 2D-COSY NMR spectra. Referenced to known compounds resolved by X-ray crystallography, we noticed that *syn*-isomers (*i.e.,* the alcohol group being *syn* to the carbonate ring) lack a strong coupling between H_D and H_E that is clearly present in the *anti*-isomer (**4A**). When comparing crystal structures, it became clear that this originates from a close to 90° torsion angle (ranging from 54 to 74º), diminishing the *J*-coupling in the *syn*-isomers compared to 173° in the *anti*-isomer **4A**, according to the Karplus relationship.[26] The compound assigned as **3A** also lacks such a coupling, and its structure was therefore proposed by exclusion of other possibilities, as all the other *syn*-isomers (**2A**, **2B** and **3B**) had been previously identified by X-ray crystallography

[26] Wu, A.; Cremer, D.; Auer, A. A.; Gauss, J. *J. Phys. Chem. A* **2002**, *106*, 657-667.

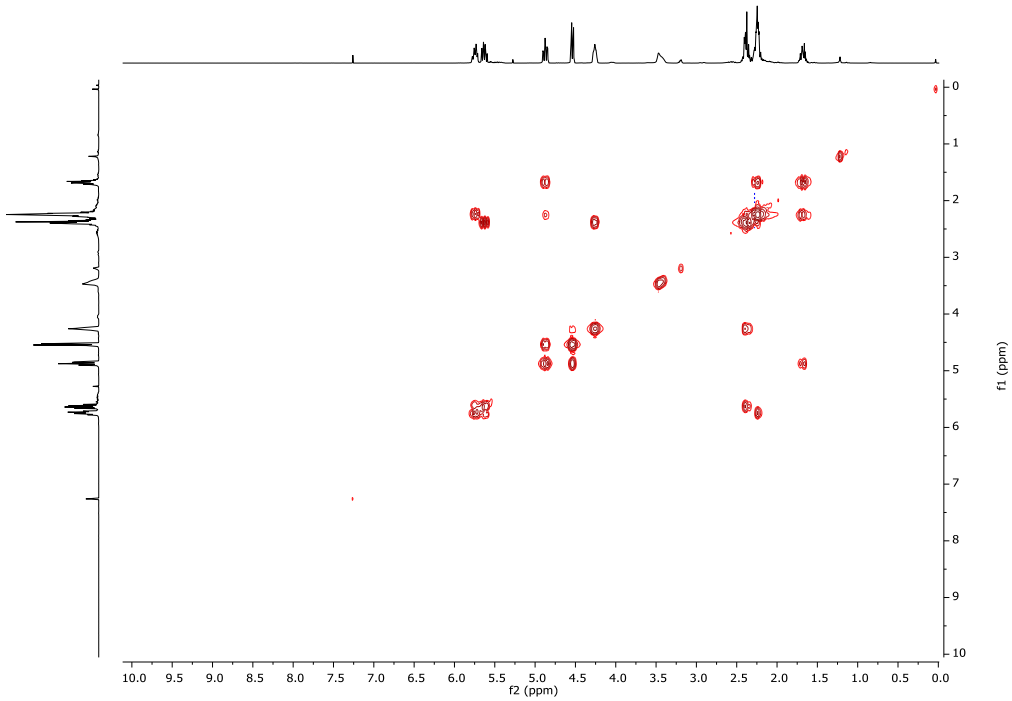

Figure 2.16. 2D ^{1}H-^{1}H COSY-NMR (500 MHz, Chloroform-*d*) for **3A**.

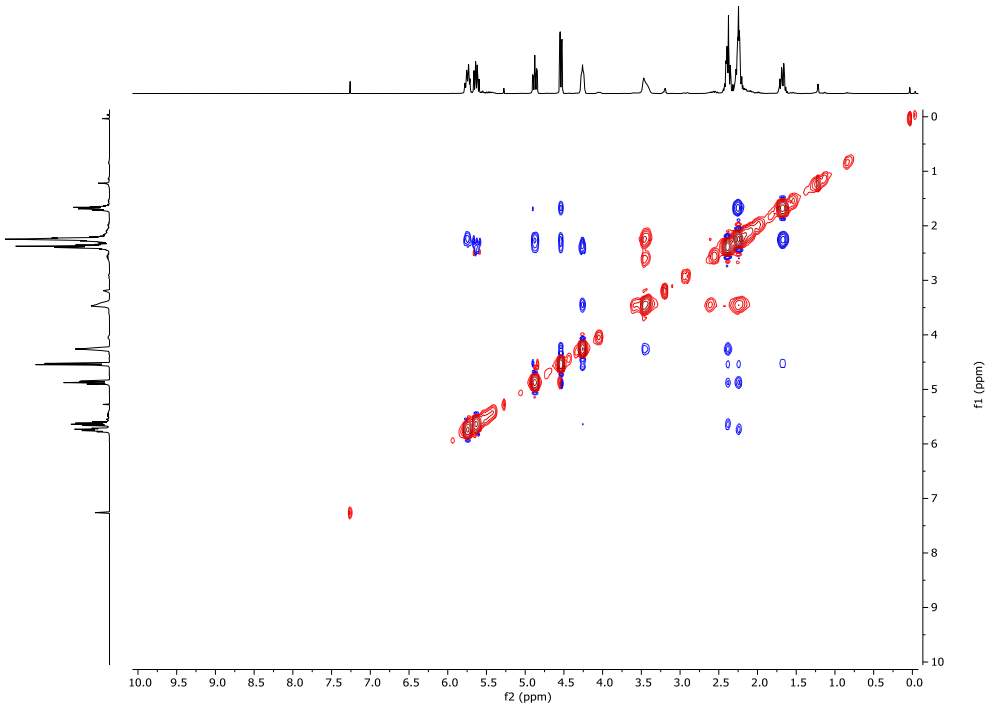

Figure 2.17. 2D ^{1}H-^{1}H NOESY-NMR (500 MHz, Chloroform-*d*) for **3A.**

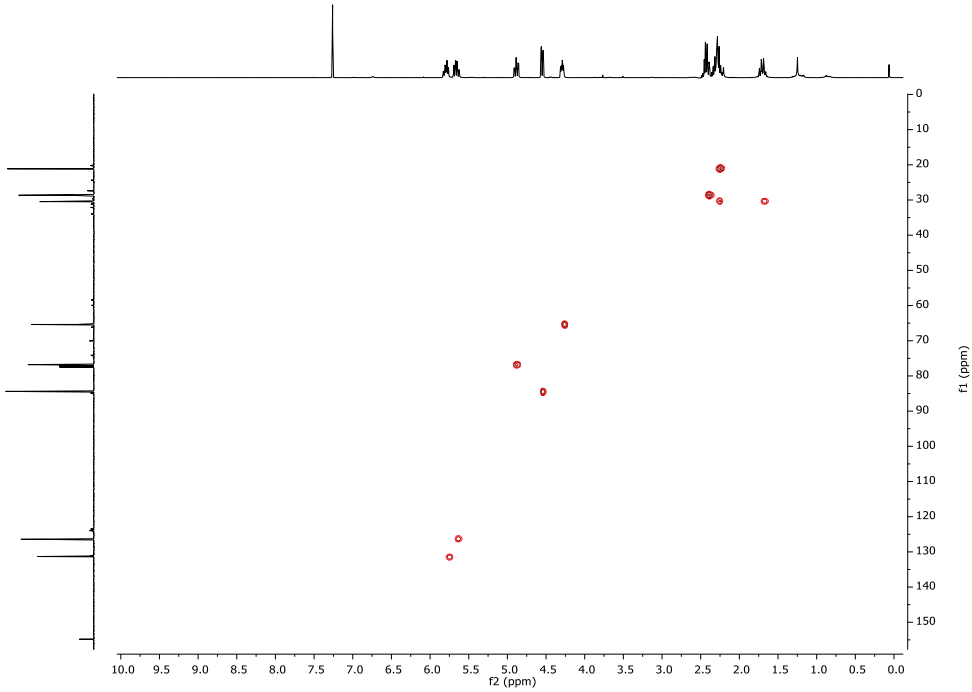

Figure 2.18. 2D ^{1}H-^{13}C HSQC-NMR (500 MHz, Chloroform-*d*) for **3A**.

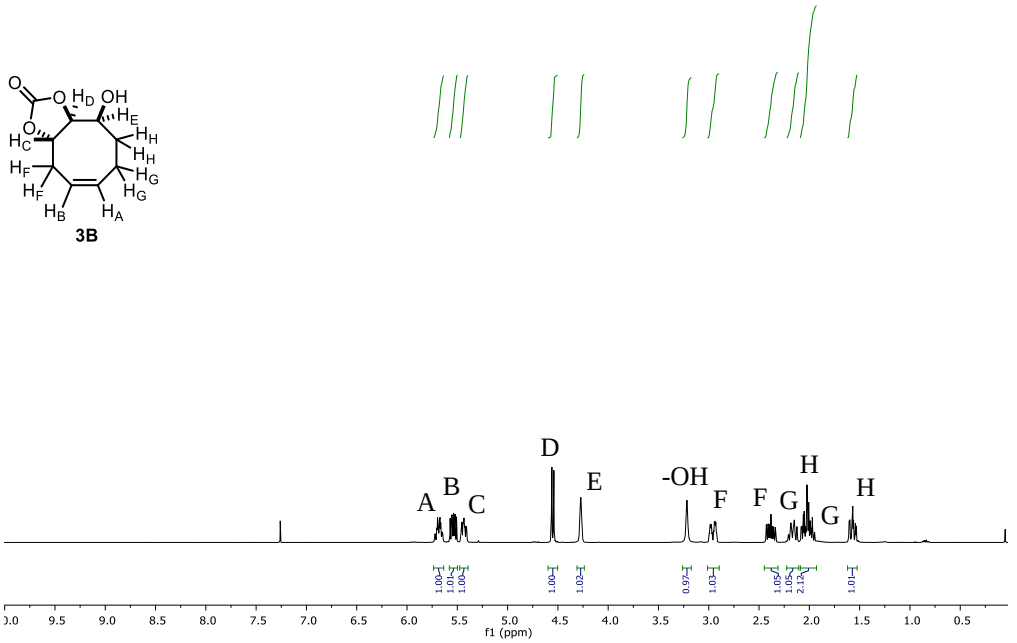

Figure 2.19. ^{1}H NMR (Chloroform-d) for pure **3B**.

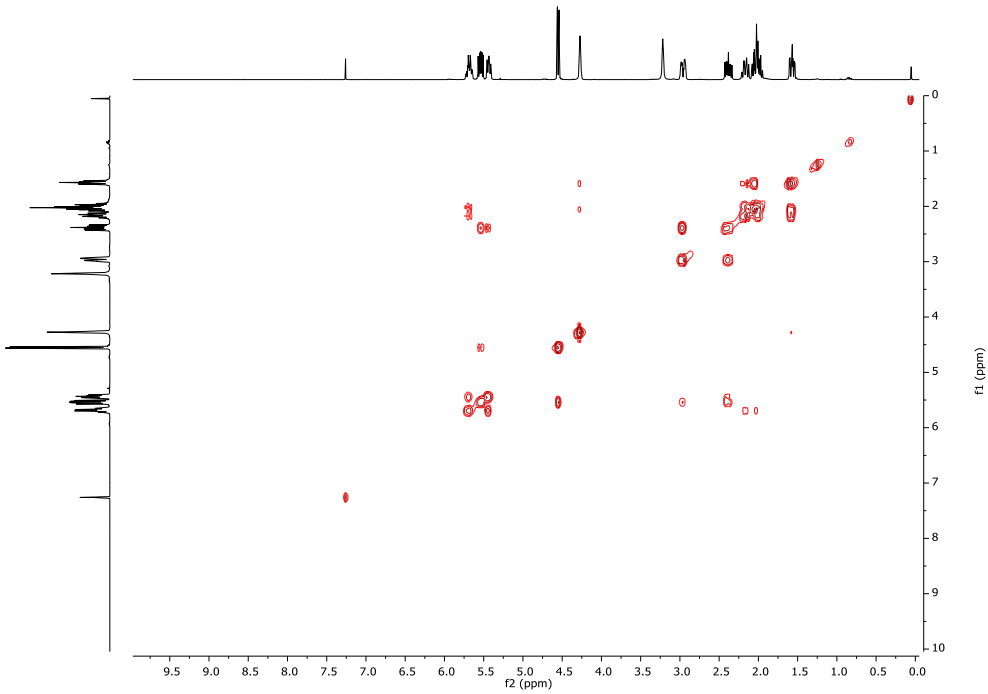

Figure 2.20. 2D ^{1}H-^{1}H COSY-NMR (500 MHz, Chloroform-*d*) for pure **3B**.

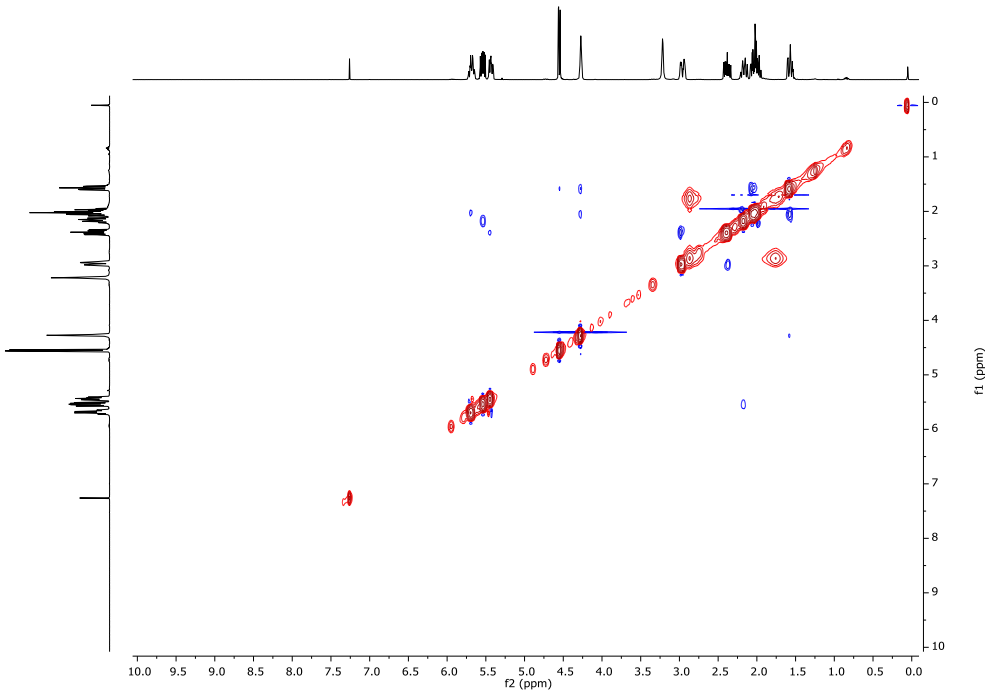

Figure 2.21. 2D ^{1}H-^{1}H NOESY-NMR (500 MHz, Chloroform-*d*) for pure **3B**.

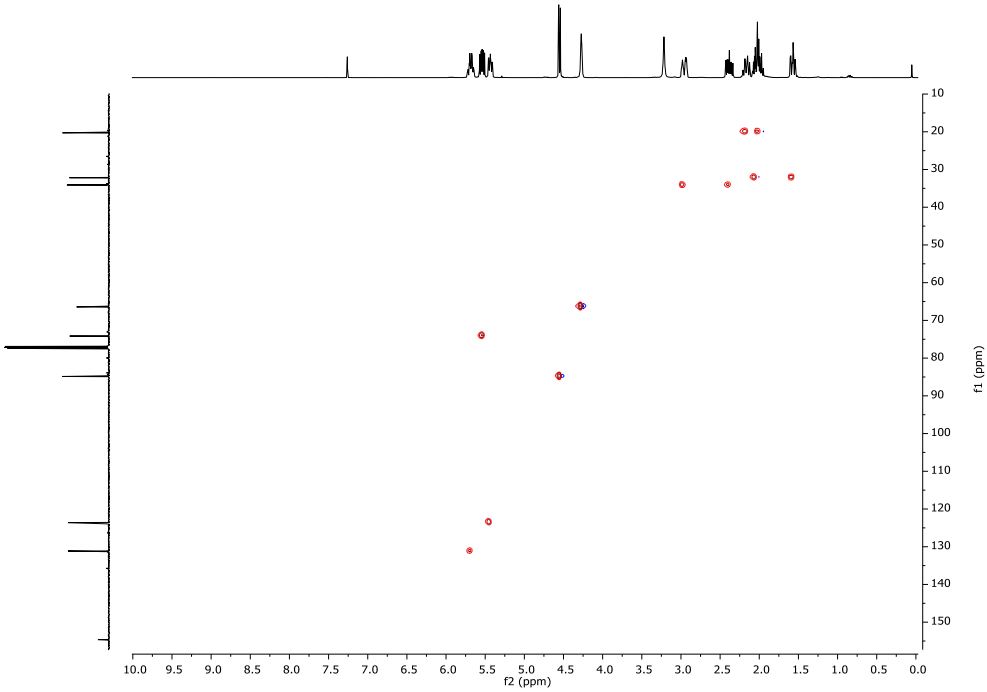

Figure 2.22. 2D ^{1}H-^{13}C HSQC-NMR (500 MHz, Chloroform-*d*) for pure **3B**.

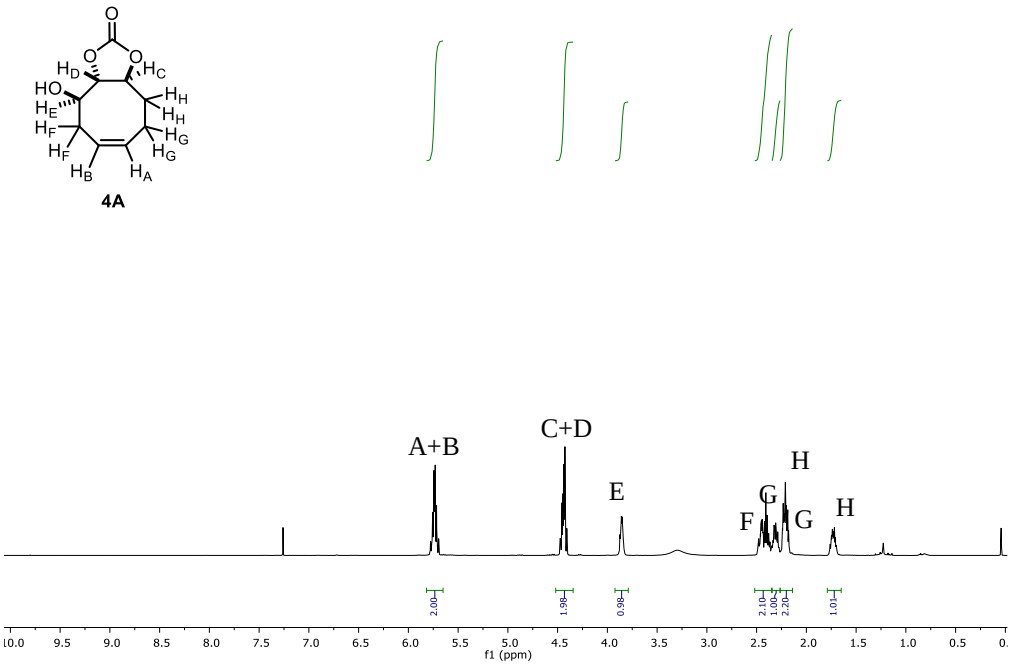

Figure 2. 23. ^{1}H NMR (Chloroform-*d*) for pure **4A**.

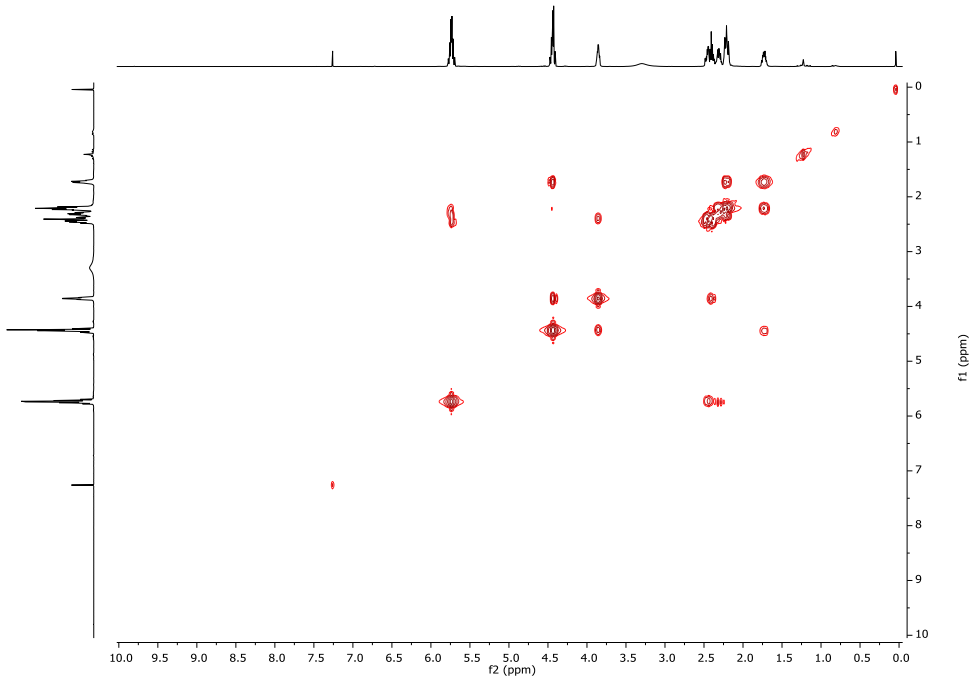

Figure 2.24. 2D ^{1}H-^{1}H COSY-NMR (500 MHz, Chloroform-d) for pure **4A**.

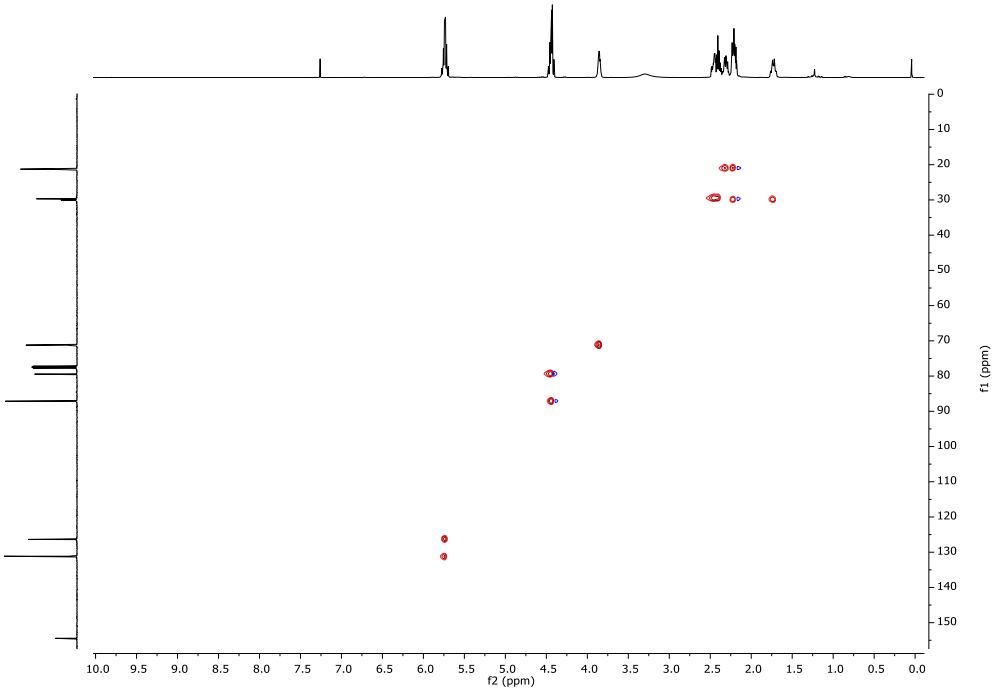

Figure 2.25. 2D ^{1}H-^{13}C HSQC-NMR (500 MHz, Chloroform-*d*) for pure **4A**.

Computational details and microkinetic model

All the calculations in this study were carried out with the Gaussian09 package, employing the B97-D371, functional (hybrid and dispersion-corrected) and a standard 6-311G(d,p) basis set for all atoms. For all structures, we carried out full non-constrained geometry optimizations and further harmonic frequency calculations in order to confirm the nature of minima and transition states. Solvent effects were included with the Solvation Model based on Density (SMD) implemented in Gaussian09, taking the parameters for butanone, the same solvent as in the experiments. The reported Gibbs free energies include the entropic corrections by Martin, already employed in previous studies, calculated at 353.15 K in order to mimic the experimental conditions. These corrections are based on the consideration of a pressure at which the ideal gas density matches the one for the solvent (in this case, butanone). A data set collection of computational results is available in the ioChem-BD repository and can be accessed through https://doi.org/10.19061/iochem-bd-1-141.

For the microkinetic model, we used the COPASI code, with reaction rates obtained from the Eyring equation assuming κ=1. The activation energies used to compute these reaction rates included corrections to account for the standard state change when going to the standard (1 atm) state in Gaussian to the (1 M) state required for working with molar concentrations (instead of the Martin ones). Table 2.9 summarizes the theoretical results and compares them to experimentally found values. Figure 2.27 (next page) shows the evolution of the conversion, selectivity and the concentration of products / starting material as a function of time.

Table 2.9. Micro-kinetic modeling of the DFT Results compared to experimental values.

Entry	[Br] (mol%)	Prediction		Experimental	
		% conv	% sel **2B**	% conv	% sel **2B**
1	25	98.1	94.8	99	92
2	20	96.9	91.3	90	87
3	15	94.8	85.1	85	89
4	10	91.4	74.1	85	88

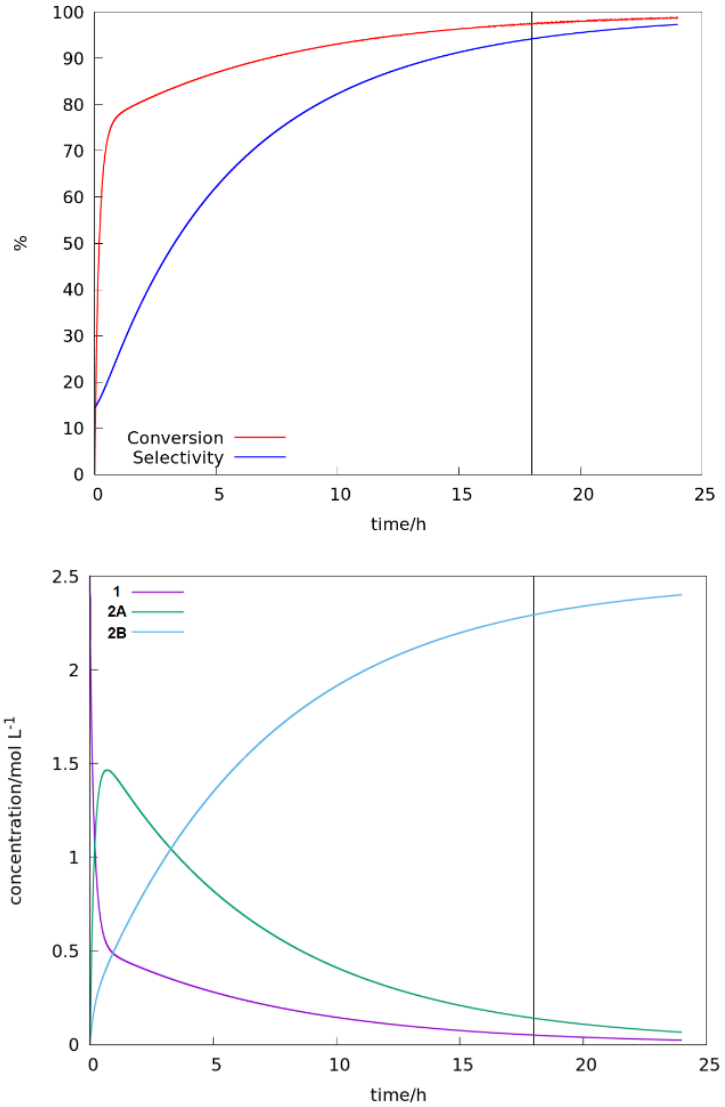

Figure 2.26. Top: Theoretical conversion and selectivity as a function of time. Down: concentration of *syn*-**1**, **2A** and **2B** as a function of time. Conditions: [**1**] = 2.5 M, pCO_2 = 40 bar, T = 80 ºC, Br^- 25 mol%.

X-ray crystallographic studies

The measured crystals of *syn-cis* **2A**, *syn-cis* **2B**, *syn-trans* **3B** and *anti-trans* **4A** were stable under atmospheric conditions; nevertheless, they were treated under inert conditions immersed in perfluoro-polyether as protecting oil for manipulation. Data Collection: measurements were made on a Bruker-Nonius diffractometer equipped with an APPEX II 4K CCD area detector, a

FR591 rotating anode with MoKα radiation, Montel mirrors and a Kryoflex low temperature device (T = −173 °C). Full-sphere data collection was used with ω and φ scans. Programs used: Data collection Apex2 V2011.3 (Bruker-Nonius 2008), data reduction Saint+Version 7.60A (Bruker AXS 2008) and absorption correction SADABS V. 2008−1 (2008). Structure Solution: SHELXTL Version 6.10 (Sheldrick, 2000)[27] was used. Structure Refinement: SHELXTL-97-UNIX VERSION.

Crystallographic details for *syn-cis* 2A: $C_9H_{12}O_4$, M_r = 184.19, monoclinic, $P2_1/c$, a = 11.8451(8) Å, b = 6.5427(5) Å, c = 12.4361(6) Å, α = 90º, β = 115.635(2)º, γ = 90º, V = 868.92(11) Å^3, Z = 4, ρ = 1.408 mg·M^{-3}, μ = 0.111 mm^{-1}, λ = 0.71073 Å, T = 100(2) K, F(000) = 392, crystal size = 0.40 × 0.10 × 0.05 mm, θ(min) = 3.293°, θ(max) = 30.536°, 4997 reflections collected, 2513 reflections unique (R_{int} = 0.0249), GoF = 1.046, R_1 = 0.0394 and wR_2 = 0.1017 [$I > 2\sigma(I)$], R_1 = 0.0455 and wR_2 = 0.1064 (all indices), min/max residual density = −0.266/0.400 [e·Å^{-3}]. Completeness to θ(30.536°) = 94.3%. CCDC number 1945737.

Crystallographic details for *syn-cis* 2B: $C_9H_{12}O_4$, M_r = 184.19, monoclinic, $P2_1/n$, a = 17.01654(16) Å, b = 5.80920(6) Å, c = 17.71629(16) Å, α = 90º, β = 92.0743(9)º, γ = 90º, V = 1750.15(3) Å^3, Z = 8, ρ = 1.398 mg·M^{-3}, μ = 0.110 mm^{-1}, λ = 0.71073 Å, T = 100(2) K, F(000) = 784, crystal size = 0.25 × 0.22 × 0.10 mm, θ(min) = 2.301°, θ(max) = 37.466°, 62800 reflections collected, 9005 reflections unique (R_{int} = 0.0459), GoF = 1.056, R_1 = 0.0348 and wR_2 = 0.1025 [$I > 2\sigma(I)$], R_1 = 0.0379 and wR_2 = 0.1048 (all indices), min/max residual density = −0.232/0.669 [e·Å^{-3}]. Completeness to θ(37.466°) = 98.1%. CCDC number 1868679.

Crystallographic details for *syn-trans* 3B: $C_9H_{12}O_4$, M_r = 184.19, orthorhombic, $P2_12_12_1$, a = 5.02716(17) Å, b = 7.4605(3) Å, c = 22.8210(7) Å, $\alpha = \beta = \gamma$ = 90º, V = 855.90(5) Å^3, Z = 4, ρ = 1.429 mg·M^{-3}, μ = 0.113 mm^{-1}, λ = 0.71073 Å, T = 100(2) K, F(000) = 392, crystal size = 0.10 × 0.10 × 0.10 mm, θ(min) = 2.873°, θ(max) = 34.662°, 10246 reflections collected, 3429 reflections unique (R_{int} = 0.0162), GoF = 1.065, R_1 = 0.0250 and wR_2 = 0.0698 [$I > 2\sigma(I)$], R_1 = 0.0264 and wR_2 = 0.0706 (all indices), Flack (x) = 0.52(18), min/max residual density = −0.172/0.273 [e·Å^{-3}]. Completeness to θ(34.662°) = 96.0%. CCDC number 1868678.

[27] Sheldrick, G. M. SHELXTL Crystallographic System, version 6.10; Bruker AXS, Inc.: Madison, WI, 2000.

Crystallographic details for *anti-trans* 4A: $C_9H_{12}O_4$, M_r = 184.19, monoclinic, $P2_1/c$, a = 11.9905(11) Å, b = 5.4556(5) Å, c = 13.3386(14) Å, α = 90º, β = 92.116(3)º, γ = 90º, V = 871.95(15) Å^3, Z = 4, ρ = 1.403 mg·M^{-3}, μ = 0.111 mm^{-1}, λ = 0.71073 Å, T = 100(2) K, F(000) = 392, crystal size = 0.20 × 0.10 × 0.05 mm, θ(min) = 1.699°, θ(max) = 29.678°, 6719 reflections collected, 2304 reflections unique (R_{int} = 0.0338), GoF = 1.030, R_1 = 0.0423 and wR_2 = 0.1041 [$I > 2\sigma(I)$], R_1 = 0.0631 and wR_2 = 0.1163 (all indices), min/max residual density = −0.257/0.355 [e·Å^{-3}]. Completeness to θ(29.678°) = 92.9%. CCDC number 1945738.

Chapter 3

Photocatalytic Synthesis of Cyclic Carbonate Monomers for Ring-Opening Polymerization

The results described in this chapter have been published in:

Maquilón, C.; Della Monica, F.; Limburg, B.; Kleij, A. W. *Adv. Synth. Catal.* **2021**, *363* (16), 4033-4040

UNIVERSITAT ROVIRA I VIRGILI
NEW AND FUNCTIONAL CYCLIC CARBONATES FOR POLYMER APPLICATIONS
Cristina Maquilón Albaladejo

3.1. Introduction

Aliphatic polycarbonates (APCs) are polymers that contain repeating carbonate units in their backbones and are devoid of aromatic side-chain segments.[1] APCs have received significant attention due to their biodegradable and biocompatible features,[2] which enable them to be useful ingredients for biomedical and advanced materials production.[3,4] The synthesis of APCs can be achieved via ring opening copolymerization (ROCOP) of epoxides and CO_2 (Scheme 3.1a);[5] however, over the years relatively few monomer combinations have shown promise towards the selective formation of fully alternating polycarbonates with tuneable properties.[6,7,8] This lack of diversity provides impetus for monomer engineering in order to be able to access novel types of functional polycarbonates whose properties can be more precisely tailored.

The ring opening polymerization (ROP) of cyclic carbonates represents another route towards the synthesis of polycarbonate macromolecules.[9] Although the synthesis of five membered cyclic carbonates (5MCCs) is well-established, [10,11,12] these heterocycles have a comparatively low ROP potential, and only a few examples exist where the reactivity of *trans*-fused, strained polycyclic carbonate structures is exploited.[13,14] Unlike their five-membered analogues, the ROP of larger-ring carbonates has been reported as a viable strategy towards the

[1] Xu J.; Feng E.; Song J. *J. Appl. Polym. Sci*. **2014**, *131*, 39822.
[2] Daia Y.; Zhang X. *Polym. Chem.* **2017**, *8*, 7492-7437.
[3] Yu W.; Maynard E.; Chiaradia V.; Arno M. C.; Dove A. P. *Chem. Rev.* **2021**, DOI:10.1021/acs.chemrev.0c00883
[4] Domiński A.; Konieczny T.; Duale K.; Krawczyk M.; Pastuch-Gawołek G.; Kurcok P. *Polymer* **2020**, *12*, 2890.
[5] Grignard B.; Gennen S.; Jérôme C.; Kleij A. W.; Detrembleur C. *Chem. Soc. Rev.* **2019**, *48*, 4466–4514.
[6] Kindermann N.; Cristòfol À.; Kleij A. W. *ACS Catal.* **2017**, *7*, 3860–3863.
[7] Li C.; Sablong R. J.; Koning C. E.; *Angew. Chem. Int. Ed.* **2016**, *55*, 11572–11576.
[8] Hauenstein O.; Agarwal S.; Greiner A. *Nat. Commun.* **2016**, *7*, 11862.
[9] Tempelaar S.; Mespouille L.; Coulembier O.; Dubois P.; Dove A. P. *Chem. Soc. Rev.* **2013**, *42*, 1312–1336.
[10] Shaikh R. R.; Pornpraprom S.; D'Elia V. *ACS Catal.* **2018**, *8*, 419–450.
[11] Della Monica F.; Kleij A. W. *Catal. Sci. Technol.* **2020**, *10*, 3483–3501.
[12] Aomchad V.; Cristòfol À.; Della Monica F.; Limburg B.; D'Elia V.; Kleij A. W. *Green Chem.* **2021**, *23*, 1077–1113.
[13] Azechi M.; Matsumoto K.; Endo T. *J. Polym. Sci. Part A* **2013**, *51*, 1651–1655.
[14] Tezuka K.; Koda K.; Katagiri H.; Haba O. *Polym. Bull.* **2015**, *72*, 615–626.

preparation of polycarbonates.[15,16,17] In particular, the ROP of six-membered carbonates (6MCCs) has been most frequently studied and takes advantage of a more diverse set of available monomers, thereby creating polycarbonate variability (Scheme 3.1b).[18] However, the synthesis of 6MCCs can be tedious and only a handful of effective methods have been reported so far.[19,20] Among the general approaches, the use of catalytic oxetane/CO_2 coupling reactions[21,22] and the stoichiometric conversion of diol reagents[23,24] are noteworthy.

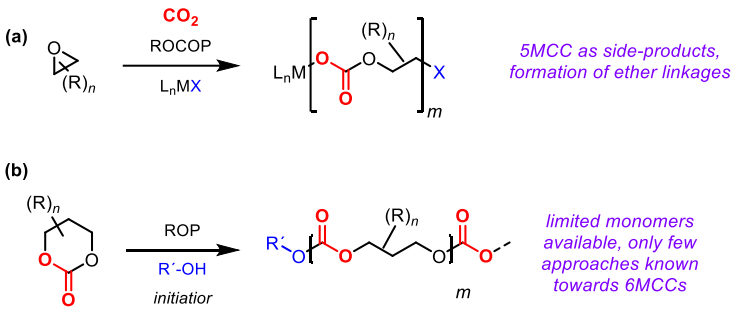

Figure 3.1. (a) Polycarbonate formation from CO_2 and epoxides via ROCOP. (b) ROP of 6MCCs leading to aliphatic polycarbonates. Some of the limitations are also provided.

In a more recent approach, our group demonstrated that tri-substituted 6MCCs can be obtained from 5MCCs that contain β-positioned (*exo*-cyclic) alcohol groups. Upon activation by a suitable base, these groups allow for an unusual isomerization process to occur.[25] In this approach, it was necessary to protect the alcohol group of the 6MCC product to prevent back-equilibration to the thermodynamically more stable 5MCC. Preliminary ROP experiments with this type of 6MCC were unsuccessful and inspired us to devise new synthetic methods to create

[15] Song Y.; Yang X.; Shen Y.; Dong M.; Lin Y.-N.; Hall M. B.; Wooley K. L. *J. Am. Chem. Soc.* **2020**, *142*, 16974–16981.
[16] McGuire T. M.; Pérale C.; Castaing R.; Kociok-Köhn G. I.; Buchard A. *J. Am. Chem. Soc.* **2019**, *141*, 13301–13305.
[17] Venkataraman S.; Ng V. W. L.; Coady D. J.; Horn H. W.; Jones G. O.; Fung T. S.; Sardon H.; Waymouth R. M.; Hedrick J. L.; Yang Y. Y. *J. Am. Chem. Soc.***2015**, *137*, 13851–13860.
[18] Bhat G. A.; Luo M.; Darensbourg D. J. *Green Chem.* **2020**, *22*, 7707–7724.
[19] Vara B. A.; Struble T. J.; Wang W.; Dobish M. C.; Johnston J. N. *J. Am. Chem. Soc.* **2015**, *137*, 7302–7305.
[20] Minakata S.; Sasaki I.; Ide T. *Angew. Chem. Int. Ed.***2010**, *49*, 1309–1311.
[21] Rintjema J.; Guo W.; Martin E.; Escudero-Adán E. C.; Kleij A. W. *Chem. Eur. J.* **2015**, *21*, 10754–10762.
[22] Buckley B. R.; Patel A. P.; Upul Wijayantha K. G. *Eur. J. Org. Chem.* **2015**, 474–478.
[23] McGuire T. M.; López-Vidal E. M.; Gregory G. L.; Buchard A. *J. CO2 Util.* **2018**, *27*, 283–288.
[24] Gregory G. L.; Ulmann M.; Buchard A. *RSC Adv.* **2015**, *5*, 39404–39408.
[25] Qiao C.; Villar-Yanez A.; Sprachmann J.; Limburg B.; Bo C.; Kleij A. W. *Angew. Chem. Int. Ed.* **2020**, *59*, 18446–18451.

different types of 6MCC monomers. In this regard, the use of metallaphotoredox catalysis was considered, as such an approach had been successfully applied to prepare 5MCCs[26] and related oxazolidinones.[27] As far as we are aware, no efforts have yet been described to create larger-ring carbonates under photocatalytic conditions.

Our envisioned approach (Scheme 3.1) is based on the use of readily available O-Boc-protected γ-substituted allylic alcohols. Under suitable photocatalytic conditions, radical addition to the allylic precursor should be feasible giving a stabilized benzylic radical. Subsequent single-electron oxidation produces a benzylic cation that can be intercepted intramolecularly by the OBoc fragment to give the 6MCC target, with expulsion of isobutylene. In this chapter, we present the results of this photocatalytic strategy towards 6MCCs and the evaluation of the carbonate ring substitution on their ROP potential.

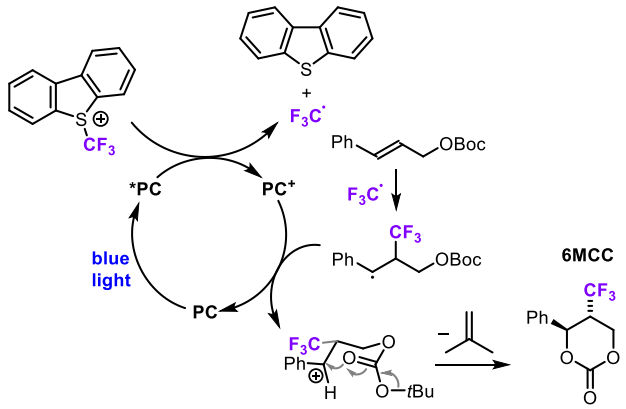

Scheme 3.1. Envisioned approach towards the photocatalytic formation of novel 6MCCs. ´PC´ stands for the photocatalyst used.

[26] Wang M.-Y.; Cao Y.; Liu X.; Wang N.; He L.-N.; Lia S.-H. *Green Chem.* **2017**, *19*, 1240–1244.
[27] Ye J.-H.; T. Huang Ju, H.; Liao L.-L.; Yu D.-G. *Acc. Chem. Res.* **2021**, *54*, 2518–2531.

3.2 Results and Discussion

All the experiments were carried out in a multi-position photoreactor that accommodates up to eight parallel reactions (Figure 3.2). It is equipped with a cooling system allowing control of the reaction temperature, and blue LED irradiation with variable intensity up to 1 A.

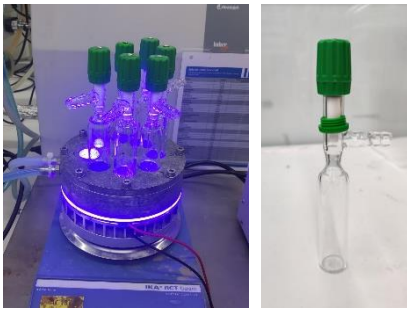

Figure 3.2. LEFT: an eight-position photoreactor. RIGHT: flat-bottom Schlenk vessel for performing photoreactions.

Optimization of the reaction conditions for the synthesis of 6MCCs

We selected Boc-protected cinnamyl alcohol as a benchmark substrate for our screening studies and the Umemoto reagent as a source of CF_3 radicals[28,29] generated under blue LED irradiation using transition metal photoredox catalysts (PC). In the presence of $NaHCO_3$, good conversion of **1a** was achieved after 30 min producing **2a** in 32% NMR yield (Table 3.1, Entry 1). A longer reaction time did not improve this result, and we found that the addition of base was not necessary (Entry 2). We thus continued without this additive and investigated the influence of the concentration (Entries 3-6). Other parameters that we screened were the solvent, the nature of the PC, the excess of Umemoto reagent and the temperature/light intensity. A concentration of 18 mM proved to be optimal producing **2a** in 54% yield (Entry 5), whereas changing the solvent did not improve the process outcome (Entries 7-10). Variation of the PC from **A** to **B**–**E** also did not lead to improved efficiency (Entries 11-14), and increasing the amount of Umemoto's reagent from 1.1 to 1.5 equiv virtually did not change the yield of **2a** (Entry 15). While decreasing the light intensity led to a drop in chemoselectivity (Entry 16), some improvement was noted when increasing the light intensity while carrying out the catalytic protocol at 0 ºC giving **2a** in 66% NMR and 62% isolated yield (Entry 17).

[28] Zhang C. *Org. Biomol. Chem.* **2014**, *12*, 6580–6589.
[29] Li H. *Synlett.* **2012**, *23*, 2289–2290.

Table 3.1. Photocatalytic conversion of *O*-Boc protected cinnamyl alcohol **1a** into 6MCC **2a** under various conditions.[a]

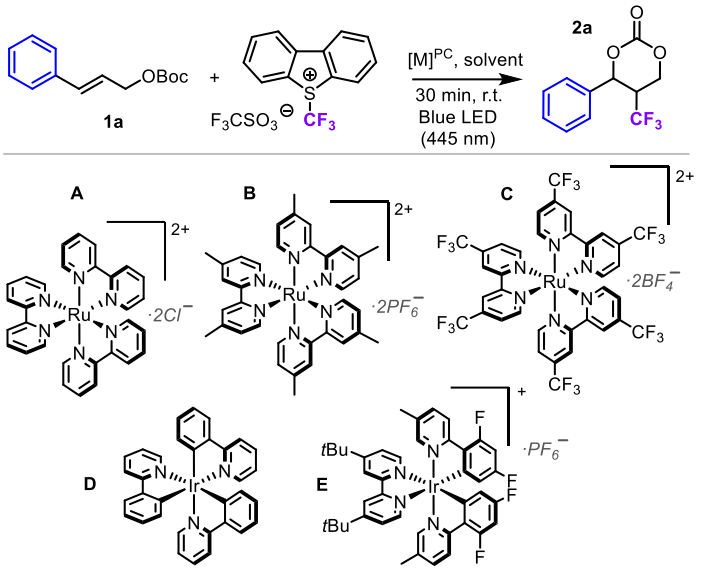

Entry	Solvent / PC	Concentration (mM)	Conv. **1a** (%)[b]	Yield **2a** (%)[c]
1[d]	MeCN / **A**	180	91	32
2[d,e]	MeCN / **A**	180	98	23
3	MeCN / **A**	180	>99	27
4	MeCN / **A**	9	>99	37
5	MeCN / **A**	18	>99	54
6	MeCN / **A**	36	>99	46
7	DCM / **A**	18	>99	13
8	DMF / **A**	18	45	5
9	DMSO / **A**	18	90	7
10	Acetone / **A**	18	>99	13
11	MeCN / **B**	18	>99	32
12	MeCN / **C**	18	0[f]	0
13	MeCN / **D**	18	91	13
14	MeCN / **E**	18	>99	21
15[g]	MeCN / **A**	18	>99	55
16[h]	MeCN / **A**	18	>99%	39
17[i]	MeCN / **A**	18	>99	66 (62)[j]

[a] **1a** (0.18 mmol for entries 1-3 and 6; 0.045 mmol for entry 4; 0.09 mmol for entries 5, 7-17), Umemoto reagent (1.1 equiv), $RuCl_2(bpy)_3 \cdot 6H_2O$ (**A**, 1.0 mol%), solvent (concentration stated), 30 min, rt, blue LED irradiation (λ_{em} = 445 nm, 700 mA, corresponding to 1.2 μeinstein/s. [b] Determined by ^1H NMR ($CDCl_3$). [c] As for [b] using mesitylene as internal standard. [d] With $NaHCO_3$ as additive (3 equiv.). [e] Reaction time was 3 h. [f] Using **C** as PC, no conversion of **1a**/Umemoto reagent observed. [g] Using 1.5 equiv Umemoto reagent. [h] LED current was 200 mA, corresponding to a photon flux of 0.4 μeinstein/s. [i] LED current was 1000 mA, corresponding to a photon flux of 1.6 μeinstein/s, T = 0 ºC. [j] In brackets, the isolated yield of **1a**.

A number of control reactions were performed to scrutinize the role of the reactants and catalyst (Table 3.2). In the dark, the chemoselectivity towards **2a** drops significantly (Entry 1). The presence of PC **A** is a requisite for product formation (Entry 2). Dioxygen only marginally affected the reaction and the product yield did not increase if the purification was omitted indicating no material is lost in the workup (Entries 3 and 4, respectively). The addition of water lowered the yield of **2a** to 46% (Entry 5). In the absence of starting material, Umemoto's reagent was fully converted to dibenzothiophene, indicating that photoexitation of PC leads to formation of CF_3 radicals in the absence of **1a** (Entry 6). The liberation of dibenzothiophene during the conversion of Umemoto's reagent and its potential effect on the catalytic efficiency was also probed but no significant decrease in product yield was noted (Entry 7). Finally, the addition of TEMPO shut down the reaction completely in line with the envisioned intermediacy of benzylic and CF_3 radicals (Entry 8). Substrates lacking benzylic stabilization of a radical intermediate such as Boc-protected prenol led to complicated product mixtures. Other protecting groups such as methoxycarbonyl or ethoxycarbonyl produced **2a** in much lower yield, indicating that the acid-labile Boc group is deprotected by the intermediate acidic benzylic cation (Entries 9-10).

Table 3.2. Control experiments carried out under the optimized screening conditions.[a]

Entry	Deviation	Yield **2a** [%][b]
1	In the dark	4
2	No PC (**A**) added	3
3	No degassing	52
4	No extraction	50
5	Added 10 μL H_2O	46
6	No **1a** added	0[c]
7	Dibenzothiophene (1 equiv) added	60
8[d]	TEMPO (2 equiv) added	0
9	Methoxycarbonyl instead of Boc	13
10	Ethoxycarbonyl instead of Boc	8

[a] See entry 17, Table 1. [b] Determined by ^{1}H NMR ($CDCl_3$) using mesitylene as internal standard. [c] Full conversion of Umemoto's reagent was observed by ^{1}H NMR. [d] TEMPO-CF_3 adduct (12%) observed by ^{19}F NMR analysis.

Other radical sources were also screened (Scheme 3.2). Alternative fluorocarbon radical precursors, such as the Ruppert-Prakash reagent, Togni's reagent II and perfluorohexyl iodide, were unproductive. This is likely due to their inability to quench the excited state. An alkyl Katritzky pyridinium salt was also tested as alkyl radical source, but this reagent was also not successful in the photocatalytic formation of the 6MCC target.

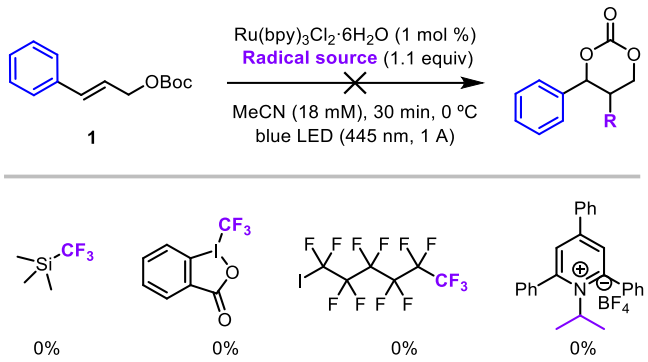

Scheme 3.2. Screening of radical sources in the photocatalytic synthesis of 6MCC.

The maximum NMR yield for **2a** was 66%, and a full kinetic profile (total time frame being 5 min) for this transformation was established (Figure 3.3). Interestingly, at the beginning of the reaction the conversion of **1a** and the formation of **2a** proceed simultaneously and the mass balance is nearly fully accounted-for, but shortly thereafter the amount of byproduct(s) quickly increases to about 34% after 5 min. ^{19}F NMR analysis of the crude product at this stage illustrated a variety of products, which we tentatively ascribe to the formation of trifluoromethylated (oligomeric) styrenes.

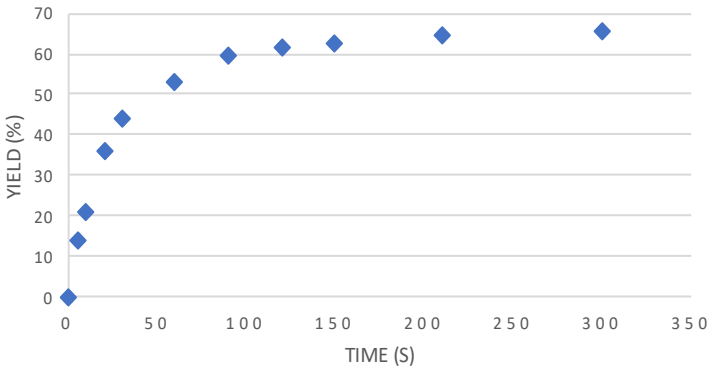

Figure 3.3. Kinetic profile for the conversion of the *tert*-butyl cinnamyl carbonate **1a** into cyclic carbonate **2a**. The time frame was 300 s (5 min).

The reason for this change in chemoselectivity during the reaction time can be explained by the instability of photocatalyst **A** under turnover conditions. As illustrated in Figure 3.4, the UV-vis spectrum shows that the characteristic band of **A** changes during the reaction indicating its decomposition. It is likely that CF_3 radicals react with the bipyridine ligands, altering the photophysical and photochemical properties of the photocatalyst rendering it unproductive for the reaction (*cf.*, efficiency of photocatalyst **A** versus **C**). Although a lower yield for **2a** is the consequence of competitive side-reactions, the targeted product can be easily isolated by column chromatography. From the kinetic data, we further infer that the initial quantum yield of the reaction is 158%, indicating a radical propagation mechanism (Scheme 3.1, see the Introduction).

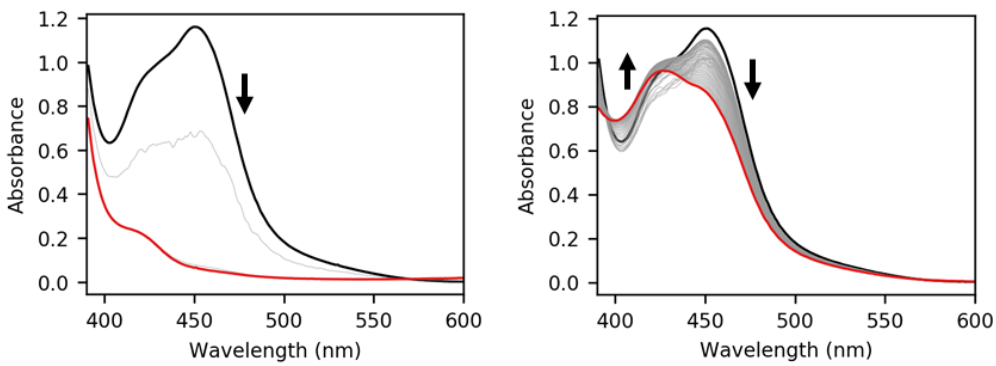

Figure 3.4. Left: Evolution of the UV-vis spectrum of a solution of $[Ru(bpy)_3]Cl_2$ (80 µM) and Umemoto's reagent (20 mM) in MeCN. $[Ru(bpy)_3]^{2+}$ is quickly oxidized by Umemoto's reagent to $[Ru(bpy)_3]^{3+}$, thereby losing the characteristic MLCT band. Right: Evolution of the UV-vis spectrum of a solution of $[Ru(bpy)_3]Cl_2$ (80 µM), **1a** (18 mM) and Umemoto's reagent (20 mM). The spectrum converts to a different species over time but does not decrease substantially in intensity (an initial dip is observed due to a photo-

stationary state being reached). This indicates the catalyst is turning over and also that it decomposes over time. **Black**: first spectrum, **grey**: intermediate spectrum, **red**: final spectrum.

Stern-Volmer analysis (Figure 3.5) shows that the reaction commences by oxidative quenching to form $[Ru(bpy)_3]^{3+}$ and a CF_3 radical which adds to the double bond. The resulting benzylic radical is then oxidized by Umemoto's reagent (radical propagation) or by $[Ru(bpy)_3]^{3+}$ (termination) following ring-closure to yield **2a** (Scheme 3.1, see Introduction).

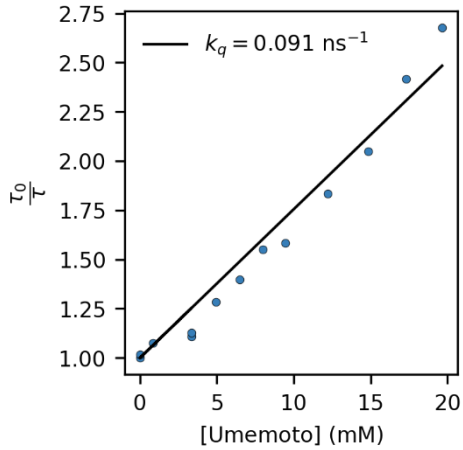

Figure 3.5. Stern-Volmer plot of the quenching of $[Ru(bpy)_3]Cl_2$ by Umemoto's reagent. Under the initial catalytic conditions, Umemoto's reagent quenches 60% of the ^{3}MLCT-state of $[Ru(bpy)_3]^{2+}$. Compound **1a** does not quench the excited state.

Scope for the photocatalytic formation of 6MCCs

The optimized reaction conditions (Table 3.1, entry 17) were then applied to the synthesis of a wider scope of 6MCCs (Scheme 3.3, **2a**-**2o**). Various mono-γ-aryl allylic carbonates could be converted into their respective 6MCCs in moderate to appreciably high NMR yields of up to 84% (**2a**-**2k**), with lower yields observed for substrates carrying electron-withdrawing substituents (**2e** and **2f**) and those equipped with a 4-methoxy-aryl (**2g**), 2-naphthyl (**2i**) or a heterobicycle (**2k**). The exact influence of each aryl substituent on the stability and reactivity of the benzylic radical/cation intermediates depicted in Scheme 3.1 is not entirely clear. However, we further noted that a di-γ-substitution in the allylic carbonate (*cf.*, syntheses of **2l**–**2o**) was beneficial providing among the highest 6MCC NMR (up to 85%) and isolated yields (up to 72%) suggesting a better control over the reactivity of the aforementioned intermediates. The larger discrepancy between some of the NMR and isolated yields is explained by the fact that some of these 6MCCs proved to be rather sensitive during column purification, yielding substantial

amounts of 1,3-diol byproduct (hydrolysis) provoked by the acidic sites of the SiO_2 stationary phase. Therefore, all 6MCC products were isolated as quickly as possible, minimizing the contact-time with the SiO_2-based column material.

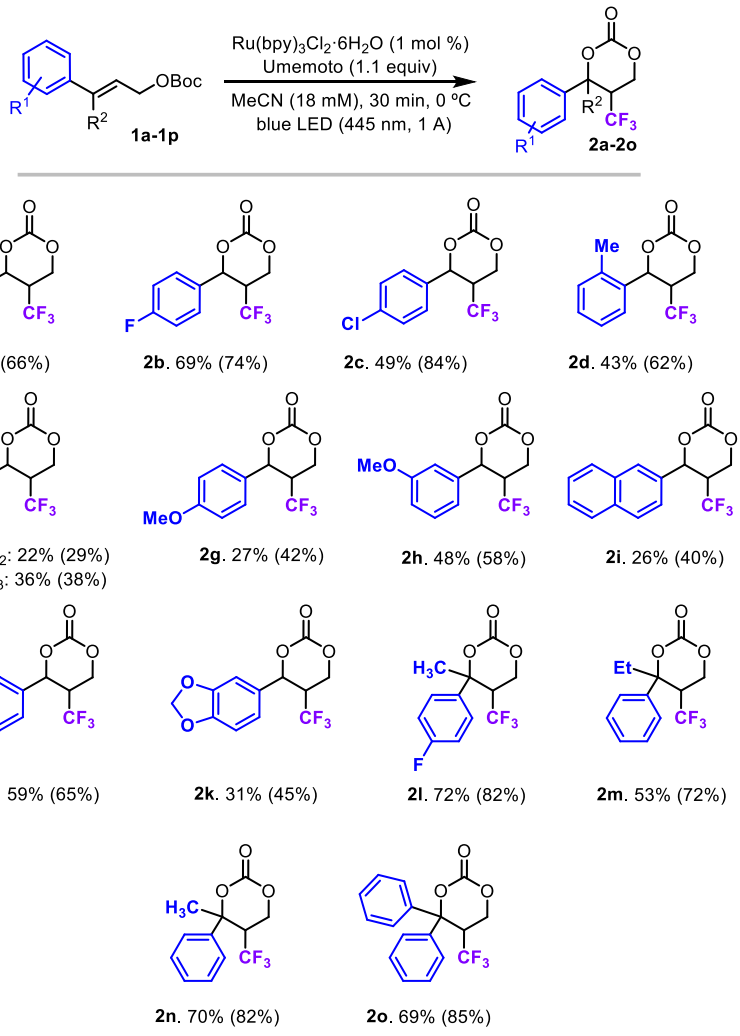

Scheme 3.3. Product scope for the photocatalytic formation of 6MCCs providing the products **2a-2o**. Yields are of the isolated products, with the NMR yield in parentheses using 1,3,5-tris(trifluoromethyl)benzene as internal standard.

All 6MCC products were fully characterized by spectroscopic and spectrometric analyses (see Experimental Section). Supplementing this, crystalline material was obtained from two different product samples. Although **2a** was initially isolated as a viscous oil, a crystallization

attempt that covered a period of several months produced a crystalline compound that was subjected to X-ray crystallography (Figure 3.6). Surprisingly, the structure of an unexpected sodium borate ion pair was revealed that incorporates four "decarbonylated" molecules of **2a**. Due to this serendipitous result, an *anti*-positioning between the CF_3 and aryl group could be determined suggesting a preferred mutual orientation in the ring-closure step leading to 6MCC **2a** (Scheme 3.1, see the Introduction).

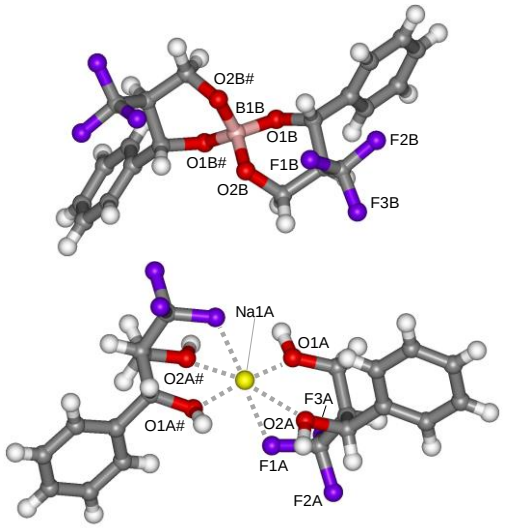

Figure 3.6. Molecular structure determined for sodium borate derived from **2a**. Top: borate anion based on two decarbonylated molecules of **2a**. Below: sodium cation stabilized by two 1,3-diols derived from **2a** showing weak F···Na cation interactions. Selected bond lengths (Å) and angles (º) with esd´s in parentheses: B1B–O1B = B1B–O1B# = 1.465(3), B1B-O2B = B1B-O2B# = 1.474(3), Na1A–O1A = 2.2119(19), Na1A–O1A# = 2.3016(19), Na1A–O2A = 2.227(2), Na1A–O2A# = 2.255(2), Na1A–F1A = 2.5089(18); O1B–B1B–O1B# = 107.2(3), O2B–B1B–O2B# = 106.2(3), O1B–B1B–O2B = 108.73(10), O1B–B1B–O2B# = 113.03(9), O1A–Na1A-O1A# = 102.93(10), O2A–Na1A-O2A# = 94.05(11), O1A–Na1A-O2A = 81.27(6), O1A–Na1A-O2A# = 171.00(8).

The molecular connectivity of carbonate product **2o** was confirmed by X-ray analysis (Figure 3.7). The structure illustrates that the three carbonate ring substituents increase the steric requirements around the carbonate unit, which may affect its reactivity in ROP studies (*vide infra*).

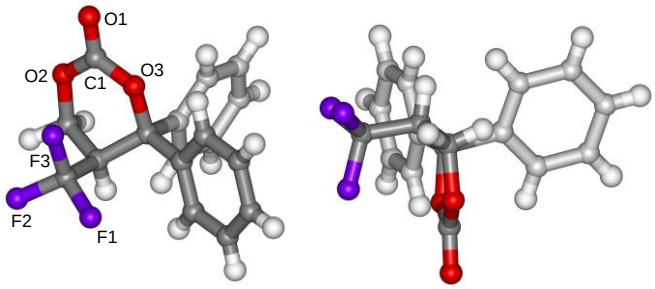

Figure 3.7. Molecular structure determined for 6MCC **2o**. Left: front view. Right: side view. Selected bond lengths (Å) and angles (º) with esd's in parentheses: O1–C1 = 1.2048(10), O2–C1 = 1.3388(9), O3–C1 = 1.3317(10); O2–C1–O3 = 119.95(7), O1–C1–O2 = 119.48(7), O2–C1–O3 = 119.95(7).

ROP potential evaluation of 6MCCs

We investigated the possibility of using cyclic carbonates **2** as monomers in ROP reactions (Table 3.3). Previous investigations showed that 1,5,7-triazabicyclo[4.4.0]dec-5-ene (TBD) is an efficient organocatalyst for the ROP of 6MCCs.[30] Thus, the TBD-catalyzed ROP of **2a**, using BnOH as initiator, was first investigated to examine the potential of the new 6MCCs in the preparation of polycarbonates (Table 3.3, next page). The reaction was first conducted in DCM under similar conditions to those used for other 6MCCs.[15,16] Low conversion of **2a** was observed after 20 h, while the conversion level increased to 34% in toluene (Entries 1 and 2). An increase in the catalyst loading to 2 mol% resulted in higher conversion of **2a** (Entry 3). Attempts to obtain full conversion by increasing the reaction temperature up to 100 ºC led to similar monomer conversion but lower polycarbonate selectivity (45%) as a result of hydrolysis producing a 1,3-diol byproduct (Entry 4). Instead, higher monomer conversion could be obtained by prolonging the reaction time, maintaining a polycarbonate selectivity of >99% and affording **P(2a)** with a M_n of 5.2 kg·mol^{-1} (Entry 5).

[30] Helou M.; Miserque O.; Brusson J.-M.; Carpentier J.-F.; Guillaume S. M. *Chem. Eur. J.* **2010**, *16*, 13805–13813.

Table 3.3. Ring-opening polymerization (ROP) of 6MCCs **2a**, **2i** and **2j** promoted by TBD/BnOH.[a]

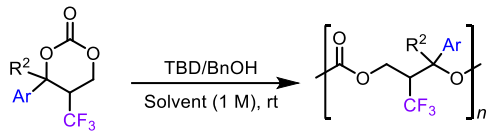

2a, 2i, 2j: R^2 = H
2n, 2o: R^2 = Me, Ar

P(2a): R^2 = H, Ar = Ph
P(2i): R^2 = H, Ar = 2-naphthyl
P(2j): R^2 = H, Ar = 4-biphenyl

Entry	**2**	TBD (mol%)	Time (h)	Conversion (%)[b]	M_n[c]	$Đ$[c]
1[d]	**2a**	1	20	17	–	–
2	**2a**	1	20	34	–	–
3	**2a**	2	20	62	3.1	1.39
4[e]	**2a**	2	20	58	–	–
5[f]	**2a**	1	60	78	5.2	1.42
6[g]	**2i**	1	76	83	5.0	1.23
7[h]	**2j**	1	66	59	2.6	1.41

[a] Monomer **2** ($8.1 \cdot 10^{-5}$ mol), TBD/BnOH = 1/1, toluene (82 µL; 1.0 M), rt. [b] Determined by ^{1}H NMR ($CDCl_3$). [c] Determined by GPC in THF calibrated with polystyrene standards. M_n values in kg·mol^{-1}. [d] The solvent was dichloromethane. [e] Reaction temperature was 100 ºC. [f] Amount of **2a** was 100 mg ($4.1 \cdot 10^{-4}$ mol). [g] Amount of **2i** was $1.1 \cdot 10^{-4}$ mol. [h] Amount of **2j** was $2.6 \cdot 10^{-4}$ mol.

Following these results obtained with monomer **2a**, other cyclic carbonates with different aryl substitutions were then tested under the same conditions as monomer **2a** (Entry 5). Naphthyl (**2i**) and biphenyl (**2j**) substituted 6MCCs were converted into oligo/polycarbonates **P(2i)** and **P(2j)** with moderate to high conversion. The molecular weight distributions ($Đ$) were comparable with that of **P(2a)** (Entries 6 and 7), but the M_n value measured for **P(2j)** was substantially lower (2.6 kg·mol^{-1}). Unfortunately, ROP attempts using either carbonates **2n** or **2o** containing quaternary carbon centers only led to the hydrolysis products. This observation is in line with the X-ray analysis of **2o,** which reveals a steric impediment around the carbonate carbon center that likely plays a role in inhibiting the ROP process.

The new **P(2a)**, **P(2i)** and **P(2j)** were characterized by NMR confirming the formation of the desired polycarbonates. Diagnostic benzylic signals were detected between 5.0 and 5.1 ppm in the ^{1}H NMR spectra and were assigned to the benzyl alcohol initiator. Decomposition temperatures ($T_d^{5\%}$) were determined by thermogravimetic analyses (TGA) under nitrogen and values of 182, 194 and 186 ºC were recorded for **P(2a)**, **P(2i)** and **P(2j)**, respectively. Despite

the fact that these values are not very high, they are close to the decomposition temperature of poly(propylene carbonate) having a similar (low) molecular weight.[31]

Glass transition temperatures (T_g's) of **P(2a)**, **P(2i)** and **P(2j)** were determined by differential scanning calorimetry (DSC) providing values of 37, 65 and 56 ºC, respectively. Comparison of these values with the T_g (–15 ºC)[32] of the simplest unsubstituted poly(trimethylene carbonate), PTMC, demonstrates that introducing substituents in the main chain of the oligo/polycarbonate reduces its flexibility resulting in substantially higher T_g values.

3.3. Conclusions

In this chapter, we present a new synthetic route for the formation of substituted 6MCCs through a photocatalytic conversion of readily available γ-substituted allylic carbonates. A good scope of 6MCCs was produced with different degrees of carbonate ring substitution. Additional ROP studies have established that these 6MCCs are indeed competent monomers for new types of polycarbonates with glass transitions that are at markedly higher than measured for the parent PTMC. The degree of substitution and identity of the ring substituents are likely the key elements to developing modular type polycarbonates from larger ring cyclic carbonates with improved thermal properties.

3.4. Experimental Section

General considerations

Solvents used in the synthesis of the complexes were dried using an Innovative Technology PURE SOLV solvent purification system. Solvents used in the catalytic screening were used as received. ^{1}H, ^{13}C and 2D NMR spectra were recorded on a Bruker AV-300, AV-400 or AV-500 spectrometer, and signals are referenced to the residual solvent peak. FT-IR measurements were carried out using a Bruker Optics FTIR Alpha spectrometer. Mass spectrometric analyses and X-ray diffraction analysis were performed by the Research Support Area (RSA) at ICIQ.

[31] Phillips O.; J Schwartz. M.; Kohl P. A. *Polym. Degrad. Stab.* **2016**, *125*, 129–139.
[32] Zhu K. J.; Hendren R. W.; Jensen K.; Pitt C. G. *Macromolecules* **1991**, *24*, 1736–1740.

General procedure for the synthesis of allyl *tert*-butyl carbonates

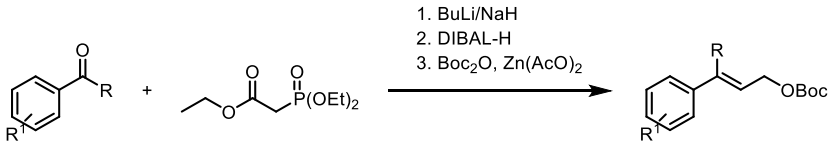

Allylic alcohols were prepared following published procedures using ketones[33] and aldehydes[34]. Protection of the allylic alcohols with a di-*tert*-butyl dicarbonate group was carried out following a literature procedure.[35]

General procedure for the synthesis of the 6MCCs

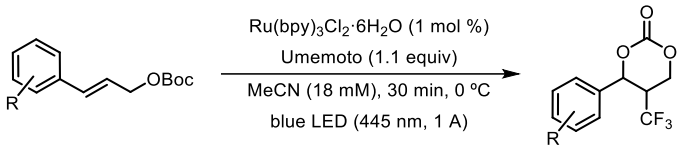

In a flat bottom Schlenk vessel, Umemoto's reagent (5-(trifluoromethyl)dibenzothiophenium trifluoromethanesulfonate) (0.99 mmol, 1.1 equiv) and $Ru(bpy)_3Cl_2 \cdot 6H_2O$ (0.9 μmol, 1 mol%) were introduced, after which three cycles of vacuum/N_2 were applied. The reagents were then dissolved in dry acetonitrile (5 mL) and finally *tert*-butyl cinnamyl carbonate (0.90 mmol, 21.1 mg) was added. The reaction mixture was allowed to reach the desired temperature in the photoreactor until a homogeneous phase was obtained and then the reaction mixture was irradiated for 30 minutes. Hereafter, the mixture was combined with dichloromethane (10 mL) and quenched with water, the aqueous phase was extracted with dichloromethane, dried over Na_2SO_4 and evaporated to dryness. The crude product was purified by column chromatography (hexane:EtOAc, gradient from 4:1 to 2:1) obtaining a colorless oil (13.7 mg, 62% yield). A scale up of product **2a**, for instance, was realized by performing several parallel reactions and combining the crude mixtures in a joint work up allowing to isolate a quantity of **2a** of >100 mg.

Analytical data for allylic *tert*-butyl carbonates

Note that relevant citations are provided for all the known carbonate precursors.

[33] Mantilli, L.; Gérard, D.; Torche, S.; Besnard, C.; Mazet, C. *Angew. Chem. Int. Ed.* **2009**, *48*, 5143–5147.
[34] Yang, B.; Wang, Z.-X. *Org. Lett.* **2019**, *21*, 7965–7969.
[35] Bartoli, G.; Bosco, M.; Carlone, A.; Dalpozzo, R.; Locatelli, M.; Melchiorre, P.; Sambri, L. *J. Org. Chem.* **2006**, *71*, 9580–9588.

Compound **1a**:[36]

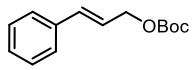

^{1}H NMR (400 MHz, $CDCl_3$) δ 7.46 – 7.24 (m, 5H), 6.69 (dt, *J* = 15.8, 1.4 Hz, 1H), 6.32 (dt, *J* = 15.9, 6.4 Hz, 1H), 4.74 (dd, *J* = 6.5, 1.4 Hz, 2H), 1.53 (s, 9H) ppm.

Compound **1b**:[36]

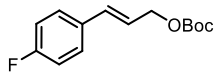

^{1}H NMR (500 MHz, $CDCl_3$) δ 7.39 – 7.31 (m, 2H), 7.05 – 6.97 (m, 2H), 6.63 (d, *J* = 15.9 Hz, 1H), 6.21 (dt, *J* = 15.9, 6.5 Hz, 1H), 4.70 (dd, *J* = 6.4, 1.4 Hz, 2H), 1.50 (s, 9H) ppm.

Compound **1c**:[36]

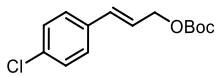

^{1}H NMR (500 MHz, $CDCl_3$) δ 7.34 – 7.24 (m, 4H), 6.61 (d, *J* = 15.9 Hz, 1H), 6.26 (dt, *J* = 15.9, 6.4 Hz, 1H), 4.70 (dd, *J* = 6.4, 1.4 Hz, 2H), 1.50 (s, 9H) ppm.

Compound **1d**:

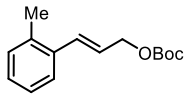

Yield: 217.8 mg (65%). **^{1}H NMR** (500 MHz, $CDCl_3$) δ 7.17 – 7.12 (m, 3H), 7.07 – 7.00 (m, 1H), 6.59 (d, *J* = 15.9 Hz, 1H), 6.24 (dt, *J* = 15.8, 6.5 Hz, 1H), 4.67 (dd, *J* = 6.4, 1.4 Hz, 2H), 2.30 (d, *J* = 0.8 Hz, 3H), 1.46 (s, 9H) ppm. **^{13}C NMR** (126 MHz, $CDCl_3$) δ 153.5, 138.2, 136.3, 134.7, 129.0, 128.6, 127.5, 123.9, 122.8, 82.3, 67.6, 27.9, 21.5 ppm. **HRMS** (ESI+, MeOH) *m/z* calcd. for ($C_{15}H_{20}NaO_3$), $(M+Na)^+$, 271.1305; found: 271.1299.

[36] Mori-Quiroz, L. M.; Londhe, S. S.; Clift, M. D. *J. Org. Chem.* **2020**, *85*, 14827–14846.

Compound **1e**:[36]

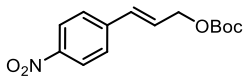

^{1}H NMR (500 MHz, $CDCl_3$) δ 8.19 – 8.13 (m, 2H), 7.53 – 7.47 (m, 2H), 6.71 (d, *J* = 16.1 Hz, 1H), 6.45 (dt, *J* = 16.0, 6.0 Hz, 1H), 4.75 (dd, *J* = 5.9, 1.5 Hz, 2H), 1.49 (s, 9H) ppm.

Compound **1f**:[37]

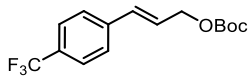

^{1}H NMR (300 MHz, $CDCl_3$) δ 7.36 – 7.23 (m, 4H), 6.62 (dt, *J* = 15.9, 1.4 Hz, 1H), 6.26 (dt, *J* = 15.9, 6.4 Hz, 1H), 4.70 (dd, *J* = 6.4, 1.3 Hz, 2H), 1.50 (s, 9H) ppm.

Compound **1g**:[37]

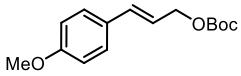

^{1}H NMR (500 MHz, $CDCl_3$) δ 7.35 – 7.29 (m, 2H), 6.89 – 6.81 (m, 2H), 6.61 (d, *J* = 15.9 Hz, 1H), 6.16 (dt, *J* = 15.9, 6.6 Hz, 1H), 4.69 (dd, *J* = 6.6, 1.3 Hz, 1H), 3.80 (s, 3H), 1.50 (s, 9H) ppm.

Compound **1h**:[36]

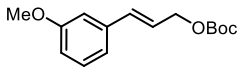

^{1}H NMR (300 MHz, $CDCl_3$) δ 7.34 – 7.23 (m, 1H), 7.08 – 6.94 (m, 2H), 6.90 (d, *J* = 8.8 Hz, 1H), 6.69 (dt, *J* = 15.9, 1.4 Hz, 1H), 6.34 (dt, *J* = 15.9, 6.4 Hz, 1H), 4.77 (dd, *J* = 6.4, 1.3 Hz, 2H), 3.86 (s, 2H), 1.55 (s, 9H) ppm.

[37] Jiang, X.; Beiger, J. J.; Hartwig, J. F. S. *J. Am. Chem. Soc.* **2017**, *139*, 87–90.

Compound **1i**:[37]

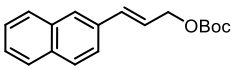

^{1}H NMR (400 MHz, $CDCl_3$) δ 7.83 – 7.73 (m, 4H), 7.62 – 7.57 (m, 1H), 7.50 – 7.41 (m, 2H), 6.84 (d, *J* = 15.8 Hz, 0H), 6.42 (dt, *J* = 15.9, 6.4 Hz, 1H), 4.78 (dd, *J* = 6.5, 1.4 Hz, 2H), 1.52 (s, 9H) ppm.

Compound **1j**:

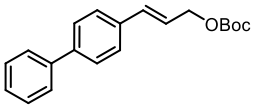

Yield: 268.8 mg (91%). **^{1}H NMR** (400 MHz, $CDCl_3$) δ 7.65 – 7.36 (m, 9H), 6.72 (dt, *J* = 15.9, 1.4 Hz, 1H), 6.35 (dt, *J* = 15.9, 6.4 Hz, 1H), 4.76 (dd, *J* = 6.5, 1.3 Hz, 2H), 1.53 (s, 9H) ppm. **^{13}C NMR** (101 MHz, $CDCl_3$) δ 153.5, 141.0, 140.7, 135.4, 134.1, 128.9, 127.5, 127.4, 127.2, 127.1, 123.1, 82.4, 67.6, 27.9 ppm. **HRMS** (ESI+, MeOH) *m/z* calcd. for ($C_{20}H_{22}NaO_3$), $(M+Na)^+$, 333.1461; found: 333.1460.

Compound **1k**:[38]

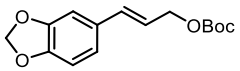

^{1}H NMR (400 MHz, $CDCl_3$) δ 6.96 – 6.71 (m, 3H), 6.57 (dt, *J* = 15.8, 1.3 Hz, 1H), 6.12 (dt, *J* = 15.8, 6.6 Hz, 1H), 5.95 (s, 2H), 4.68 (dd, *J* = 6.6, 1.3 Hz, 2H), 1.50 (s, 9H) ppm.

[38] Hutchings-Goetz, L. S.; Yang, C.; Fyfe, J. W. B.; Snaddon, T. N. *Angew. Chem. Int. Ed.* **2020**, *59*, 17556–17564.

Compound **1l**:[39]

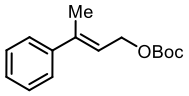

^{1}H NMR (500 MHz, $CDCl_3$) δ 7.43 – 7.37 (m, 2H), 7.37 – 7.29 (m, 2H), 7.29 – 7.23 (m, 1H), 5.92 (tq, *J* = 6.9, 1.4 Hz, 1H), 4.81 – 4.76 (m, 2H), 2.12 (dt, *J* = 1.5, 0.7 Hz, 3H), 1.50 (s, 9H) ppm.

Compound **1m**:

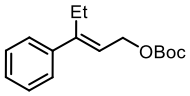

Yield: 307.2 mg (95%). **^{1}H NMR** (400 MHz, $CDCl_3$) Major isomer (*E*): δ 7.43 – 7.23 (m, 5H), 5.78 (t, *J* = 7.0 Hz, 1H), 4.78 (d, *J* = 7.0 Hz, 2H), 2.57 (q, *J* = 7.5 Hz, 0H), 1.50 (s, 9H), 1.00 (t, *J* = 7.5 Hz, 3H) ppm. **^{13}C NMR** (101 MHz, $CDCl_3$) Major isomer (*E*): δ 153.7, 147.3, 141.8, 128.4, 127.5, 126.6, 120.9, 82.2, 63.8, 27.9, 23.6, 13.9 ppm. **HRMS** (ESI+, MeOH) *m/z* calcd. for ($C_{16}H_{22}NaO_3$), $(M+Na)^+$, 285.1461; found: 285.1472. Note that the (*Z*)-isomer was present in small amounts.

Compound **1n**:

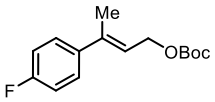

Yield: 298.6 mg (93%). **^{1}H NMR** (300 MHz, $CDCl_3$) δ 7.42 – 7.29 (m, 2H), 7.07 – 6.93 (m, 2H), 5.86 (tq, *J* = 7.0, 1.3 Hz, 1H), 4.76 (dt, *J* = 7.0, 0.8 Hz, 2H), 2.09 (dt, *J* = 1.5, 0.8 Hz, 3H), 1.50 (s, 9H) ppm. **^{19}F NMR** (376 MHz, $CDCl_3$) δ -115.09 – -115.29 (m) ppm. **^{13}C NMR** (101 MHz, $CDCl_3$) δ 162.5 (d, *J* = 246.6 Hz), 153.7, 139.6, 138.7 (d, *J* = 3.3 Hz), 127.6 (d, *J* = 7.9 Hz), 121.2 (d, *J* = 1.4 Hz), 115.2 (d, *J* = 21.4 Hz). 82.3, 64.0, 27.91, 16.5 ppm. **HRMS** (ESI+, MeOH) *m/z* calcd. ($C_{15}H_{19}NaO_3$) 289.1210; $(M+Na)^+$ found: 289.1214.

[39] Lin, L.-Z.; Che, Y.-Y.; Bai, P.-B.; Feng, C. *Org. Lett.* **2019**, *21*, 7424–7429.

Compound **1o**:

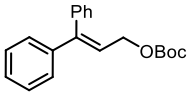

Yield: 221.3 mg (75%). **^{1}H NMR** (400 MHz, $CDCl_3$) δ 7.57 – 7.11 (m, 10H), 6.25 (t, *J* = 7.0 Hz, 1H), 4.69 (d, *J* = 7.0 Hz, 2H), 1.53 (s, 9H) ppm. **^{13}C NMR** (101 MHz, $CDCl_3$) δ 153.6, 146.5, 141.6, 138.7, 129.8, 128.4, 128.3, 128.0, 127.9, 127.8, 122.3, 82.3, 65.1, 27.9 ppm. **HRMS** (ESI+, MeOH) *m/z* calcd. ($C_{20}H_{22}NaO_3$), $(M+Na)^+$, 333.1461; found: 333.1472.

Six-membered ring cyclic carbonates, 6MCCs

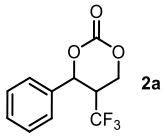

2a

Yield: 13.7 mg, 62% (66% by NMR). **^{1}H NMR** (400 MHz, $CDCl_3$) δ 7.53 – 7.37 (m, 3H), 7.36 – 7.32 (m, 2H), 5.73 (d, *J* = 5.0 Hz, 1H), 4.64 – 4.46 (m, 2H), 3.08 – 2.93 (m, 1H) ppm. **^{19}F NMR** (376 MHz, $CDCl_3$) δ -68.11 (d, *J* = 8.3 Hz) ppm. **^{13}C NMR** (101 MHz, $CDCl_3$) δ 147.3, 136.1, 129.8, 129.4, 125.7, 124.7 (q, *J* = 280.3 Hz), 77.9 (q, *J* = 2.2 Hz), 63.0 (q, *J* = 2.9 Hz), 42.9 (q, *J* = 27.4 Hz) ppm. **IR** (neat) ν = 1761 (C=O) cm^{-1}. **HRMS** (ESI+, MeOH) *m/z* calcd. ($C_{11}H_9F_3NaO_3$), $(M+Na)^+$, 269.0396; found: 269.0390.

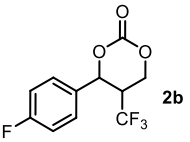

2b

Yield: 16.3 mg, 69% (74% by NMR). **^{1}H NMR** (400 MHz, $CDCl_3$) δ 7.39 – 7.29 (m, 2H), 7.21 – 7.04 (m, 2H), 5.67 (d, *J* = 6.1 Hz, 1H), 4.64 – 4.48 (m, 2H), 3.09 – 2.94 (m, 1H) ppm. **^{19}F NMR** (376 MHz, $CDCl_3$) δ -68.16 (d, *J* = 8.1 Hz), -110.91 – -111.07 (m) ppm. **^{13}C NMR** (101 MHz, $CDCl_3$) δ163.5 (d, *J* = 249.9 Hz), 147.3, 131.8 (d, *J* = 3.3 Hz), 128.1 (d, *J* = 8.6 Hz), 124.5 (q, *J* = 280.2 Hz), 116.5 (d, *J* = 22.1 Hz), 77.6 (q, *J* = 2.2 Hz), 63.3 (q, *J* = 3.0 Hz), 43.2 (q, *J* = 27.2 Hz) ppm. **IR** (neat) ν 1762 (C=O) cm^{-1}. **HRMS** (ESI+, MeOH) *m/z* calcd. ($C_{11}H_8F_4NaO_3$), $(M+Na)^+$, 287.0302; found: 287.0302.

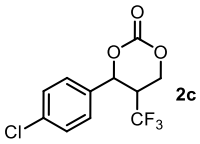

2c

Yield: 12.3 mg, 49% (84% by NMR). **^{1}H NMR** (500 MHz, $CDCl_3$) δ 7.45 – 7.40 (m, 2H), 7.31 – 7.21 (m, 2H), 5.65 (d, *J* = 5.8 Hz, 1H), 4.59 – 4.46 (m, 2H), 3.04 – 2.92 (m, 1H) ppm. **^{19}F NMR** (471 MHz, $CDCl_3$) δ -68.20 (d, *J* = 8.2 Hz) ppm. **^{13}C NMR** (101 MHz, $CDCl_3$) δ 147.2, 136.0, 134.4, 129.7, 124.5 (q, *J* = 280.3 Hz), 127.4, 77.6 – 77.3 (m), 63.3 (q, *J* = 2.9 Hz), 43.0 (q, *J* = 27.4 Hz) ppm. **IR** (neat) ν 1768 (C=O) cm^{-1}. **HRMS** (ESI+, MeOH) *m/z* calcd. ($C_{11}H_8ClF_3NaO_3$), $(M+Na)^+$, 303.0006; found: 302.9992.

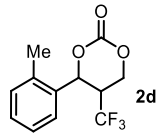

2d

Yield: 10.2 mg, 43% (62% by NMR). **^{1}H NMR** (500 MHz, $CDCl_3$) δ 7.37 – 7.30 (m, 1H), 7.28 – 7.20 (m, 1H), 7.15 – 7.04 (m, 2H), 5.70 (d, *J* = 4.7 Hz, 1H), 4.58 – 4.46 (m, 2H), 3.04 – 2.93 (m, 1H), 2.39 (s, 3H) ppm. **^{19}F NMR** (471 MHz, $CDCl_3$) δ -68.58 (d, *J* = 8.4 Hz) ppm. **^{13}C NMR** (101 MHz, $CDCl_3$) δ 147.4, 139.4, 136.1, 130.5, 128.9, 126.2, 126.2 (q, *J* = 280.4 Hz), 122.7, 77.8 (q, *J* = 2.2 Hz), 62.9 (q, *J* = 2.9 Hz), 42.8 (q, *J* = 27.4 Hz). 21.5 ppm. **IR** (neat) ν 1763 (C=O) cm^{-1}. **HRMS** (ESI+, MeOH) *m/z* calcd. ($C_{12}H_{11}F_3NaO_3$), $(M+Na)^+$, 283.0552; found: 283.0549.

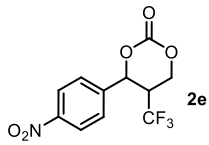

2e

Yield: 5.7 mg, 22% (29% by NMR). **^{1}H NMR** (400 MHz, $CDCl_3$) δ 8.37 – 8.30 (m, 2H), 7.64 – 7.48 (m, 2H), 5.78 (d, *J* = 6.2 Hz, 1H), 4.66 – 4.48 (m, 2H), 3.14 – 2.99 (m, 1H) ppm. **^{19}F NMR** (376 MHz, $CDCl_3$) δ -67.93 (d, *J* = 8.0 Hz) ppm. **^{13}C NMR** (101 MHz, $CDCl_3$) δ 148.9, 146.7, 127.3, 126.0 (q, *J* = 263.2 Hz), 124.7, 77.1 (q, *J* = 2.1 Hz), 66.7 – 58.4 (m), 43.2 (q, *J* = 27.7 Hz) ppm. **IR** (neat) ν 1767 (C=O) cm^{-1}. **HRMS** (ESI+, MeOH) *m/z* calcd. ($C_{11}H_8F_3NNaO_5$), $(M+Na)^+$, 314.0247; found: 314.0243.

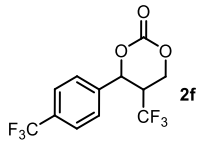

2f

Yield: 10.2 mg, 36% (38% by NMR). **^{1}H NMR** (400 MHz, $CDCl_3$) δ 7.73 (d, *J* = 8.2 Hz, 2H), 7.50 (d, *J* = 8.1 Hz, 2H), 5.76 (d, *J* = 5.7 Hz, 1H), 4.63 – 4.47 (m, 2H), 3.12 – 2.97 (m, 1H) ppm. **^{19}F NMR** (376 MHz, $CDCl_3$) δ -63.04, -68.22 (d, *J* = 8.2 Hz) ppm. **^{13}C NMR** (101 MHz, $CDCl_3$) δ 147.0, 139.9, 132.2 (q, *J* = 33.0 Hz), 126.5 (q, *J* = 4.1 Hz), 126.5(overlap), 125.8 (q, *J* = 280.2 Hz), 123.7 (q, *J* = 272.5 Hz), 77.3 (q, *J* = 2.1 Hz), 63.2 (q, *J* = 3.0 Hz), 43.1 (q, *J* = 27.6 Hz) ppm. **IR** (neat) ν 1765 (C=O) cm^{-1}. **HRMS** (ESI+, MeOH) *m/z* calcd. ($C_{12}H_8F_6NaO_3$), $(M+Na)^+$, 337.0270; found: 337.0268.

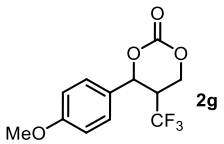

2g

Yield: 6.7 mg, 27% (42% by NMR). **^{1}H NMR** (500 MHz, $CDCl_3$) δ 7.29 – 7.23 (m, 2H), 6.99 – 6.91 (m, 2H), 5.64 (d, *J* = 5.9 Hz, 1H), 4.57 – 4.50 (m, 2H), 3.83 (s, 3H), 3.06 – 2.95 (m, 1H) ppm. **^{19}F NMR** (471 MHz, $CDCl_3$) δ -68.31 (d, *J* = 8.5 Hz) ppm. **^{13}C NMR** (101 MHz, $CDCl_3$) δ 160.7, 147.6, 127.8, 127.4, 124.6 (q, *J* = 280.3 Hz), 114.7, 78.0 (q, *J* = 2.2 Hz), 63.4 – 63.2 (m), 55.5, 43.0 (q, *J* = 27.1 Hz) ppm. **IR** (neat) ν 1761 (C=O) cm^{-1}. **HRMS** (ESI+, MeOH) *m/z* calcd. ($C_{12}H_{11}F_3NaO_4$), $(M+Na)^+$, 299.0502; found: 299.0496.

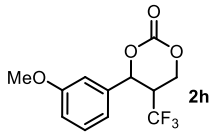

Yield: 12.0 mg, 48% (58% by NMR). **^{1}H NMR** (400 MHz, $CDCl_3$) δ 7.42 – 7.29 (m, 1H), 7.01 – 6.82 (m, 3H), 5.70 (d, *J* = 4.6 Hz, 1H), 4.63 – 4.45 (m, 2H), 3.82 (s, 3H), 3.06 – 2.92 (m, 1H) ppm. **^{19}F NMR** (376 MHz, $CDCl_3$) δ -68.61 (d, *J* = 8.4 Hz) ppm. **^{13}C NMR** (126 MHz, $CDCl_3$) δ 160.4, 147.2, 137.7, 130.6, 124.7 (q, *J* = 280.4 Hz), 117.6, 114.9, 111.6, 77.6 (q, *J* = 2.3 Hz), 62.9 (q, *J* = 3.0 Hz), 55.5, 42.8 (q, *J* = 27.4 Hz) ppm. **IR** (neat) ν 1763 (C=O) cm^{-1}. **HRMS** (ESI+, MeOH) *m/z* calcd. ($C_{12}H_{11}F_3NaO_4$), $(M+Na)^+$, 299.0502; found: 299.0502.

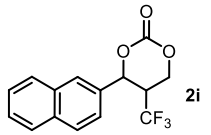

Yield: 6.9 mg, 26% (40% by NMR). **^{1}H NMR** (400 MHz, $CDCl_3$) δ 7.97 – 7.75 (m, 4H), 7.62 – 7.46 (m, 2H), 7.46 – 7.31 (m, 1H), 5.89 (d, *J* = 4.9 Hz, 1H), 4.64 – 4.46 (m, 2H), 3.20 – 3.01 (m, 1H) ppm. ^{19}F NMR (376 MHz, $CDCl_3$) δ -68.42 (d, *J* = 8.3 Hz) ppm. **^{13}C NMR** (101 MHz, $CDCl_3$) δ 147.4, 133.6, 133.2, 133.0, 129.7, 128.4, 127.9, 127.4, 127.3, 125.6, 124.7 (q, *J* = 280.8 Hz), 122.3, 78.0 (q, *J* = 2.2 Hz), 63.0 (q, *J* = 2.9 Hz), 42.7 (q, *J* = 27.5 Hz) ppm. **IR** (neat) ν 1762 (C=O) cm^{-1}. **HRMS** (ESI+, MeOH) *m/z* calcd. ($C_{15}H_{11}F_3NaO_3$), $(M+Na)^+$, 319.0552; found: 319.0559.

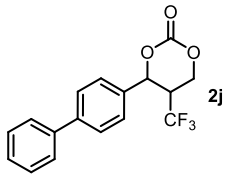

Yield: 17.0 mg, 59% (65% by NMR). **^{1}H NMR** (400 MHz, $CDCl_3$) δ 7.73 – 7.35 (m, 9H), 5.77 (d, *J* = 5.1 Hz, 1H), 4.64 – 4.50 (m, 2H), 3.13 – 2.99 (m, 1H) ppm. **^{19}F NMR** (376 MHz, $CDCl_3$) δ -68.38 (d, *J* = 8.3 Hz) ppm. **^{13}C NMR** (101 MHz, $CDCl_3$) δ 147.3, 142.8, 139.9, 134.9, 129.1, 128.1, 127.2, 126.2, 24.7 (q, *J* = 280.5 Hz), 77.8 (q, *J* = 2.1 Hz), 63.1 (q, *J* = 3.0 Hz), 42.9 (q, *J* = 27.4 Hz) ppm. **IR** (neat) ν 1760(C=O) cm^{-1}. **HRMS** (ESI+, MeOH) *m/z* calcd. ($C_{17}H_{14}F_3O_3$), $(M+Na)^+$, 323.0890; found: 323.0889.

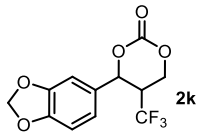

2k

Yield: 8.0 mg, 31% (45% by NMR). **^{1}H NMR** (400 MHz, $CDCl_3$) δ 6.90 – 6.70 (m, 3H), 6.01 (s, 2H), 5.58 (d, *J* = 6.0 Hz, 1H), 4.53 (d, *J* = 5.6 Hz, 2H), 3.08 – 2.93 (m, 1H) ppm. **^{19}F NMR** (376 MHz, $CDCl_3$) δ -68.27 (d, *J* = 8.1 Hz) ppm. **^{13}C NMR** (101 MHz, $CDCl_3$) δ 148.9, 148.7, 147.4, 129.5, 124.5 (q, *J* = 280.3 Hz), 120.2, 108.8, 106.2, 101.9, 78.1 (q, *J* = 2.2 Hz), 63.3 (q, *J* = 3.1 Hz), 43.1 (q, *J* = 27.2 Hz) ppm. **IR** (neat) ν 1759 (C=O) cm^{-1}. **HRMS** (ESI+, MeOH) *m/z* calcd. ($C_{12}H_9F_3NaO_5$), $(M+Na)^+$, 313.0294; found: 313.0291.

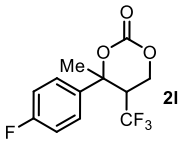

2l

Yield: 18.0 mg, 72% (82% by NMR). **^{1}H NMR** (400 MHz, $CDCl_3$) δ 7.38 – 7.29 (m, 2H), 7.19 – 7.08 (m, 2H), 4.53 (dd, *J* = 12.3, 2.6 Hz, 1H), 4.20 – 4.10 (m, 1H), 3.07 – 2.95 (m, 1H), 1.92 – 1.82 (m, 3H) ppm. **^{19}F NMR** (376 MHz, $CDCl_3$) δ -63.29 (d, *J* = 8.6 Hz), -112.44 – -112.83 (m) ppm. **^{13}C NMR** (101 MHz, $CDCl_3$) δ 162.8 (d, *J* = 249.5 Hz), 147.0, 138.4 (d, *J* = 3.4 Hz), 25.8 (d, *J* = 8.4 Hz), 125.0 (q, *J* = 281.8 Hz), 116.6 (d, *J* = 21.9 Hz), 83.8, 63.7 (q, *J* = 3.4 Hz), 44.3 (q, *J* = 26.9 Hz), 27.4 (d, *J* = 2.2 Hz) ppm. **IR** (neat) ν 1751 (C=O) cm^{-1}. **HRMS** (ESI+, MeOH) *m/z* cacld. ($C_{12}H_{10}F_4NaO_3$), $(M+Na)^+$, 301.0458; found: 301.0467.

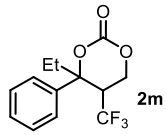

Yield: 13.0 mg, 53% (72% by NMR). **^{1}H NMR** (400 MHz, $CDCl_3$) δ 7.58 – 7.22 (m, 5H), 4.50 (dd, *J* = 12.3, 1.5 Hz, 1H), 4.13 – 4.03 (m, 1H), 3.04 – 2.92 (m, 1H), 2.40 – 2.25 (m, 1H), 2.17 – 2.03 (m, 1H), 0.71 (t, *J* = 7.3 Hz, 3H) ppm. **^{19}F NMR** (376 MHz, $CDCl_3$) δ -62.57 (d, *J* = 8.9 Hz). **^{13}C NMR** (101 MHz, $CDCl_3$) δ 147.3, 139.9, 129.6, 128.9, 125.2 (q, *J* = 282.1 Hz), 124.5, 87.0, 64.1 (q, *J* = 3.6 Hz), 44.1 (q, *J* = 26.5 Hz), 31.9 (q, *J* = 2.2 Hz), 7.3 ppm. **IR** (neat) ν 1758 (C=O) cm^{-1}. **HRMS** (ESI+, MeOH) *m/z* calcd. ($C_{13}H_{13}F_3NaO_3$), $(M+Na)^+$, 297.0709; found: 297.0719.

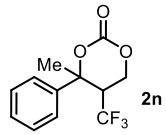

Yield: 16.5 mg, 70% (82% by NMR). **^{1}H NMR** (400 MHz, $CDCl_3$) δ 7.49 – 7.29 (m, 5H), 4.51 (dd, *J* = 12.4, 2.1 Hz, 1H), 4.17 – 4.07 (m, 1H), 3.09 – 2.96 (m, 1H), 1.86 (q, *J* = 1.9 Hz, 3H) ppm. **^{19}F NMR** (376 MHz, $CDCl_3$) δ -62.84 (d, *J* = 9.0 Hz) ppm. **^{13}C NMR** (101 MHz, $CDCl_3$) δ 147.2, 142.5, 129.6, 129.0, 125.1 (q, *J* = 281.7 Hz), 123.6, 84.1, 63.8 (q, *J* = 3.4 Hz), 44.1 (q, *J* = 26.7 Hz), 27.5 (q, *J* = 2.2 Hz) ppm. **IR** (neat) ν 1742 (C=O) cm^{-1}. **HRMS** (ESI+, MeOH) *m/z* calcd. ($C_{12}H_{11}F_3NaO_3$), $(M+Na)^+$, 283.0552; found: 283.0561.

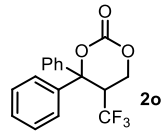

Yield: 20.0 mg, 69% (85% by NMR). **^{1}H NMR** (500 MHz, $CDCl_3$) δ 7.57 – 7.18 (m, 10H), 4.70 (dd, *J* = 12.4, 1.4 Hz, 0H), 4.60 – 4.51 (m, 1H), 3.84 – 3.74 (m, 1H) ppm. **^{19}F NMR** (471 MHz, $CDCl_3$) δ -62.43 (dd, *J* = 8.3, 1.6 Hz) ppm. **^{13}C NMR** (126 MHz, $CDCl_3$) δ 147.2, 141.8, 139.2, 130.1, 129.4, 128.9, 128.6, 127.2 – 123.1 (m), 125.1, 124.7, 85.4, 65.2 (q, *J* = 3.0 Hz), 43.0 (q, *J* = 25.8 Hz) ppm. **IR** (neat) ν 1752 (C=O) cm^{-1}. **HRMS** (ESI+, MeOH) *m/z* calcd. ($C_{17}H_{13}F_3NaO_3$), $(M+Na)^+$, 345.0709; found: 354.0705.

Typical procedure for the ROP of selected 6MCCs

In a glovebox, monomer **2a** (20 mg, 81 μmol) was introduced into a vial equipped with a magnetic stirrer. Then, benzyl alcohol (27 μL from a 59.2 mM solution in toluene, 1.62 μmol, 2.0 mol%) and TBD (55 μL of a 29.5 mM solution in toluene, 1.62 μmol, 2 mol%) were added in this sequence. Out of the glovebox, the vial was sealed with electric insulator tape. After stirring for 20 h, the reaction mixture was quenched with benzoic acid (30 μL of a 83.5 mM solution in toluene, 1.22 μmol) and a sample was analyzed by NMR ($CDCl_3$) to determine the monomer conversion. The polymer product was collected by precipitation from hexane and filtration. Conversion of **2a** under these conditions was 62%. M_n (GPC) =3.1 kDa. For the M_n and $Đ$ values of all three isolated polymers, see Table 3.3.

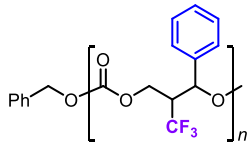

P(2a)

^{1}H NMR (δ ppm, 400 MHz, $CDCl_3$): 7.35 (bs, 4H, Ar-H); 7.23 (bs, 1H, Ar-H); 6.04 (bs, 1H, -$CHCF_3$-Ph**C*H***-O-); 5.19 (bs, Ph**C*H*$_2$**-** chain end); 4.48-4.43 (overlapped bs, 2H, -COO-**C*H*$_2$**-**$CHCF_3$-); 2.94 (bs, 1H, -CH_2-**C*H***CF_3- PhCH-) ppm.

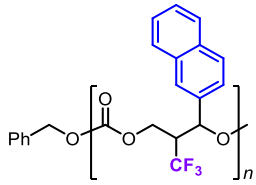

P(2i)

^{1}H NMR (δ ppm, 400 MHz, $CDCl_3$): 7.76 (bs, 4H, Ar-H); 7.46 (bs, 2H, Ar-H); 7.24 (bs, 1H, Ar-H); 6.16 (bs, 1H, -$CHCF_3$-Ph**C*H***-O-); 5.29 (bs, Ph**C*H*$_2$**-** chain end); 4.42-4.29 (overlapped bs, 2H, -COO-**C*H*$_2$**-**$CHCF_3$); 2.96 (bs, 1H, -CH_2-**C*H***CF_3- PhCH-) ppm.

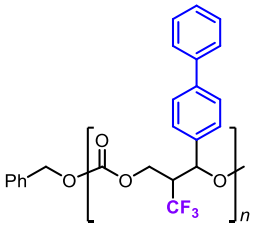

P(2j)

^{1}H NMR (δ ppm, 400 MHz, $CDCl_3$): 7.6-7.2 (overlapped bs, 9H, Ar-H); 6.10 (bs, 1H, -CHCF$_3$-PhC***H***-O-); 5.22 (bs, PhC***H*$_2$**- chain end); 4.54-4.44 (overlapped bs, 2H, -COO-C***H*$_2$**-CHCF$_3$-); 3.00 (bs, 1H, -CH$_2$-C***H***CF$_3$- PhCH-) ppm.

X-ray molecular determinations

Note that the measurements were carried out following the same procedure described as in Chapter 2.

Crystallographic details for the sodium borate derived from 2a: $C_{40}H_{40}BF_{12}NaO_8$, M_r = 910.52, monoclinic, *I*2/a, a = 21.8987(6) Å, b = 9.4206(2) Å, c = 19.8167(6) Å, α = 90°, β = 90.507(3)°, γ = 90°, V = 4088.00(19) Å^3, Z = 4, ρ = 1.479 mg·M^{-3}, μ = 0.145 mm^{-1}, λ = 0.71073 Å, T = 100(2) K, F(000) = 1872, crystal size = 0.20 × 0.20 × 0.03 mm, θ(min) = 2.055°, θ(max) = 27.133°, 16469 reflections collected, 3888 reflections unique (R_{int} = 0.0371), GoF=1.028, R_1 = 0.0484 and wR_2 = 0.1217 [I> 2σ(I)], R_1 = 0.0969 and wR_2 = 0.1413 (all indices), min/max residual density= −0.301/0.465 [e·Å^{-3}]. Completeness to θ(27.133°) = 86.0%. CCDC number 2074284.

Crystallographic details for 2o: $C_{17}H_{13}F_3O_3$, M_r = 322.27, monoclinic, *P*21/n, a = 8.32649(10) Å, b = 16.25304(18) Å, c = 10.67489(14) Å, α = 90°, β = 92.3904(12)°, γ = 90°, V = 1443.38(3) Å^3, Z =4, ρ = 1.483 mg·M^{-3}, μ = 0.126 mm^{-1}, λ = 0.71073 Å, T = 100(2) K, F(000) = 664, crystal size = 0.25 × 0.20 × 0.10 mm, θ(min) = 2.506°, θ(max) = 34.42°, 29596 reflections collected, 5868 reflections unique (R_{int} = 0.0243), GoF = 1.049, R_1 = 0.0378 and wR_2 = 0.1078 [I>2σ(I)], R_1 = 0.0436 and wR_2 = 0.1111 (all indices), min/max residual density = −0.267/0.525 [e·Å^{-3}]. Completeness to θ(34.42°) = 96.8%. CCDC number 2074285.

Chapter 4

New Biobased Nonisocyanate Polyurethane Synthesis from β-Elemene Dicarbonate

The results described in this chapter are part of a manuscript in preparation:

Maquilón, C.; Della Monica, F.; Brandolese, A.; Hoevelmann, C.; Kleij, A. W. **2021**, *to be submitted*

UNIVERSITAT ROVIRA I VIRGILI
NEW AND FUNCTIONAL CYCLIC CARBONATES FOR POLYMER APPLICATIONS
Cristina Maquilón Albaladejo

4.1. Introduction

Accounting for about 7 wt % of all plastic production, polyurethanes (PUs) represent one of the most important polymeric materials in industry and society.[1] PUs have excellent properties that make them precursors to fabricate high quality adhesive and coating materials with the automotive and transportation industry being the largest consumers. Due to their versatile applications, PUs are widely used in modern life as insulating plastics, foams, elastomers, paint-and-varnish materials, adhesives and synthetic fibers among other applications.[2]

Traditionally, PU production relies on polyaddition reactions between polyisocyanates and polyols. Although this approach has been well established in industry since the 1930s,[3] it presents important drawbacks in terms of safety and environmental effects. First, phosgene is a highly toxic compound involved in the synthesis of isocyanates, while the latter are also considered as toxic (Figure 4.1a). As a result of the toxicity of isocyanates, REACH regulations increasingly restricts their manipulation and use on an industrial scale.[4] Furthermore, the production of commonly used polyols is based on fossil fuel feedstock contributing to a non-ideal sustainability (carbon) footprint for the overall PU production process.[5] Therefore, finding greener alternatives for PU synthesis poses a huge challenge in industry, and in this respect the design and preparation of *non-isocyanate based polyurethanes* (NIPUs) has recently emerged as promising surrogates and a potential sustainable solution.

One of the most popular synthetic routes towards NIPUs is the polyaddition of diamines to cyclic dicarbonates (Figure 4.1b).[6] The resulting polyurethanes are also known as poly-*hydroxy*-urethanes (PHUs) due to the presence of alcohol groups in their structure. In order to tailor the polymer properties for a specific purpose in industrial applications, a common post-modification

[1] Geyer, R.; Jambeck, J. R.; Law, K. L. *Sci. Adv.* **2017**, *3*, e1700782.
[2] Gomez-Lopez, A.; Panchireddy, S.; Grignard, B.; Calvo, I.; Jerome, C.; Detrembleur, C.; Sardon, H. *ACS Sustainable Chem. Eng.* **2021**, *9*, 9541–9562.
[3] Bayer, O.; Siefken, W.; Rinke, H.; Orthner, L.; Schild, H. A Process for the Preparation of Polyurethanes or Polyureas. DRP 728981, 1937.
[4] REACH stands for Registration, Evaluation, Authorisation and Restriction of Chemicals Regulation.
[5] Khatoon, H.; Iqbal, S.; Irfan, M.; Darda, A.; Rawat, N. K. *Prog. Org. Coat.* **2021**,*154*, 106124.
[6] Guan, J.; Song, Y.; Lin, Y.; Yin, X.; Zuo, M.; Zhao, Y.; Tao, X.; Zheng, Q. *Ind. Eng. Chem. Res.* **2011**, *50*, 6517.

carried out in PU chemistry is the cross-linking of the polymer chains.[7] In this regard, the pendant hydroxyl groups that are present in each repeating unit of the NIPU allow for such a modification.

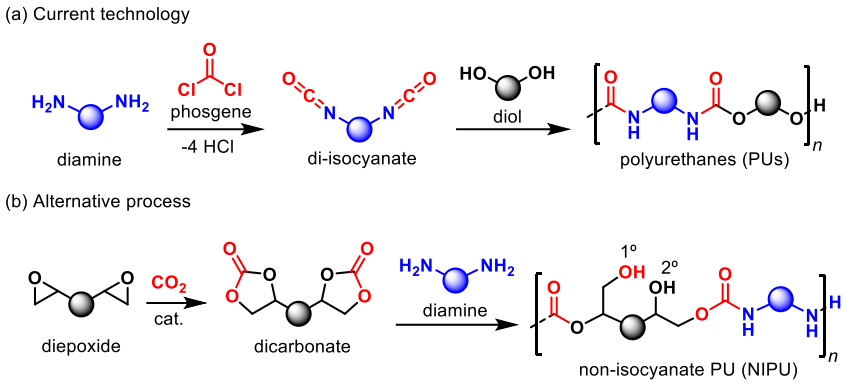

Figure 4.1. (a) Traditional route towards PUs. (b) Alternative route providing non-isocyanate PUs. The abbreviation 1º and 2º stand for primary and secondary, respectively.

In contrast to isocyanates, cyclic carbonates are presumed non- or low-toxic materials and readily accessible from [3+2] cycloaddition reactions between CO_2 and bio-based epoxides.[8] Many additional research efforts are focused on the sustainable preparation of diamines from renewable sources, since they are used as intermediates in various synthetic processes.[9] The development of efficient and environmentally friendly methods for cyclic carbonate synthesis and the sustainable production of diamines enables an increasingly attractive approach towards NIPUs. However, only a limited number of renewable bio-based monomers are available to produce NIPUs.[10] Expanding the range of these monomers will therefore open up new opportunities in the area of NIPU-derived materials, especially in those cases where the monomers combine features such as renewability, cost-effectiveness and structural modularity.

[7] Maisonneuve, L.; Lamarzelle, O.; Rix, E.; Grau, E.; Cramail, H. *Chem. Rev*. **2015**, *115*, 12407-12439.
[8] (a) Aomchad, V.; Cristòfol, À.; Della Monica, F.; Limburg, B.; D'elia, V.; Kleij, A.W. *Green Chem.* **2021**, *23*, 1077-1113. (b) de la Cruz-Martínez, F.; Martínez de Sarasa Buchaca, M.; Martínez, J.; Fernández-Baeza, J.; Sánchez-Barba, L. F.; Rodríguez-Diéguez, A.; Castro-Osma, J. A.; Lara-Sánchez, A. *ACS Sustainable Chem. Engin*. **2019**, *7*, 20126-20138. (c) Martínez, J.; Fernández-Baeza, J.; Sánchez-Barba, L. F.; Castro-Osma, J. A.; Lara-Sánchez, A.; Otero, A. *ChemSusChem* **2017**, *10*, 2886-2890.
[9] Froidevaux, V.; Negrell, C.; Caillol, S.; Pascault, J.-P.; Boutevin, B. *Chem. Rev.* **2016**, *116*, 14181-14224.
[10] Schimpf, V.; Ritter, B. R.; Weis, P.; Parison, K.; Mülhaupt, R. *Macromolecules* **2017**, *50*, 3, 944-955.

In recent years, terpenes have been recognized as useful and functional bio-monomers for the preparation of polymeric materials.[11] The preparation of several types of terpene-based polymers has shown the immense potential of functional and commercially available terpene-derived monomers for sustainable materials and product development, contributing thus towards a gradual transition to a biobased (circular) economy.[12] However, very few terpene-based carbonates have been used in polyurethane synthesis. In this context, limonene has been the subject of various investigations with a focus on new NIPU synthesis.[10,13,14] The group of Mülhaupt reported the preparation of linear PHUs by reaction of limonene dicarbonate and diamines thereby obtaining oligomers with glass transition temperatures (T_g) ranging from 33 to 62 ºC (Figure 4.2a),[15a] while other types of NIPUs have also been reported.[15b]

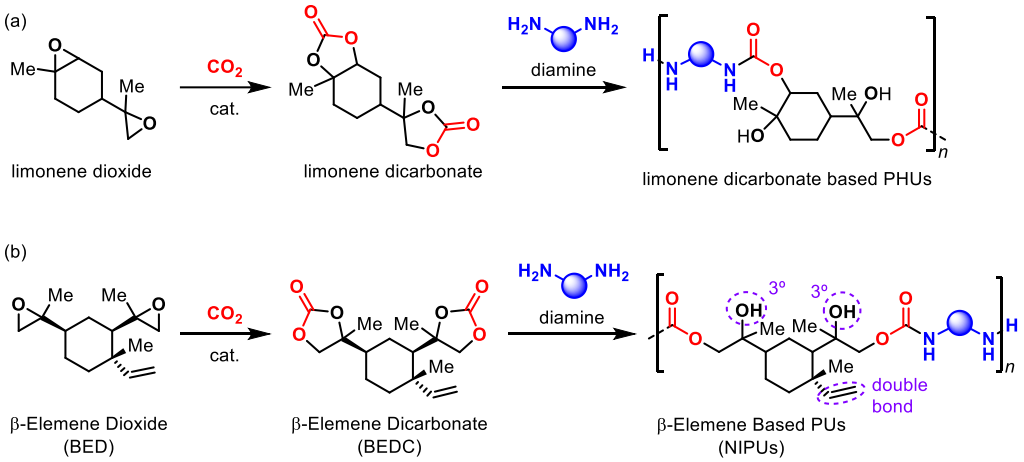

Figure 4.2. (a) Previously reported limonene-dicarbonate based PHUs. (b) Synthetic approach for β-elemene-based PUs

We envisioned that alternative, rigid and functional terpene-derived cyclic carbonates such as β-elemene dicarbonate (BEDC, Figure 4.2b) would offer highly attractive building blocks to promote biobased NIPUs with tailor-made properties. The terpene β-elemene (BE) is a natural

[11] Chaudhari, A.; Gite, V.; Rajput, S.; Mahulikar, P.; Kulkarni, R. *Ind. Crops Prod.* **2013**, *50*, 550-556.
[12] Hauenstein, O.; Agarwal, S.; Greiner, A. *Nature Commun.* **2016**, *7*, 11862.
[13] Maltby, K. A.; Hutchby, M.; Plucinski, P.; Davison, M. G.; Hintermair, U. *Chem. Eur. J.* **2020**, *26*, 7405-7415.
[14] Firdaus, M.; Meier, M. A. R. *Green Chem.* **2013**, *15*, 370-380.
[15] (a) Bahr, M.; Bitto, A.; Mulhaupt, R. *Green Chem.* **2012**, *14*, 1447-1454. For another recent work on NIPU synthesis from unsaturated epoxidized fatty acids, see: (b) Martínez, J.; de la Cruz-Martínez, F.; Martínez de Sarasa Buchaca, M.; Fernández-Baeza, J.; Sánchez-Barba, L. F.; North, M.; Castro-Osma, J. A.; Lara-Sánchez, A. *ChemPlusChem* **2021**, *3*, 460-468.

sesquiterpene commonly extracted from ginger root but is also present in citrus fruit. More recently, BE has become available on multi-ton scale as a byproduct from a biocatalytic process that produces fragrances and is commercialized by Isobionics.[16]

Here, we describe the preparation of new PHU based oligomers that are derived from BEDC, a new biobased dicarbonate building block. These new functional NIPU oligomers, upon suitable formulation, have further been tested in coating applications using UV and thermal curing procedures.

4.2 Results and discussion

β-Elemene dicarbonate synthesis

Very recently, we described the synthesis of β-elemene epoxides via oxidation of β-elemene using *meta*-chloroperbenzoic acid (*m*CPBA).[17] In order to facilitate the preparation of NIPU samples, the procedure was scaled up yielding up to 8 g of pure β-elemene dioxide (BED) in a single reaction (see Experimental Section for details). Afterwards, we explored the reaction of BED with carbon dioxide in the presence of commercial halide salts using high pressure autoclave reactor systems. Tetrabutylammonium chloride (TBAC), tetrabutylammonium bromide (TBAB) and bis(triphenylphosphine)iminium chloride (PPNCl) were chosen at the onset of these preliminary studies (Table 4.1). After 24 h under reaction conditions similar to those used with other bis-epoxides (100 ºC, 40 bar of CO_2),[10] β-elemene was fully converted into a mixture of β-elemene mono-carbonate (**BEMC**) and β-elemene dicarbonate (**BEDC**) products, with PPNCl giving consistently higher **BEDC**:**BEMC** ratio (entries 1-3). The BEMC formation was confirmed by NMR, HRMS and FT-IR analyses of the isolated product (Experimental Section). The reaction time was then extended using PPNCl as catalyst (entries 4-5) reaching a **BEDC**:**BEMC** ratio of 91:9 after 72 h. Complete conversion of **BED** into **BEDC** was achieved increasing the catalyst loading to 2 mol%. Conversely, increasing the initial quantity of **BED** to 1.0 g resulted in a significantly lower **BEDC**:**BEMC** ratio (entry 7), likely due to more difficult CO_2 diffusion towards the reactive sites, and a temperature of 130 ºC was necessary to reach quantitative formation of **BEDC** (entries 8-10). Finally, under these latter conditions, the

[16] http://isobionics.com/index-Beta%20Elemene.html. A 100 g sample was kindly provided recently to the Kleij group at ICIQ.
[17] Della Monica, F.; Kleij, A. W. *ACS Sustainable Chem. Eng.* **2021**, *9*, 2619-2625.

reaction could be scaled up to the use of 4.0 g of **BED** without affecting the conversion (entry 11).

Table 4.1. Cycloaddition of CO_2 to β-elemene dioxide **BED** to afford β-elemene dicarbonate **BEDC**.

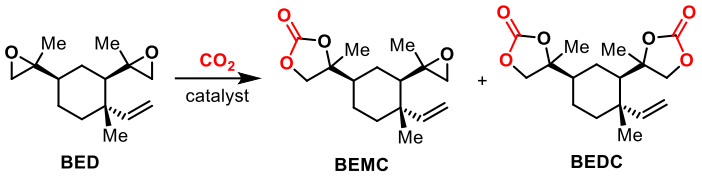

BED **BEMC** **BEDC**

Entry[a]	Catalyst (mol%)[b]	Temperature (ºC)	Time (h)	**BEDC:BEMC** (%)
1	TBAB (1.5)	100	24	38:62
2	TBAC (1.5)	100	24	39:61
3	PPNCl (1.5)	100	24	53:47
4	PPNCl (1.5)	100	48	78:22
5[d]	PPNCl (1.5)	100	72	91:9
6[d]	PPNCl (2)	100	72	>99:1
7[e]	PPNCl (2)	100	72	80:20
8[e]	PPNCl (2)	115	72	86:14
9[e]	PPNCl (2)	130	72	>99:1
10[f]	PPNCl (2)	130	72	>99:1

[a] Reaction conditions: BED = 50 mg ($2.1 \cdot 10^{-4}$ mol), 40 bar CO_2, neat. conditions Conversion of β-elemene dioxide was always > 99% as determined by ^{1}H NMR. [b] With respect to [epoxide groups]. [c] Determined by ^{1}H NMR by integration of epoxide/carbonate/olefin signals. [d] **BED** = 200 mg ($8.5 \cdot 10^{-4}$ mol). [e] **BED** = 1.0 g ($4.2 \cdot 10^{-3}$ mol). [f] **BED** = 4.0 g ($1.7 \cdot 10^{-2}$ mol).

The new dicarbonate **BEDC** was obtained as an oil after column chromatography, which was needed to remove the catalyst. A complete NMR, HRMS and FT-IR characterization was performed revealing the formation of several diastereoisomers analogous to the starting epoxide. Attempts to obtain crystals suitable for X-ray analysis were unsuccessful, however precipitation of one enriched diastereoisomer in the form of white solid could be achieved.

Diurethane synthesis from β-elemene dicarbonate and diamines

The reaction of **BEDC** with *n*-hexylamine was performed as a model reaction before the polyaddition attempts in order to get insight into the reactivity of this new carbonate and to have a reference compound useful for the characterization of the NIPUs (Figure 4.3).

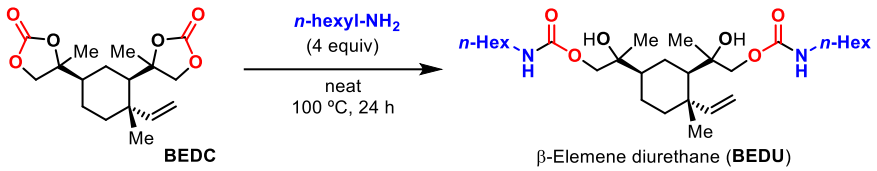

Figure 4.3. Synthesis of model compound β-elemene diurethane (**BEDU**).

Full conversion of **BEDC** was achieved after 24 h at 100 ºC. However, a mixture of stereoisomers was obtained, resulting in broad ^{1}H NMR signals. In order to get clearer spectra, the reaction was performed using precipitated **BEDC** under the same conditions. In this case, NMR analyses revealed the formation of one species, and the exclusive formation of tertiary alcohols was observed as a result of the high regio-selective ring-opening of the cyclic carbonate moieties.

Polyaddition reactions of BEDC and diamines

With the reference compound **BEDU** in hand, polyaddition reactions of various diamines were performed. Five different diamines were used (Table 4.2). Commercially relevant linear and cyclic substrates were employed, and also α- and β-methyl substituted amines were probed. The range of molecular weights (number average molecular weights, M_n´s) range from 1.3 to 6.2 kg/mol, pointing at the formation of oligomeric NIPUs species. Not surprisingly, the higher molecular weight and the more flexible the diamine reagent, the less viscous the NIPU that is produced. Along this tendency, similar notions are made for the T_g values with temperatures ranging from -59 to 86ºC for the lowest and highest viscosity of the prepared NIPUs.

Table 4.2. Properties of β-elemene-based NIPUs. Note the conversion levels provided for each of the reactions utilizing the five amine reagents.[a]

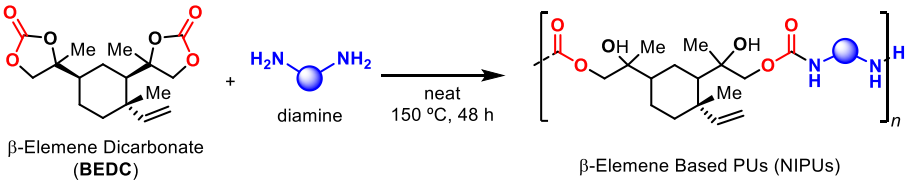

β-Elemene Dicarbonate (**BEDC**)

β-Elemene Based PUs (NIPUs)

1,6-hexamethyldiamine (HMDA)
NIPU1
83%

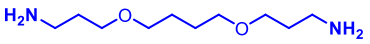

Baxxodur® EC 280
NIPU2
76%

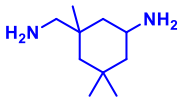

Isophorone diamine (IPDA)
NIPU3
92%

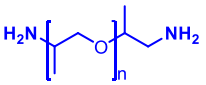

Baxxodur® EC 302
(M.W. = 400 g/mol)
NIPU4
74%

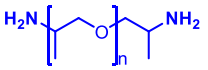

Jeffamine® D-2010
(M.W. = 2000 g/mol)
NIPU5
57%

Entry	Sample	M_n (kDa)[b]	$Đ$[b]	T_g (ºC)[c]	T_d (ºC)[d]
1	**NIPU1**	1.6	1.5	-6	243
2	**NIPU2**	1.8	1.5	-26	248
3	**NIPU3**[e]	1.3	1.3	84	247
4	**NIPU4**	2.0	1.6	-25	256
5	**NIPU5**	6.3	2.1	-59	310

[a] Reaction conditions: **BEDC** = 1.0 g ($3.1 \cdot 10^{-3}$ mol), diamine = $3.1 \cdot 10^{-3}$ mol, temperature = 150 ºC, time = 48 h. [b] Obtained by GPC analyses in DMAc + 1% TFAc + 0.5% LiBr at 40 ºC and calibrated with PMMA standards. [c] Obtained by DSC analyses with a scan rate of 10 ºC/min. [d] Onset decomposition temperature (T_d^0) obtained by TGA under nitrogen. [e] After 6 h the reaction mixture solidified preventing further substrate conversion.

For the purpose of showing the scope of application of these NIPUs, cross-linking reactions were assessed (see below). Since **NIPU5** showed the lowest viscosity, we decided to scale its synthesis up to 6 g in order to have enough starting material for the cross-linking experiments.

Initial cross-linking tests

As mentioned in the introduction section, a distinct feature of NIPUs generated from aminolysis of polycarbonates is the presence of hydroxyl groups in the final product. In addition, an additional pendant double bond is also present in the structure of the oligomers produced from **BEDC**. These double bonds can be used for crosslinking via well-established radical-mediated thiol-ene chemistry, creating dithio-ether linkages between the polymer chains (Figure 4.4). Consequently, the network created this way would represent a hard and dry film suitable for testing various physical properties.

In this context, a commonly used linker is pentaerythritol tetrakis(3-mercaptopropionate) (**PEMTP**) that contains four thiol moieties. Thus, we explored the conditions for the thermal curing of **BEDC** by **PEMTP** while adding AIBN as catalyst and performing these experiments in an oven for 40 minutes. Ratios from 1:0.8 to 1:2 of double bond equivalents (C=C) versus thiol moieties (SH) were considered, and temperatures ranging from 100 ºC to 140 ºC were screened (see Experimental Section). These thermal curing attempts only gave sticky layers and hence were not suitable for physical tests. When using higher relative amounts of thiols (C=C vs. SH = 1:1.2), a lower stickiness was obtained at 140 ºC.

Thus, we decided to try a different, bifunctional cross-linker (ethylene glycol bis(3-mercaptopropionate, **GDMP**), as likely the steric requirements of **PEMTP** affects the rate of the crosslinking reaction. The best temperature conditions from the experiments carried out with **PEMTP** (140 ºC) were used during 40 min in the presence of 2 wt % AIBN, and ratios of 1:0.8, 1:1 and 1:1.2 between the C=C bonds and the thiol groups of **GDMP**. Unfortunately, the resulting layers were even stickier compared to the ones obtained with **PETMP** produced at a 1:1.2 ratio at 140 ºC.

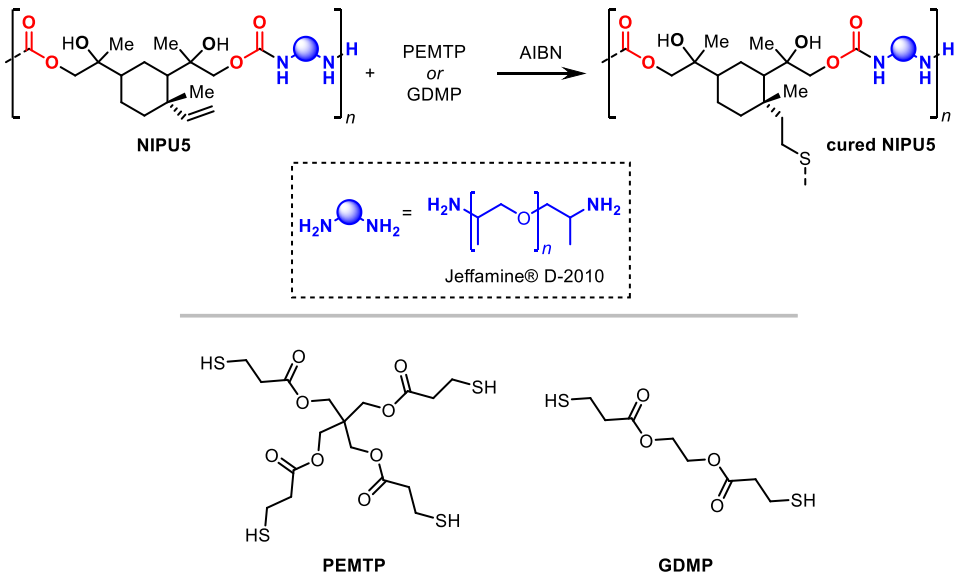

Figure 4.4. Thermal curing of **NIPU5** via thiol-ene reactions using **PEMTP** and **GDMP** as cross-linkers.

The cross-linking reactions using thiols did not work as desired, and the layers obtained after thermal curing were too sticky for physical tests. The difference in the physical state of the reaction mixture before and after curing point out that the crosslinking reaction had likely taken place. At this stage, we believed that the amount of double bonds in **NIPU5** is probably too low to generate enough thiol bridges, and thus the resulting macromolecular structures are not suitable coatings for further analysis. As a possible solution, we then thought about *dual curing* using a possible oligomeric additive to increase the double bond density (vide infra), since **NIPU5** is probably the one with the lowest density of double bonds among the synthesized NIPUs due to the high molecular weight of Jeffamine® 2010.

Dual curing cross-linking reactions and physical tests

Dual cure processes imply two type of reactions taking place to cure a coating, and more specifically in our case, the photocatalytic coupling of the double bonds and the thermal coupling of -OH and -NH_2 groups with the isocyanate (NCO) functionalities of an additional oligomer added in order to increase the amount of double bonds present in the reaction mixture (Figure 4.5).

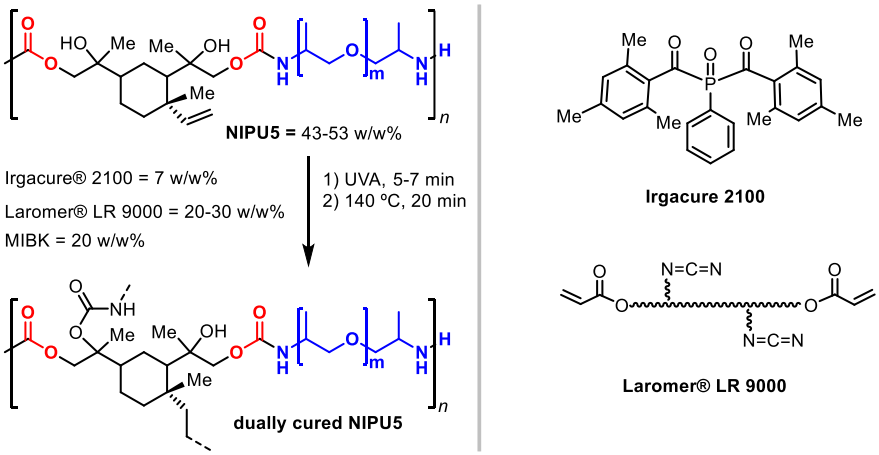

Figure 4.5. Curing of **NIPU5** in the presence of Irgacure® 2100 (photo-initiator) and Laromer® LR 9000 isocyanate acrylate curing agent.

First, we tried the curing of the selected non-isocyanate polyurethane (Table 4.3, entry 1, Formulation 1) and premixed 73 wt % **NIPU5** with 7 wt % Irgacure® 2100 (initiator) dissolved in 20 wt % of methyl isobutyl ketone (MIBK) in a vial and then applied a metallic panel employing a spiral squeegee or coating knife with a certain thickness associated. Then, the wet film was cured for 5 min under UV irradiation and subsequently heated for 20 min in an oven at 140 ºC. Unfortunately, this curing procedure did not result in a dry coating, presumably due to the low density of double bond equivalents. To overcome this limitation, we considered the addition of a polyacrylate with isocyanate functionalities in its structure (Laromer® 9000). We screened different combinations of thickness, concentration of Laromer® 9000 and UV curing time, while keeping the percentage in weight of solvent and photo-initiator constant (entries 2-3: Formulations 2 and 3). Also, a test with laromer 9000 self-curing was performed to compare with the combinations of **NIPU5** with laromer 9000 (entry 4, Formulation 4).

Table 4.3. Formulations used for the coating preparation from **NIPU5** and laromer 9000.

Entry	Code	**NIPU5** (wt %)	Laromer (wt %)
1	Formulation 1	73	0
2	Formulation 2	53	20
3	Formulation 3	43	30
4	Formulation 4	0	73

With these different formulations in hand, we then carried out a series of physical tests on the coatings produced in order to check their physical properties. These assays were performed in BASF and are typically optimized for the evaluation of coatings with application in the automotive industry. The different analyses are discussed below.

Dryness test

A first evaluation of the film dryness was required in order to continue with the measurement of further physical properties. The protocol consisted of placing an "L" shaped metal piece in the middle of a panel with a 100 g weight on it for 20 seconds. Hereafter, the weight is removed. If the metal piece takes one or more seconds to fall, the panel is not completely dry and therefore not appropriate for any further physical tests. We were happy to observe that formulations 2, 3 and 4 resulted in a dry coatings suitable for further analysis. These analyses will be first explained below in some detail.

Figure 4.6. Dryness test example with an "L" shape metal piece placed in the middle of the panel containing the coating.

Gloss

If one thinks about the surface of a car body, the way the light is reflected on it is an important factor from an aesthetic point of view. This effect is known as "gloss" and it is measured in three different points of the coating using a gloss reflectometer. Interestingly, the choice of solvent can affect the gloss result. Solvents with a higher boiling point will evaporate slowly giving time for the coating to result in a flat and homogeneous surface. Also, the use of some additives such as silicon derivatives can help to get a flatter layer.

Figure 4.7. Reflectometer measuring the gloss of a coating sample.

Thickness measurement

Interestingly, the thickness of a dry coating will determine the size of the crosscut blade used for the upcoming cross-cut test. To check the thickness of the dry layer, a thickness-meter is used to measure five different points of the coating. The value given by the instrument is an average of these five measurements.

Figure 4.8. Thickness measurement of a dry coating.

Cross-cut

Another property also important in the production of coatings is how well the layer is adhered to the base surface, in this case the panel. With the thickness value in hand, the proper cross-cut blade is placed in the cross-cut knife and two cuts in cross shape are made. Right after, the cut is brushed 5 times in both diagonal directions. A piece of tape is placed on the cut and quickly removed from it. After evaluation of the cross-cut area, depending on the degree of damage, the results are classified between classes 1 to 5, with low values corresponding to low

erosion and vice versa. When the network in the layer is good, the cross-cut classification is higher, since the coating is a hard film and usually does not fix well to the panel base layer.

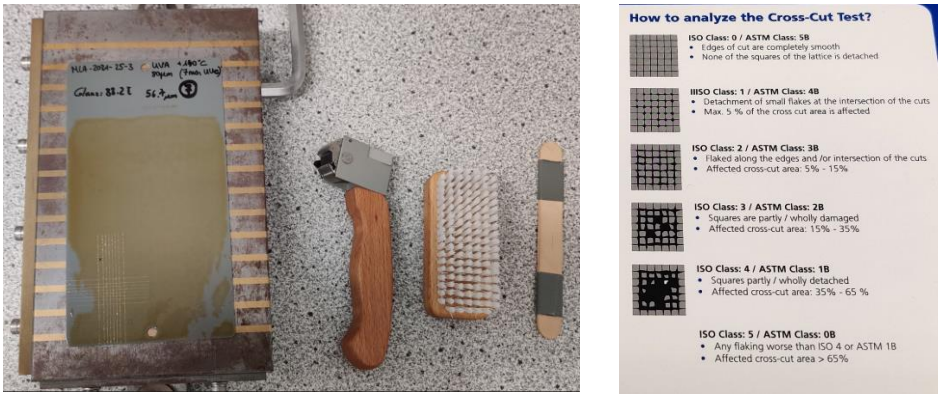

Figure 4.9. LEFT: Instrumentation for cross-cut test. RIGHT: Classification of cross-cut result tests.

Buchholz indentation hardness

The next technique is the measure of the coating hardness. To proceed with the measurement, the indenter is placed in the panel for 30 seconds. Once removed, typically within 30 additional seconds, one should measure the length of the cut with a magnifying glass equipped with a measuring scale. Marking the area of the cut helps to analyze the result within the limited time.

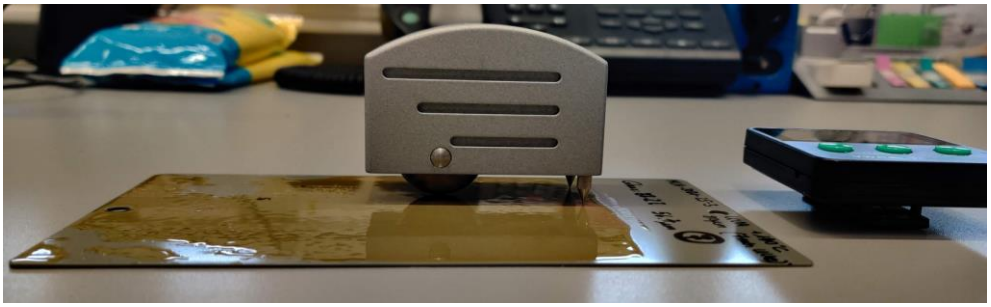

Figure 4.10. Buchholz hardness indenter placed on the surface of a panel to perform a hardness test.

MEK test

Finally, to prove the resistance of the coating to solvent a MEK test is performed. The procedure starts by fixing a clean wipe in the MEK hammer with the help of a Teflon ring. Then, there is a hollow section on the opposite side of the hammer's head where the MEK is added. Once the wipe is soaked with solvent, the hammer is placed on the side of the panel and it is moved over the surface up and down until completing 25 double rubs (DR). After checking the quality of the coating, 25 extra double rubs are performed in case the surface is not damaged. This procedure is repeated until 200 rubs, or when the surface has eroded.

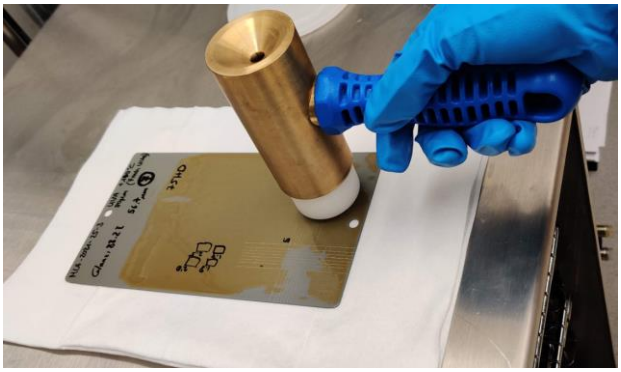

Figure 4.11. MEK hammer used for the solvent resistant test.

Physical test results

Once the cured coatings were prepared following the formulations previously described (Table 4.3 in the previous section), we moved forward with the testing of the physical properties of the different panels. In Figure 4.12 cured coatings *before* and *after* the physical tests are shown.

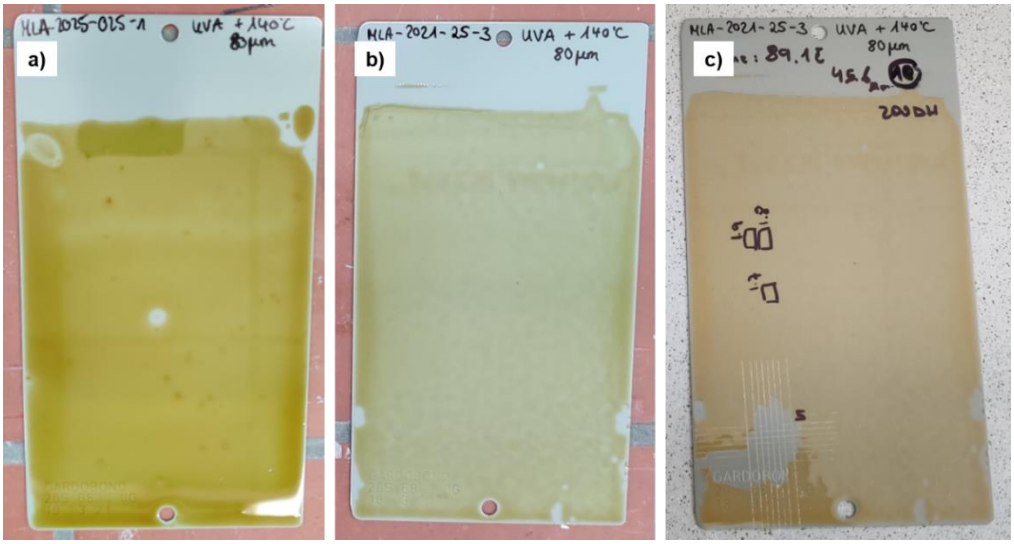

Figure 4.12. Comparison between coating samples obtained from (a) **NIPU5** + 7 wt% Irgacure® 2100, and (b) **NIPU5** + 7 wt% Irgacure® 2100 + 30 wt% Laromer® 9000 cured coating (c) Result of the physical test of the coating.

All the results for the physical tests are gathered in Table 4.4. As mentioned previously, the self-curing of **NIPU5** (formulation 1) did not result in a dry layer, and consequently it was not possible to perform any physical test on it (Entry 1) but the dryness test was positive for the other curing conditions allowing for further evaluation. These showed in the case of the gloss results no dependency on the formulation, obtaining rather similar results in a small range of 87-96 E. One of the variations applied in the film preparation was the associated thickness of the coating knife. Two different coating knife sizes, viz. 60 µm and 80 µm, were used for the application of the mixture in the panel before the dual curing reaction. After the UV and thermal curing, the dry panels showed reproducibility on the thickness obtaining these with about 24-25 µm and 50-57 µm when using the 60 µm and the 80 µm coating knife respectively. Cross-cut tests revealed a big difference between the formulations containing a combination of **NIPU5** and Laromer® 9000 (Formulations 2 and 3) in contrast with the self-curing of the latter, representing a class 5 and class 0, respectively, in this assay.

This fact suggests that coatings produced with our polymer were not adhering perfectly to the panel surface. Similarly, the Buchholz hardness test offers numbers from 1.6 to 2.2 for formulations 2 and 3 and a slightly lower result, 1.3, for Formulation 4. Finally, the MEK test was crucial to conclude that coating with a larger amount of Laromer® 9000 and thicker layer

shows better results (Entries 2-5). Formulation 3 employing an 80 µm coating knife turned out as good as formulation 4 in terms of solvent resistance (entry 4 vs 6), and only in these two cases the coating was able to resist 200 DR.

Table 4.4. Physical test results for the different curing conditions employed.[a]

Entry	Form.[b]	Dryness	Gloss (GU)	Thickness (µm)	Cross-cut	Buchholz hardness	MEK test (DR)
1	Form. 1 80 µm	Not okay	-	-	-	-	-
2	Form. 2 80 µm	Okay	87.7	50.9	5	2.2	50
3	Form. 2 60 µm	Okay	89.7	24.3	5	1.7	0
4	Form. 3 80 µm	Okay	89.1	50.5	5	1.8	200
5[c]	Form. 3 80 µm	Okay	88.2	56.7	5	1.8	75
6	Form. 3 60 µm	Okay	87.4	25.7	5	1.6	25
7	Form. 4 80 µm	Okay	96.4	57.5	0	1.3	200

[a] Curing conditions: 5 minutes UV curing followed by 20 minutes in an oven at 140 ºC. [b] Form. stands for formulation. [c] 7 minutes UV curing followed by 20 minutes in an oven at 140 ºC.

4.3. Conclusions

The results presented in this chapter demonstrate that a bis-cyclic carbonate derived from β-elemene (a natural terpene, **BE**) allows for the formation of new non-isocyanate based oligourethanes (NIPUs) using commercial and relevant diamines. Five different diamines were tested offering appreciable conversion of the carbonate groups, and modest molecular weights of up to 6.3 kg·mol^{-1} and dispersities in the range 1.3-2.1. A first set of trials were performed to investigate the application of these oligomeric NIPUs to serve as a starting point for coating preparation. The initial results show some degree of promise after applying a dual curing process.

Subsequent testing of various physical properties points towards the potential of renewable **BE** in devising new polyurethane formulations of value in coating applications.

4.4. Experimental section

General considerations

All water-sensitive operations were carried out under a nitrogen atmosphere using standard vacuum line and Schlenk techniques. Solvents were purchased from Sigma-Aldrich (HPLC grade) and dried using an MBraun MBSPS800 purification system. NMR spectra were recorded on a Bruker AV-400 spectrometer operating at 400 MHz to collect ^{1}H and 100 MHz for ^{13}C NMR spectral data. ^{1}H NMR spectra are referenced to the residual solvent peak at δ 7.26 ppm for $CDCl_3$, and δ 2.50 ppm for DMSO-d_6. ^{13}C NMR spectra are referenced to the residual solvent peak at δ 77.16 ppm for $CDCl_3$, and δ 39.52 ppm for DMSO-d_6. Differential scanning calorimetry (DSC) analyses for determination of the glass transition temperatures (T_g) were measured under a N_2 atmosphere using a Mettler Toledo equipment (model DSC822e). Samples were weighed into 40 μL aluminum crucibles and subjected to two heating cycles at a heating rate of 10 °C/min. Thermogravimetric analyses (TGA) were recorded under N_2 atmosphere using Mettler Toledo equipment (model TGA/SDTA851). Samples were weighed into 40 μL aluminum crucibles and heated to 400 ºC at a heating rate of 10 °C/min. Gel permeation chromatography (GPC) measurements were performed using an Agilent 1200 series HPLC system, equipped with PSS SDV Analytical linear M GPC column (8 × 300 mm; 5 μm particle size) in tetrahydrofuran at 30 °C at a flow rate of 1 mL·min^{-1}. Samples were analyzed at a concentration of 1 mg·mL^{-1} after filtration through a 0.45 μm pore-size membrane. M_n, M_w, and $Đ$ data were derived from the RI signal by a calibration curve based on polystyrene standards (PS from Polymer Standards Service) for the analysis of the polymers.

Reagents

All reagents were purchased from commercial suppliers (Aldrich and Acros) and used as received. The catalyst bis(triphenylphosphine)iminium chloride (PPNCl) is commercially available and was used after recrystallization from dichloromethane and drying under vacuum for 48 h. β-elemene was kindly provided by Isobionics. The diamines and formulation reagents (Irgacure® 2100 and Laromer® 9000) were supplied by BASF Coatings GmbH (Münster).

Synthesis of β-elemene dioxide (BED)

The β-elemene dioxide (**BED**) was prepared by modification of a previously reported procedure.[17] Beta-elemene (93%, 10.0 g, 45.5 mmol) was dissolved in DCM (455 mL) in a 1 L flask and cooled at 0 ºC with an ice bath. *m*CPBA (77 % w/w, 23.0 g, 0.10 mol) was added during 20 minutes and the reaction mixture stirred at 0 ºC. After 4 hours from the first addition, the suspension was filtered, the solid washed with hexane and the solvent removed by rotary evaporation. The resulting mixture was suspended in hexane, filtered and dried again until obtaining a colorless oil. The oil was dissolved in hexane (250 mL) and washed with sat. $NaHCO_3$ (250 mL, 3 times). The organic phase was dried over Na_2SO_4, filtered and the solvent removed by rotary evaporation. The mixture was purified by column chromatography on silica gel (eluent from Hex/EtOAc = 8/2 to Hex/EtOAc = 6/4). In Hex/EtOAc = 8/2, the R_f (monoxide) = 0.76; the R_f (dioxide) = 0.48-0.57. Yield: 8.1 g (75.3%). NMR data were consistent with the data in the literature.[17]

Reaction conditions for β-elemene dicarbonate (BEDC) formation

The reaction of **BED** with CO_2 for the synthesis of **BEDC** led to the formation of a mixture of diastereoisomers reminiscent to the composition of the starting bis-epoxide. The formation of **BEDC** proceeds through **BEMC** intermediates and, for which eight possible isomers can form. Nevertheless, NMR characterization of isolated **BEMC** samples supports the formation of a simpler mixture, likely due to the preferred reaction of the sterically more accessible epoxide moiety. This results in the selective formation of one major *regio*-isomer in the form of four different diastereoisomers (**Figure S2**). This scenario is supported by the different reactivity observed for the double bonds in the 3,4 and 11,12 position of β-elemene during epoxidation with *m*CPBA.[17]

BEMC

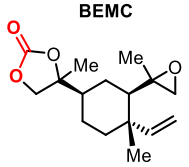

^{1}H NMR (400 MHz, $CDCl_3$) δ 6.08 – 5.56 (m, 1H), 5.31 – 4.68 (m, 2H), 4.50 – 3.69 (m, 4H), 2.20 – 0.71 (m, 17H) ppm. **IR** (neat) ν 1791 (C=O) cm^{-1}. **HRMS** (ESI+, MeOH) *m/z* calcd. ($C_{16}H_{24}NaO_4$), $(M+Na)^+$, 303.1568; found: 303.1567.

BEDC

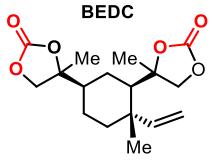

^{1}H NMR (400 MHz, $CDCl_3$) δ 5.98 – 5.63 (m, 1H), 5.11 – 4.83 (m, 2H), 4.40 – 4.19 (m, 1H), 4.12 – 4.01 (m, 1H), 2.70 – 2.31 (m, 2H), 2.01 – 0.85 (m, 17H). **^{13}C NMR** (101 MHz, $CDCl_3$) δ 154.64, 154.62, 154.47, 154.44, 154.42, 154.05, 154.03, 154.00, 150.68, 150.66, 149.88, 149.83, 148.62, 148.55, 148.36, 148.23, 111.85, 111.68, 111.08, 110.41, 87.14, 87.02, 86.88, 86.80, 85.66, 85.63, 85.38, 85.32, 85.28, 75.61, 75.50, 73.29, 73.27, 73.15, 73.08, 73.06, 72.90, 72.79, 67.11, 63.66, 53.52, 52.48, 52.45, 52.25, 51.13, 51.08, 46.84, 46.79, 45.84, 45.26, 45.12, 45.07, 45.01, 42.32, 41.83, 41.80, 41.75, 39.39, 39.27, 39.22, 38.67, 38.59, 38.58, 27.88, 27.78, 26.32, 25.95, 23.79, 23.32, 22.99, 22.93, 22.81, 22.62, 21.95, 21.89, 21.81, 21.74, 21.69, 21.61, 21.45, 21.40, 21.38, 21.35, 16.91, 16.82, 16.64, 16.57, 15.88 ppm. **IR** (neat) ν 1783 (C=O) cm^{-1}. **HRMS** (ESI+, MeOH) *m/z* calcd. ($C_{17}H_{24}NaO_6$), $(M+Na)^+$, 347.1479; found: 347.1465.

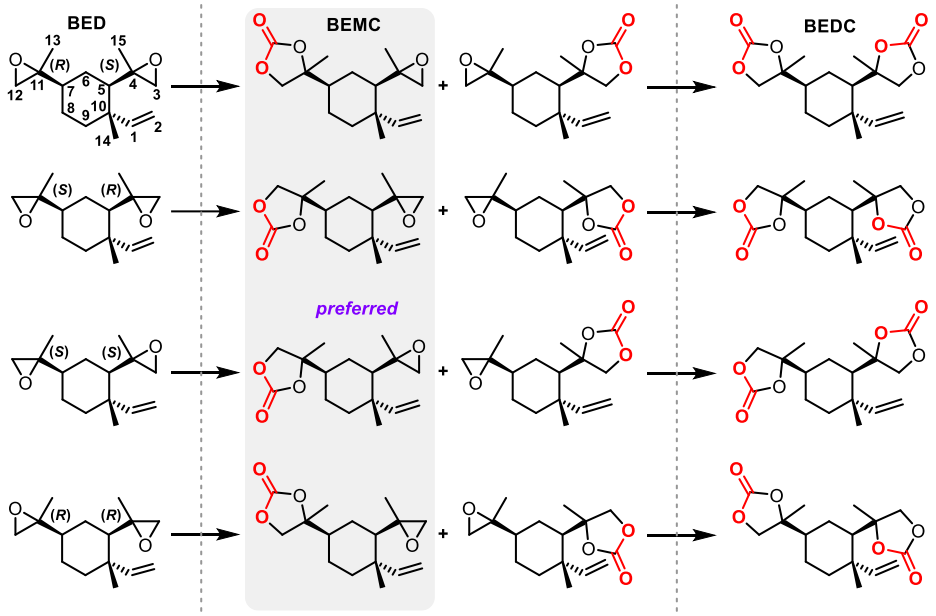

Figure 4.13. Possible *regio*- and *stereo*-isomers for **BEMC** and **BEDC** obtained from **BED**. Proposed preferred **BEMC** regioisomers highlighted in the gray zone.

Screening of halide salt catalysts

Screening of halide salt catalysts TBAC, TBAB and PPNCl was conducted in parallel under the same conditions using high pressure autoclave reactors according to the following procedure. **BED** (50 mg, $2.1 \cdot 10^{-4}$ mol) and the selected halide salt catalyst (1.5 mol% with respect to epoxide groups) were weighed into a Teflon vessel equipped with a magnetic stirring bar. The lid was closed, and the system pressurized with CO_2 (10 bar) and purged three times. Then, the reactor was pressurized at the selected pressure of 40 bar and placed in a heating mantel set at 100 ºC. After stirring for 24 h, the reactor was cooled down with an ice bath. Mesitylene (5.9 µL, 10 mol%) was added as an internal standard, and each reaction was analyzed by ^{1}H NMR ($CDCl_3$) to determine the conversion and selectivity (Figure S2). The reaction mixtures were purified by column chromatography (Hex:EtOAc, gradient from 4:1 to 2:1).

Screening of BEDC formation using PPNCl

Screening of reaction conditions for the formation of **BEDC** in the presence of PPNCl was conducted using a 40 mL autoclave reactor according to the following procedure. **BED** (0.1 – 1.0 g, $4.23 \cdot 10^{-4}$ – $4.23 \cdot 10^{-3}$ mol) and PPNCl (1.5 – 2.0 mol% with respect to epoxide groups) were weighed into a Teflon vessel equipped with a magnetic stirring bar and placed into the reactor. The lid was closed, and the system pressurized with CO_2 (5 bar) and vented three times. Then, the reactor was pressurized at the selected pressure of 40 bar and placed in a heating mantel set at 100 – 130 ºC. After stirring for 48-72 h, the reactor was cooled down with an ice bath. Mesitylene (10 mol%) was added as an internal standard, and the reaction analyzed by ^{1}H NMR ($CDCl_3$) to determine the conversion and selectivity.

Multigram-scale synthesis of BEDC under optimized conditions

BED (4.0 g, $1.69 \cdot 10^{-2}$ mol) and PPNCl (388 mg, $6.77 \cdot 10^{-4}$ mol, 2.0 mol% with respect to epoxide groups) were weighed into a 100 mL Teflon vessel equipped with a magnetic stirring bar and placed into a 150 mL autoclave reactor. The lid was closed, and the system pressurized with CO_2 (5 bar) and vented three times. Then, the reactor was pressurized at the selected pressure of 40 bar and placed in a heating mantel set at 130 ºC. After stirring for 72 h, the reactor was cooled down with an ice bath. Mesitylene (10 mol%) was added as an internal standard, and the reaction analyzed by ^{1}H NMR ($CDCl_3$) to determine the conversion and selectivity. The reaction mixture was purified by column chromatography (Hex:EtOAc: gradient from 4:1 to 2:1). Yield: 4.8 g (87%).

Typical procedure for NIPU synthesis using various diamines and BEDC

In a Schlenk tube, both **BEDC** and the corresponding diamine were combined in a 1:1 ratio. After purging with N_2, the reaction mixture was heated up to 130 ºC and let stirring for 48 h. Hereafter, the reaction mixture was allowed to reach room temperature, dissolved in MeOH and precipitated by addition of hexane. This work up procedure was repeated three times and the precipitated polymer was then dried under vacuum. For the M_n, $Đ$ and T_g values of all isolated NIPU oligomers, see Table 4.2. For reference data concerning the IR assignments, see footnote 15b.

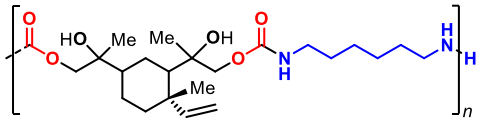

NIPU1

^{1}H NMR (500 MHz, DMSO-d_6) δ 6.02 – 5.62 (m, 1H), 5.15 – 4.60 (m, 2H), 4.19 – 3.55 (m, 4H), 3.03 – 2.66 (m, 4H), 1.89 – 0.81 (m, 24H) ppm. **^{13}C NMR** (125 MHz, DMSO-d_6) δ 156.82, 154.81, 154.38, 153.59, 153.37, 152.73, 152.68, 152.13, 151.66, 150.68, 150.21, 149.64, 110.57, 110.48, 110.00, 109.95, 108.18, 87.79, 87.77, 87.57, 86.48, 86.32, 86.29, 86.23, 75.08, 74.66, 74.26, 74.23, 74.05, 72.85, 72.49, 72.39, 72.24, 72.20, 72.16, 70.77, 69.76, 69.58, 69.40, 69.24, 65.63, 52.34, 51.86, 51.46, 50.91, 47.67, 46.71, 45.76, 45.66, 45.61, 45.18, 44.84, 44.48, 44.25, 44.08, 42.98, 41.23, 29.88, 29.72, 26.44, 26.25, 26.06, 25.85, 24.47, 23.06, 22.83, 22.64, 22.51, 22.37, 22.25, 22.13, 21.99, 21.86, 21.80, 21.64, 21.50 ppm. **IR** (neat) ν 3339 (NH and NH_2), 2931, 2863, 1790 (carbonate), 1692 (C=O amide), 1637, 1520 (NH amide), 1460, 1379, 1251 (C–O urethane), 1058, 906, 774, 668 cm^{-1}.

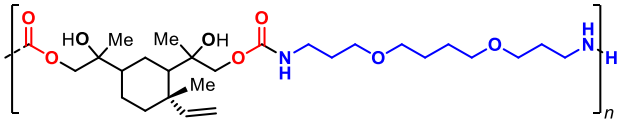

NIPU2

^{1}H NMR (500 MHz, DMSO-d_6) δ 6.16 – 5.69 (m, 1H), 5.09 – 4.38 (m, 2H), 4.21 – 3.55 (m, 4H), 3.51 – 3.12 (m, 16H), 3.06 – 2.74 (m, 4H), 1.90 – 0.81 (m, 21H) ppm. **IR** (neat) ν 3336 (NH and NH_2), 2936, 2862, 1794 (carbonate), 1692 (C=O amide), 1542 (NH amide), 1465, 1376, 1252 (C–O urethane), 1105, 1059, 906, 774 cm^{-1}.

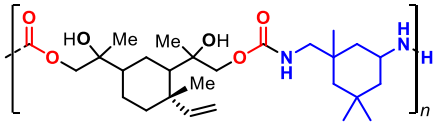

NIPU3

^{1}H NMR (500 MHz, DMSO-d_6) δ 6.13 – 5.55 (m, 1H), 5.17 – 4.58 (m, 2H), 4.51 – 3.09 (m, 4H), 1.55 – 1.26 (m, 4H), 1.23 – 0.57 (m, 21H) ppm. **^{13}C NMR** (125 MHz, DMSO-d_6) δ 156.19, 154.72, 154.68, 154.20, 152.12, 152.07, 150.98, 150.06, 150.00, 149.65, 149.63, 110.95, 110.39, 109.97, 109.94, 87.83, 87.67, 87.51, 87.48, 87.39, 86.25, 86.23, 86.18, 86.11, 86.08, 75.63,

75.14, 75.05, 74.94, 74.83, 74.81, 74.70, 73.54, 73.38, 73.33, 72.93, 72.91, 72.77, 72.72, 72.55, 71.24, 68.14, 67.87, 67.46, 65.76, 65.68, 65.65, 52.32, 51.83, 51.46, 51.45, 50.94, 50.86, 49.02, 47.10, 46.96, 46.90, 46.71, 46.68, 45.67, 45.63, 45.36, 45.18, 44.93, 44.77, 44.76, 43.77, 43.10, 43.01, 41.99, 41.97, 41.94, 38.85, 38.83, 31.43, 27.82, 27.73, 25.58, 24.62, 24.48, 24.37, 23.02, 22.92, 22.83, 22.58, 22.52, 22.48, 22.45, 22.24, 22.01, 21.97, 21.91, 21.82, 21.80, 21.70, 21.65, 21.55, 21.50, 21.47, 21.41, 20.70, 18.76, 18.57, 18.38, 17.75, 17.69, 17.63, 17.53, 17.51, 16.77, 16.75, 16.71, 16.49, 16.45, 16.32, 16.21, 14.38 ppm. **IR** (neat) ν 3339 (NH and NH_2), 2924, 1790 (carbonate), 1695 (C=O amide), 1537 (NH amide), 1462, 1385, 1241 (C–O urethane), 1059, 905, 774 cm^{-1}.

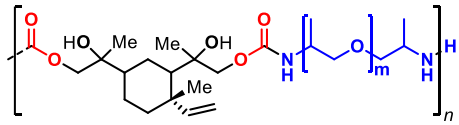

NIPU4

^{1}H NMR (500 MHz, DMSO-d_6) δ 6.03 – 5.59 (m, 1H), 5.11 – 4.67 (m, 2H), 4.54 – 3.65 (m, 4H), 3.61 – 3.14 (m, 19H), 2.01 – 0.61 (m, 33H) ppm. **^{13}C NMR** (125 MHz, DMSO-d_6) δ 157.57, 156.10, 154.80, 154.79, 154.73, 154.70, 154.43, 154.37, 154.26, 154.22, 154.21, 153.39, 152.92, 152. 84, 152.72, 152.67, 152.11, 152.06, 151.28, 150.96, 150.87, 150.70, 150.21, 150.04, 149.98, 149.66, 149.63, 132.39, 126.79, 110.99, 110.96, 110.56, 110.48, 110.43, 110.36, 109.98, 109.95, 109.45, 109.25, 87.86, 87.85, 87.79, 87.77, 87.59, 87.56, 87.54, 87.53, 87.51, 87.48, 87.41, 86.74, 86.57, 86.53, 86.47, 86.29, 86.26, 86.24, 86.20, 86.14, 86.11, 75.51, 75.29. 75.23, 75.10, 75.04, 74.32, 74.09, 73.63, 73.48, 73.44, 73.41, 73.40, 73.30, 73.25, 73.12, 73.01, 72.89, 72.84, 72.48, 72.33, 72.23, 70.82, 68.13, 68.04, 67.86, 67.78, 66.99, 65.66, 65.63, 63.47, 63.38, 61.38, 60.20, 55.93, 54.82, 54.54, 52.69, 52.32, 52.27, 52.21, 51.81, 51.46, 51.44, 50.92, 50.85, 48.23, 47.76, 47.75, 47.66, 47.58, 47.53, 47.44, 47.08, 46.94, 46.71, 46.67, 46.53, 45.75, 45.66. 45.62, 44.92, 44.91, 44.79, 44.76. 44.66, 44.61, 44.45, 43.76, 43.51, 43.30, 43.12, 43.09, 42.99, 41.98, 41.95, 41.23, 41.05, 40.76, 38.85, 38.83, 37.88, 36.86, 36.73, 36.52, 36.23, 36.10, 36.05, 35.47, 35.33, 35.30, 35.27, 31.98, 31.91, 31.87, 31.78, 31.76, 31.74, 31.70, 30.33, 30.08, 29.75, 28.51, 27.98, 27.89, 27.86, 27.84, 27.82, 27.72, 27.32, 26.66, 25.88, 25.56, 25.34, 25.24, 24.86, 24.69, 24.62, 24.56, 24.47, 24.37, 24.25, 23.64, 23.59, 23.47, 23.37, 23.02, 22.93, 22.81, 22.61, 22.58, 22.47, 22.44, 22.36, 22.25, 22.14, 22.04, 21.98, 21.95, 21.85, 21.80, 21.77, 21.70, 21.64, 21.57, 21.50, 21.47, 21.40, 21.12, 17.53, 17.26, 17.18, 17.05, 16.80, 16.78, 16.76, 16.75, 16.62, 16.54,

16.53, 16.50, 16.48, 16.46, 16.25, 14.55 ppm. **IR** (neat) ν 3348 (NH and NH_2), 2971, 2870, 1796 (carbonate), 1714, 1650, 1537 (NH amide), 1455, 1375, 1258 (C–O urethane), 1089, 1059, 909, 775 cm^{-1}.

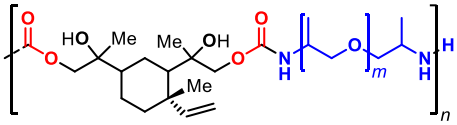

NIPU5

^{1}H NMR (500 MHz, DMSO-d_6) δ 5.98 – 5.65 (m, 1H), 5.11 – 4.66 (m, 2H), 4.52 – 3.71 (m, 4H), 3.69 – 3.57 (m, 4H), 3.56 – 3.13 (m, 84H) ppm. **^{13}C NMR** (125 MHz, DMSO-d_6) δ 157.42, 156.22, 154.81, 154.79, 154.74, 154.70, 154.44, 154.42, 154.40, 154.36, 154.30, 154.26, 154.22, 154.21, 152.12, 152.07, 151.25, 150.98, 150.89, 150.39, 150.05, 150.00, 149.66, 149.64, 111.02, 110.98, 110.47, 110.34, 110.29, 109.97, 109.94, 109.75, 87.87, 87.85, 87.80, 87.77, 87.75, 87.55, 87.51, 87.49, 87.42, 86.29, 86.27, 86.25, 86.21, 86.15, 86.12, 75.36, 75.31, 75.29, 75.23, 75.15, 75.09, 75.04, 74.99, 74.96, 74.92, 74.83, 74.68, 73.49, 73.43, 73.41, 73.40, 73.30, 73.11, 73.01, 72. 90, 72.85, 72.63, 72.55, 70.65, 69.21, 68.13, 68.05, 67.87, 65.76, 65.68, 65.66, 65.63, 52.69, 52.31, 52.26, 51.81, 51.45, 51.44, 50.92, 50.85, 47.75, 47.14, 47.00, 46.92, 46.71, 46.67, 45.66, 45.62, 45.37, 45.18, 44.92, 44.76, 44.74, 44.30, 44.19, 43.76, 43.31, 43.12, 43.09, 42.99, 41.98, 41.95, 38.85, 38.83, 27.81, 27.72, 25.86, 25.67, 25.54, 24.91, 24.86, 24.72, 24.63, 24.48, 24.38, 23.02, 22.83, 22.58, 22.47, 22.25, 22.14, 22.03, 21.97, 21.94, 21.84, 21.81, 21.70, 21.64, 21.56, 21.50, 21.46, 21.40, 20.75, 18.71, 18.36, 18.04, 17.72, 17.64, 17.60, 17.54, 17.50, 17.40, 17.17, 17.05, 16.79, 16.78, 16.76, 16.74, 16.73, 16.52, 16.50, 16.46, 16.06, 15.91, 15.79 ppm. **IR** (neat) ν 3310 (NH and NH_2), 2970, 2886, 1803 (carbonate), 1453, 1373, 1093, 925 cm^{-1}. Other representative signals were not clearly observed by IR.

Thermal curing with thiol-ene reactions

In 10 vials, 100 mg of the **NIPU5** was charged and then AIBN (2 mg, 2 wt.%) was added as initiator, and hereafter the desired amount of linker. Three out of these ten vials were mixed with a 1:1 ratio of alkene:thiol (that means 1 equiv of alkene to ¼ equiv of **PETMP**, 5.2 mg), three of them with a 1:1.2 ratio (i.e., 6.2 mg **PETMP**) and the other three with a 1:0.8 ratio (i.e., 4.2 mg **PETMP**). The remaining vial was used as a blank (absence of linker). The reaction

mixtures were poured into an aluminum tray providing a homogeneous film. Then, temperatures of 100 ºC, 120 ºC and 140 ºC were screened for the three ratios of alkene:thiol used. After cooking for 40 minutes, the trays were allowed to cool down and the dryness of the films obtained in all experiments was evaluated.

In the case of **GDMP**, the reaction conditions were 140 ºC during 40 min, using 2 wt % AIBN, and functional group ratios of 1:0.8 (4.1 mg **GDMP**), 1:1 (5.1 mg **GDMP**) and 1:1.2 (6.1 mg **GDMP**). Further on, the procedure followed was the same as explained above for those reactions done with **PETMP**.

Figure 4.14. Aluminum tray with a film after thermal curing corresponding to a 1:1 alkene:thiol ratio.

Selected spectra:

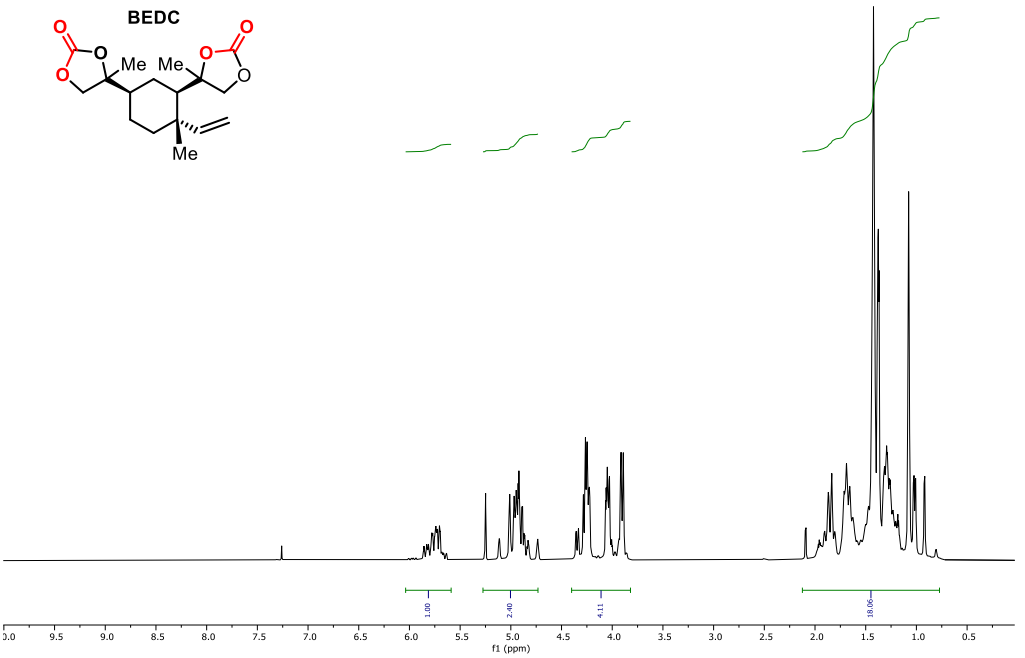

Figure 4.15. ^{1}H NMR analysis (400 MHz, Chloroform-*d*) for **BEDC**.

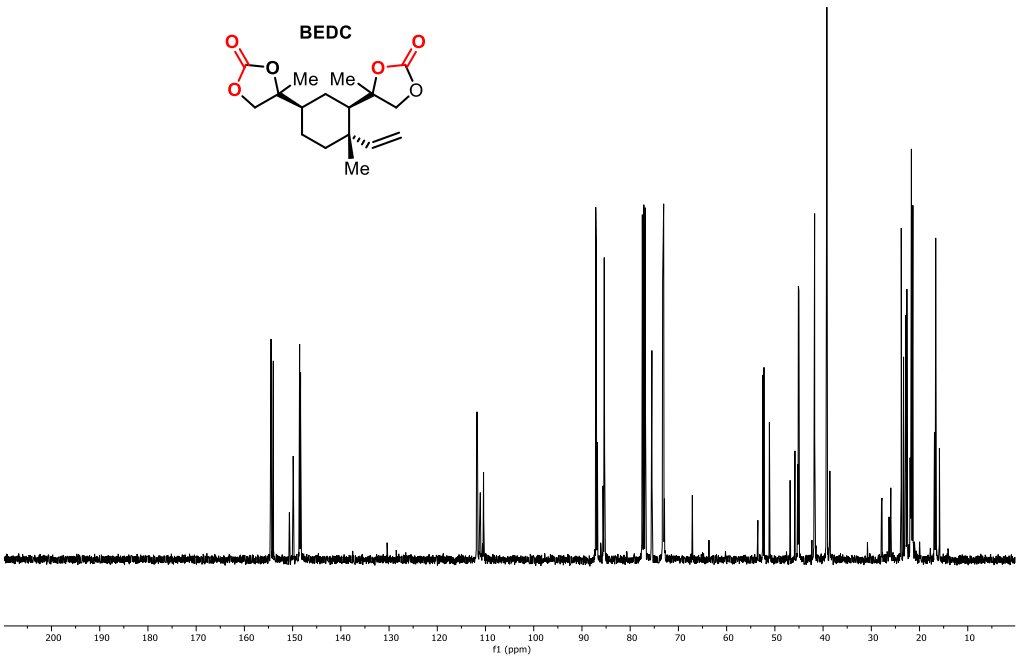

Figure 4.16. ^{13}C NMR analysis (400 MHz, Chloroform-*d*) for **BEDC**.

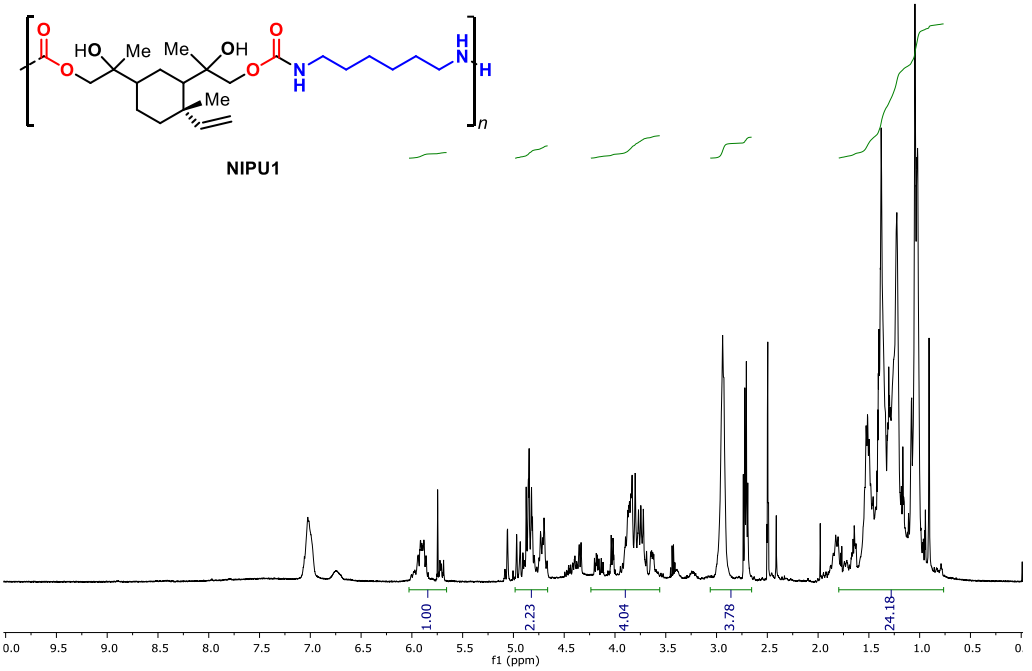

Figure 4.17. ^{1}H NMR analysis (500 MHz, DMSO-d_6) for **NIPU1**.

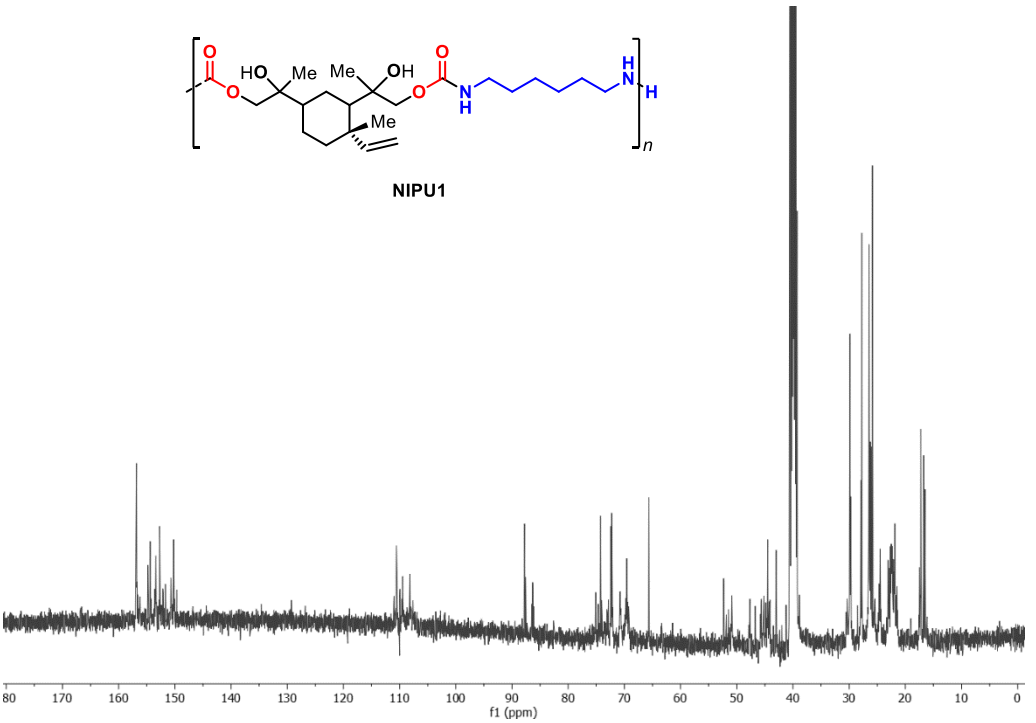

Figure 4.18. ^{13}C NMR analysis (125 MHz, DMSO-d_6) for **NIPU1**.

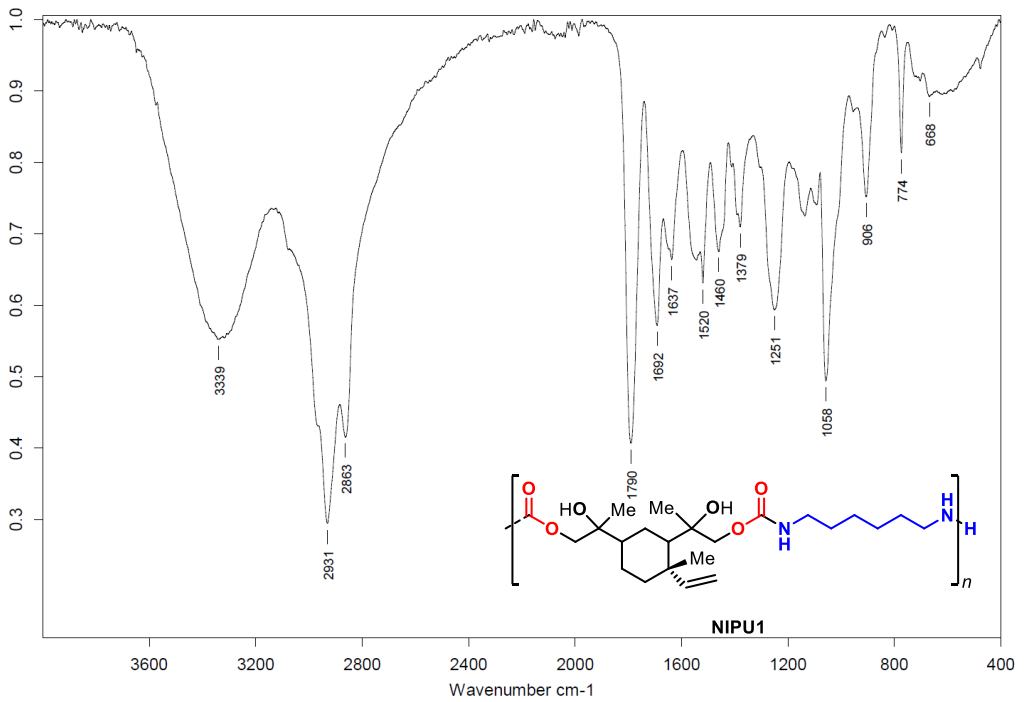

Figure 4.19. IR (neat) for **NIPU1**.

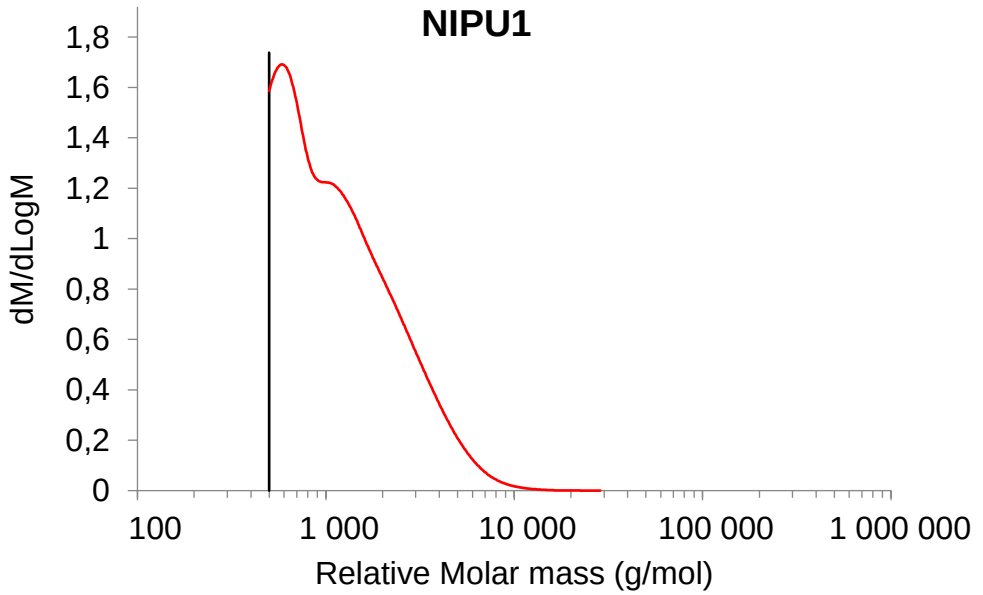

Figure 4.20. GPC analysis for **NIPU1.**

Chapter 5

Summary and General Conclusions

UNIVERSITAT ROVIRA I VIRGILI
NEW AND FUNCTIONAL CYCLIC CARBONATES FOR POLYMER APPLICATIONS
Cristina Maquilón Albaladejo

Carbon dioxide has been present in our atmosphere since the early stages of our planet creating essentially the prerequisites for life. The carbon cycle has been a means to regulate the global temperature being influenced directly by the atmospheric concentration of gases such as CO_2. However, ever since the 1860s the emissions of this gas to the atmosphere have been growing dramatically because of the industrial revolution, with a current record-high concentration of >420 ppmv. Nowadays, the high concentration of CO_2 is connected to drastic changes observed in the global climate, and new technologies that can mitigate on the short and long term these effects are being considered to reduce carbon emissions and atmospheric CO_2 concentration. In this respect, the utilization of CO_2 in synthesis through CCU has become an attractive approach to valorize CO_2 thereby setting an example for the reuse/recycling of this waste gas.

The field of catalytic CO_2 reutilization can be mainly divided into reductive and nonreductive transformations. Within the latter area, the Kleij group has long focused on the coupling of CO_2 with epoxides and oxetanes to form 5- and 6-membered cyclic carbonates (CCs). This topic has become increasingly popular in the last decades, and the development of new CCs has resulted into interesting novel applications as these scaffolds represent versatile organic synthetic intermediates and precursors for polymeric materials, among others.

Polymeric materials are widely use in the daily life due to their broad applicability in consumer end-products. However, virtually none of the most employed polymers are biodegradable and consequently they accumulate in the natural environment, with potential adverse side-effects (cf., plastic soup, microplastics issues, toxic degradation products). New approaches that can unleash protocols for biobased polymer substitutes with an improved carbon footprint and degradation features can help to advance the transition to a more sustainable polymer production with polycarbonates, polyesters and polyurethanes as exemplary cases. The development of new polymer chemistry based on CCs is here presented as a way to contribute to the challenge posed by the production of greener and more environmentally friendly materials.

Chapter 2 introduces the [3 + 2] cycloaddition of CO_2 to a bicyclic epoxy alcohol with the aim to unravel new stereo- and regio-selective manifolds, which further expands the knowledge towards the preparation of the more challenging carbonate compounds. The results presented show the influence of the nature of the catalytic system on the chemo-selectivity and stereo/regio preference towards a specific isomer. X-ray studies and a combination of spectroscopic analyses confirmed the synthesis and identification of 5 out of 8 possible isomers from a single epoxy

substrate by simply changing the reaction conditions. Two rare *trans*-configured CCs were structurally characterized, which should have potential in ROP.

Chapter 3 describes a new photocatalytic approach towards the synthesis of 6MCCs using γ-mono and γ,γ-disubstituted, *O*-protected allylic alcohols. A product 6MCC scope is presented with moderate to appreciable yields and high diastereoselectivity. In addition, the potential of selected 6MCCs towards ROP was evaluated. These studies revealed a steric influence of the substitution pattern of the monomers on their "polymerizability". Moreover, the 6MCC structure had indeed an influence on the thermal properties (T_d, T_g) of the polycarbonates obtained by ROP.

Chapter 4 presents the formation of a terpene based dicarbonate produced from the natural compound β-elemene. A scale up of this β-elemene dicarbonate facilitated the study of polyaddition reactions using commercially relevant diamines (in collaboration with BASF Coatings GmbH) in order to access new NIPUs. A coating application of one of the NIPUs was evaluated and the results of various physical tests are summarized and discussed in this chapter.

As a **General Conclusion** of this thesis, it is clear that new designs of CCs can be developed using catalytic CO_2 valorization approaches providing new CO_2-derived monomers for polymer synthesis. The newly developed syntheses of CCs in chapters 2 and 3 show that a larger diversity of monomers has become available to expand the portfolio of (future) polycarbonates with modular properties. While these protocols are not necessarily greener, they do start with an alternative carbon feedstock which ultimately may prove beneficial once further optimized. Greener polymer synthesis using newly developed CCs is attractive as a general objective, which has the potential to reduce the overall carbon footprint of the process and allow to explore new formulations depending on the structure of the carbonate monomer. In chapter 4, the introduction of a biobased reagent (β-elemene) further helps to "green" polymer synthesis and lowers the carbon footprint, and preliminary results do indicate that carbonates derived from this terpene may be useful in the development of novel NIPUs.

However, there is still room for synthetic improvement, and a better understanding of the relationship between the monomer structure and polymer properties should be achieved by a combination of empirical and computational efforts. Thus, future work with a focus on the development of a wider variety of bio-CCs can boost the access and study of more attractive and functional polymer materials and composites.

UNIVERSITAT
ROVIRA i VIRGILI